NASA TECHNICAL NOTE

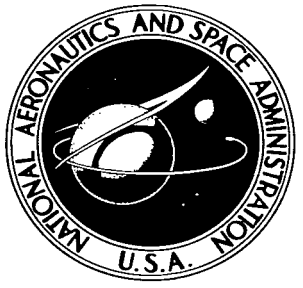


NASA TN D-2189



NASA TN D-2189

# DESCRIPTION OF VEHICLE SYSTEM AND FLIGHT TESTS OF NINE TRAILBLAZER I REENTRY PHYSICS RESEARCH VEHICLES

*by William N. Gardner, Clarence A. Brown, Jr.,*
*Allen B. Henning, W. Ray Hook,*
*Reginald R. Lundstrom, and Ira W. Ramsey, Jr.*

*Langley Research Center*
*Langley Station, Hampton, Va.*

NATIONAL AERONAUTICS AND SPACE ADMINISTRATION • WASHINGTON, D. C. • APRIL 1964

TECHNICAL NOTE D-2189

# DESCRIPTION OF VEHICLE SYSTEM AND FLIGHT TESTS OF NINE TRAILBLAZER I REENTRY PHYSICS RESEARCH VEHICLES

By William N. Gardner, Clarence A. Brown, Jr., Allen B. Henning, W. Ray Hook, Reginald R. Lundstrom, and Ira W. Ramsey, Jr.

Langley Research Center
Langley Station, Hampton, Va.

NATIONAL AERONAUTICS AND SPACE ADMINISTRATION

For sale by the Office of Technical Services, Department of Commerce, Washington, D.C. 20230 -- Price $2.25

# DESCRIPTION OF VEHICLE SYSTEM AND FLIGHT TESTS OF NINE TRAILBLAZER I REENTRY PHYSICS RESEARCH VEHICLES

By William N. Gardner, Clarence A. Brown, Jr., Allen B. Henning, W. Ray Hook, Reginald R. Lundstrom, and Ira W. Ramsey, Jr.

## SUMMARY

A unique six-stage solid-fuel rocket system was designed for the purpose of performing experimental reentry physics research in such a manner that a test object is caused to reenter the atmosphere at ICBM speeds at a location near the launching site. Preliminary results obtained from flight tests of nine Trailblazer I vehicles indicated that the design concept of a rearward-firing reentry rocket research vehicle was valid.

This system resulted in placing a small reentry body of hemispherical shape and of different materials close enough to ground-based optical and radar stations that good reentry data were obtained on six of the nine vehicles. Some problems with the vehicle became evident during the initial phase of the program but were eliminated as the program progressed.

## INTRODUCTION

In order to solve the many technical and operational problems involved in atmospheric reentry of satellites, space probes, manned space stations, and ballistic missiles, it is necessary that the available limited knowledge of the subject be expanded. At the present time there are numerous ground research facilities available which are capable of simulating some of the phenomena encountered by reentering bodies. None of these facilities, however, is capable of simultaneously simulating more than a few of the many stringent requirements. Actual satellite and ICBM reentry offers the best available means of simultaneously generating all reentry conditions. For purposes of studying reentry phenomena, however, satellites and ICBM vehicles are not a simple solution for many obvious reasons paramount of which are geographical reentry location and cost.

The purpose of this report is to describe a unique six-stage solid-fuel rocket vehicle designed for the sole purpose of performing experimental reentry physics research by reentering a test object into the atmosphere near the launch site at ICBM speeds. Although the vehicle has severely limited payload capability, its cost is approximately one-fiftieth to one-hundredth the cost of an ICBM or satellite, and it is possible to place all of the ground reentry monitoring instrumentation on the U.S. mainland within a range of less than 200 miles from the launch site or approximately 100 miles or less from the reentry event.

In addition to describing the vehicle which is known as Trailblazer I, this report presents limited preliminary data obtained from nine flight tests. These tests were made primarily for purposes of vehicle-system and ground-instrumentation-system development and to determine the effects of various materials on the reentry phenomena which were observed. Two configurations of the reentry object were utilized. Both configurations were essentially a 5-inch-diameter sphere; one has a cylindrical spike on the forward or leading face, and the other is a near hemisphere-cylinder shape.

The vehicle system was conceived, designed, and developed by the Langley Research Center, and all flight tests have been conducted at the NASA Wallops Station. The reentry research program is a cooperative enterprise between the NASA and the Massachusetts Institute of Technology - Lincoln Laboratory wherein the NASA has provided all vehicle-system management and technical responsibility with the Lincoln Laboratory providing funding for six of the vehicles reported. Data acquisition and analysis tasks are performed jointly by both organizations. Lincoln Laboratory funds are derived from the Air Force through an order from the Defense Department - Advanced Research Projects Agency.

## DESCRIPTION OF ROCKET VEHICLE SYSTEM AND METHOD OF FUNCTIONING

### Trajectory Considerations

The Trailblazer I rocket vehicle is unique in that its trajectory causes reentry to occur at a point near the launching site without having to resort to the use of automatic guidance or control systems aboard the vehicle. Figure 1 is a schematic presentation of a typical vehicle trajectory. Such a trajectory permits locating all the ground-based reentry monitoring instrumentation on the U.S. mainland within a horizontal range of 100 miles or less from the reentry location. Consequently, it is possible to use rather elaborate radar and optical equipment at convenient permanent instrument sites.

### Vehicle General Description

Figure 2 is a photograph of the complete vehicle mounted on a launcher ready for firing, and figure 3 is a sketch of the vehicle and velocity-package assemblies. The reentry trajectory is obtained by boosting a so-called velocity package to an altitude near one million feet and firing rocket stages out of the package backward toward the atmosphere on a near-vertical path. Three solid-fuel rocket stages are used to boost the velocity package to altitude and three rearward-orientated smaller solid-fuel rocket stages are contained in the spin-stabilized package. (See fig. 3.) A standard Honest John M6 booster rocket is utilized as the first-stage booster motor; a standard Nike M5 booster rocket, as the second-stage booster motor; and a TX77 rocket motor, as the third-stage booster motor. The fourth, fifth, and sixth stages contained in the velocity package are, respectively, a T40, and T55, and an NASA developed 5-inch-diameter spherical rocket motor (specific impulse in a vacuum, 236 seconds). The burned-out empty case of the 5-inch spherical motor together with any attachments is the

primary experimental reentry object. Figure 4 is a photograph of the velocity-package components laid out in their relative assembled positions. The upper part of the photograph shows the nose casting, timer, and battery-package housing, and the velocity-package shell or skin sections; and the lower part of the photograph shows the three small rocket motors together with their adapter hardware.

## Vehicle Functions and Design Considerations

Booster phase.- In order to achieve the trajectory shown in figure 1 without the use of onboard guidance and control equipment, it is necessary to employ both aerodynamic and spin stability. Aerodynamic fins are used on the three booster motors to achieve the ascending trajectory, and spin stabilization is used to maintain the velocity-package attitude so that the three motors which fire out of the package will follow the desired reentry trajectory. Aerodynamic stabilization can be used for the booster system in this case because all the booster propulsion effort is expended prior to the time that the vehicle leaves the sensible atmosphere. The fins on each successive booster stage are designed so as to provide sufficient static stability for that stage. References 1, 2, and 3 present the results of wind-tunnel tests made to determine the vehicle static aerodynamic stability.

During vehicle ascent the first-stage booster is drag separated from the remainder of the vehicle immediately after burnout. Following a short coasting period the second stage is ignited by ground-energized delay squibs. After burnout of this stage the empty motor remains attached to the vehicle during another coasting period. The purpose of the coasting periods is to allow the vehicle to gain sufficient altitude so that skin temperatures caused by aerodynamic heating will not become excessively high during third-stage burning, and to allow the aerodynamics forces and moments to become negligible at about the same time that the third-stage motor burns out. At the end of the second coasting period the third-stage motor is ignited by an internal timer and power supply and simultaneously separates from the empty case of the second stage. The second and third stages are mechanically held together by a thin metal diaphragm which has a threaded flange or rim and is radially slotted. The diaphragm is threaded directly into the lip of the third-stage nozzle exit cone and into a threaded adapter which is bolted to the forward end of the second-stage motor. At third-stage ignition the motor exhaust pressure collapses the diaphragm and, thus, disengages the threads and permits the motors to separate. A more complete description of this diaphragm may be found in reference 4.

Booster-trajectory dispersion control.- In order to meet range safety requirements and to avoid large errors in the location of the reentry trajectory, the ascending trajectory must be controlled within reasonable dispersion limits. Several methods are employed to minimize the trajectory dispersion. During lift-off, before the vehicle attains sufficient velocity to generate aerodynamic forces on the fins, any thrust misalinement of the motor can cause large trajectory dispersion. In order to minimize the effects of any thrust misalinement, small rockets are employed on the first stage to spin the vehicle very rapidly in a counterclockwise direction to a rate of nearly 1 cycle per second. These rockets are ground fired by a special trailing-wire ignition system which allows

the first-stage fins to clear the launcher before the spin motors are energized. The spin rockets burn for only 1 second, and the vehicle spin rate decreases very rapidly after spin-rocket burnout because of the large roll damping of the vehicle fins. In order to maintain vehicle spin, the first-stage fins are canted at an angle of approximately $0.5^{\circ}$. Shortly after the spin rockets burn out as the vehicle increases speed, the fins become effective in producing roll and cause the spin rate to increase again to about 1 cycle per second. This spin rate is sufficient to effectively cancel any thrust or fin misalinements in pitch or yaw.

Immediately after first-stage burnout and separation, the vehicle spin rate damps to some low rate consistent with the roll out-of-trim of the second-stage fins. Because the dynamic pressure and vehicle static stability are greater during most of the second-stage thrusting period than during the first-stage period, it has not been found necessary to spin the second stage to overcome thrust misalinement. The effects of any pitch and yaw fin misalinements are minimized by the large vehicle static stability. The third-stage fins are canted primarily to provide sufficient spin rate to spin stabilize the velocity package; however, this spin rate also counteracts any disturbances caused by third-stage thrust or fin misalinements in pitch or yaw. Fin misalinements for all stages for either pitch or yaw were held to an angle of less than $0^{\circ}10'$ for each fin. As shown by reference 2 the canted third-stage fins have a negligible effect on the second-stage roll rate. Figure 5 shows a time history of the nominal vehicle spin rate from launch through third-stage burning. The earliest peak spin rate shown is that caused by the first-stage spin rockets, and the second peak is caused by the first-stage canted fins. The large increase in spin at 34 seconds after launch is caused by the third-stage canted fins.

In spinning the vehicle either for dispersion control or for stabilization, care must be exercised to avoid resonance both with the aerodynamic pitch and structural frequencies. In the present case both a rigorous structural analysis and vehicle shake tests were made to determine the structural frequencies, and an analysis of the aerodynamic pitch frequency was made based on the data of references 1 and 2. The analysis indicated that the spin rate was less than the structural first-bending frequency at all times. A structural-natural-frequency curve is shown in figure 5. The spin-rate curve exceeds the aerodynamic-pitch-frequency curve during first-stage burning and crosses the pitch-frequency curve very rapidly to become less than the pitch frequency at first-stage separation. Roll-pitch resonance can be safely encountered only during a transient condition where the resonance point is rapidly traversed as in the present case. During third-stage burning as the vehicle rapidly increases altitude, the pitch frequency decreases and again the spin-rate curve crosses and exceeds the pitch-frequency curve. In this case, also, the roll-pitch resonance point is traversed rapidly enough so that no vehicle dispersion results.

A computed time history of the flight-path angle is presented in figure 6 for the first-stage thrust period. The data are for a thrust misalinement of $0.1^{\circ}$ with and without spin rockets and canted first-stage fins.

Atmospheric winds both at the surface of the earth and throughout the atmospheric altitude range have a large effect on trajectory dispersion. Vehicle velocity, acceleration, and aerodynamic static stability are the primary factors which determine the sensitivity of the vehicle trajectory to winds. If a vehicle

has low take-off acceleration, low velocity, or high static stability, then the atmospheric winds will have the greatest effects on the vehicle dispersion. In order to minimize trajectory dispersion, the launcher elevation and azimuth angles must be adjusted for the integrated wind effects. Prior to flight time the winds are measured by balloon soundings to an altitude corresponding to third-stage burnout and by ground instruments for the first 250 feet. A computer program tailored to the vehicle characteristics continuously determines launcher elevation and azimuth corrections for the existing winds up until 10 minutes prior to launch time. The method used to compensate the launcher settings to allow for atmospheric winds is presented in reference 5.

The booster-trajectory dispersion-control methods outlined herein have been successfully applied to several vehicle flights and have generally produced an error in azimuth and elevation angles of less than about $5^{\circ}$ and $1^{\circ}$, respectively. Nominal elevation angles have been either $80^{\circ}$ or $82^{\circ}$ in the subject flights. Normal variations in rocket-motor performance caused by variations in propellant-mix performance and motor temperature are other possible major causes of trajectory dispersion. In the present case, however, no effort has been made to control these factors nor has it been found necessary to either correct for or control them.

Coast during ascent.- During third-stage burning as the vehicle spin rate is rapidly increased, the vehicle passes through a transition region from aerodynamic stability to spin stability. In order to assist this transition, the third-stage fins are designed to provide sufficient aerodynamic static stability at third-stage ignition and a much smaller amount at third-stage burnout. This is achieved by taking advantage of the decrease in fin lift effectiveness as Mach number increases during third-stage burning. As the vehicle is spun, any angle between the thrust vector and the missile center line, or displacement of the missile center of gravity from the center line, will cause the vehicle to have a wobbling motion. This wobbling motion is further increased as the vehicle makes the transition from aerodynamic stability, where the vehicle tends to aline itself with the relative wind, to spin stability, where the vehicle axis tends to remain at a constant attitude angle. These two stabilities tend to oppose each other as the flight-path angle decreases. The high vehicle velocity after third-stage burning minimizes the decrease in flight-path angle, and the near neutral aerodynamic stability at third-stage burnout minimizes the resultant wobble motion.

This transition is shown in figure 7 where angle of attack has been computed and is presented as a function of time. Angle of attack is the angle between the missile axis and the relative wind projected onto a plane determined by the missile longitudinal axis and the local earth's vertical. The frequency decreases rapidly after third-stage burnout, and the amplitude increases until the dynamic pressure falls below any appreciable value. The amplitude of the wobble then remains constant, a fact which cannot be noticed well on this plot since the velocity-package separation occurs also at this point where the dynamic pressure becomes essentially zero. However, after separation, the amplitude is noticeably constant. Also noticeable is the increasing angle of attack caused by the decreasing flight-path angle and the essentially constant spin-stabilized missile attitude. The effect of the wobble angle is to cause dispersion of the reentry

trajectories of the three rocket stages contained in the velocity package. No attempt has been made to provide special wobble damping features in the vehicle.

After the vehicle has coasted to an altitude above the sensible atmosphere, the velocity package is separated from the third-stage motor case by a special separation mechanism. Figure 8 is a schematic drawing which helps to show how the mechanism works, and figure 9 shows photographs of the unit. Figure 9(a) is an exploded view of the mechanism parts in their relative assembled positions, and figure 9(b) shows the complete assembled unit together with the vehicle performance-monitoring telemeter section. This mechanism functions on the same principle as the blowout diaphragm mentioned previously. A threaded radially slotted disk mechanically holds the third stage and the velocity package together. At separation, a timer-initiated powder charge structurally buckles the diaphragm to release the velocity package. In order to minimize any possible disturbance to the velocity package and to provide some distance between the velocity package and the third-stage motor case, the powder-charge gases are expanded into a cylinder which pushes the velocity package and motor apart. Flight experience has shown no measurable disturbance caused by the separation-mechanism action.

After separation, the differential velocity of approximately 10 feet per second produced by the separation mechanism causes the empty third-stage motor and the velocity package to drift apart. At the time of fourth-stage firing the velocity package and third-stage motor are approximately 2,000 feet apart, and there is no interference between the fourth-stage and the third-stage motor even though their trajectories cross. During ascent after separation, both the third-stage motor and the velocity package remain spin stabilized at an attitude equivalent to the vehicle flight-path angle just prior to third-stage burnout.

Reentry phase.- The purpose of the boomerang-type trajectory flown by the Trailblazer I vehicle is to cause the high-speed reentry event to be located as near the launching site as may be reasonable. The downward-firing final three rocket stages must be completely burned out and up to maximum speed before descending below an altitude of about 500,000 feet. Therefore, it is necessary first to launch the vehicle at as high an elevation angle as is consistent with range safety requirements, and secondly to obtain a peak altitude sufficient to allow burnout of the final reentry stage above 500,000 feet. If the downward-firing stages are fired prior to reaching peak altitude, an appreciable velocity loss results from having to overcome the vehicle upward velocity component. Therefore, in the Trailblazer I system, fourth-stage ignition is timed to occur after apogee when the angle between the velocity-package spin axis and the vehicle flight-path angle is approximately 90°. Timing the fourth-stage firing event to occur in this manner permits full utilization of the velocity potential of the final rocket stages and simultaneously results in the reentry event occurring at a horizontal range approximately equivalent to the horizontal range at trajectory apogee.

As indicated by the sketch in figure 3, the fourth-, fifth-, and sixth-stage rocket motors are assembled as a unit and installed in the velocity package. The fourth-stage motor is supported by guide rails along its length and is attached to the velocity package by a blowout diaphragm threaded into its nozzle. At fourth-stage firing the diaphragm ruptures and leaves the motors free to

accelerate out of the package shell. Rearward directed vent holes are provided in the forward shell section to relieve any pressure buildup in the shell caused by rocket exhaust at ignition. The vent holes are visible in the photograph shown in figure 4, and they have a combined vent area greater than the nozzle-throat area of the fourth-stage motor.

The three rockets are simultaneously energized by an internal timer-battery package. Appropriate delay igniters are used in the fifth and sixth stages, and a short-delay igniter is used in the fourth stage to assure that the final two stages are energized before fourth-stage ignition. The fifth and sixth stages are assembled to the fourth stage and to each other by means of blowout diaphragms, and the motors fire in rapid succession in accordance with their time-delay igniters.

Since the sixth stage is physically a near-spherical shape and has a small spin inertia and a ratio of spin inertia to pitch inertia of near 1, it is necessary to employ a high spin rate for stabilization. An analysis by the method of reference 6 shows that a spin rate of 30 cycles per second is required at the time of sixth-stage ignition in order to maintain a wobble angle of less than $10^{\circ}$ in the average case. Because of structural considerations it is not possible to spin the complete velocity package to 30 cycles per second by means of the third-stage fins. A special torque nozzle was therefore designed for the fourth-stage motor to provide an increment in spin rate of 20 cycles per second during fourth-stage burning. This nozzle consists of seven small canted nozzles arranged in a circle around a small central nozzle. Each of the small nozzles is machined into a single nozzle block. Figure 10 shows a photograph of a fourth-stage torque nozzle together with a schematic diagram of the nozzle arrangement.

One of the conditions necessary to achieving less than $10^{\circ}$ wobble at sixth-stage burnout is dynamic balance with reference to the nominal thrust axis of each of the three reentry rocket motors. This necessitated dynamically balancing several different configurations. Configurations that were balanced were: fifth and sixth stages; fourth, fifth, and sixth stages; and the velocity package with the fourth, fifth, and sixth stages within. Weights were added to each configuration until the principal-axis inclination was less than $0.02^{\circ}$ for the combination of fifth and sixth stages and less than $0.01^{\circ}$ for the velocity package with the internal stages. A photograph of the fourth-, fifth-, and sixth-stage motors assembled on a vertical dynamic balancing machine is shown in figure 11.

Reference 3 presents a limited analysis of the motions of the Trailblazer I reentry body, which shows that at an altitude of 120,000 feet a maximum yaw angle as high as $50^{\circ}$ is possible. It will be shown subsequently that of the payloads considered in this report, either melting or burning of the payload generally takes place at an altitude above 150,000 feet. Reference 3 also shows that for altitudes above 120,000 feet the maximum yaw angle is greatly reduced.

## Vehicle Performance

Reference 7 is a performance analysis of several rocket booster systems similar to and including the Trailblazer system. The nominal computed trajectory

of each vehicle stage is shown in figure 12 for a launch angle of 80°. Time notations on the trajectories indicate the relative position of the various stages throughout their flight times. A time history of the nominal computed vehicle altitude, horizontal range, flight-path angle, and velocity until the time of fourth-stage firing is shown in figure 13 for a launch angle of 80°. A family of vehicle ascending trajectories and sixth-stage reentry trajectories is shown in figure 14 for various launch angles (only variable changed); and summary curves showing the effect of launch angle on vehicle altitude, horizontal range, flight-path angle, and velocity at two significant times during the flight are presented in figure 15. The two significant times selected are 40.6 and 300 seconds after launch.

Third-stage burnout nominally occurs at 40.6 seconds after launch, and the fourth stage is ignited at 300 seconds. Maximum booster velocity is obtained at third-stage burnout and peak altitude is a direct function of this velocity and the flight-path angle. The flight-path angle at third-stage burnout is also the approximate spin-stabilized attitude of the velocity package and therefore is a major factor in determining the angle of the sixth-stage reentry trajectory. The sixth-stage trajectory is fixed by the combined influence of the vehicle velocity and flight-path angle at fourth-stage ignition and by the velocity-package attitude. Slant range from the launch site to the sixth-stage reentry is approximately equivalent to the horizontal range at fourth-stage ignition. The summary curves and the family of trajectories show that the sixth-stage reentry angle is affected only slightly by small changes in the vehicle launch angle; however, the slant range from launch site to reentry more than doubles as the launch angle is decreased from 84° to 76°.

Curves which show the velocity-altitude and velocity-time relationships for the three final stages during their reentries are presented in figures 16 and 17, respectively. These nominal curves are computed for a sixth-stage reentry weight of approximately 2 pounds and a vehicle launch angle of 80°. A curve which shows the variation of sixth-stage reentry velocity with reentry weight is shown in figure 18. Reentry weight is the weight of the sixth stage after burnout of the sixth-stage 5-inch-diameter spherical rocket motor and includes the weight of the empty motor. The minimum weight of the empty spherical motor is approximately 0.5 pound.

## FLIGHT TESTS

The primary purpose of the nine vehicle flight tests reported herein has been to determine the effects of variations in the reentry-body material on the reentry phenomena which can be observed by various ground-based radar and optical instrumentation. The first three tests, which are designated Iα, Iβ, and Iγ, were intended to serve the purpose of combined vehicle-system and ground-instrumentation-system development; and the later six tests were expected to yield reentry data. The tests planned to yield reentry data are herein designated as Ia to If. A summary of the materials used in the tests, the reentry weight, and the nominal expected reentry velocity is made in table I. A weight

breakdown for each vehicle is presented in table II. Nominal launch angles, spin rate at velocity-package separation, cant angle of the third-stage fins, and ignition times are presented in table III. Moment-of-inertia measurements were not taken for all vehicles, but representative mass parameters for one such vehicle are presented in table IV. Mass parameters are presented for the loaded and empty conditions for each of the seven configurations.

## Reentry-Body Configuration

In all tests the burned-out or empty case of the 5-inch-diameter rocket motor was the primary test object. Except for the phenolic nylon and copper tests, the rocket case was manufactured of the test material. For both the phenolic nylon and copper tests, the rocket case was made of thin aluminum. The phenolic nylon was bonded directly to the case, whereas the copper was machined as a cap and threaded to a boss on the front of the case. Thin aluminum cases were used for the first two system-development tests. Detailed sketches of each of the test configurations are shown in figure 19, and photographs of typical test configurations are shown in figure 20.

A radio beacon, as shown in the sketches and photographs, was added to the configurations as a tracking aid. In the first two development tests the beacon was contained in a small cylinder attached to the front face of the sphere, and in all the other tests the beacon was contained in a torus can surrounding the motor nozzle. For the tests with the torus-beacon installation the can was in each case made of the test material. The torus beacon also served as a shield to prevent contamination of the experiments by the magnesium rocket-motor nozzle.

In all the reentry tests, the reentry bodies are completely destroyed, or consumed, when they reenter the atmosphere, and survival to impact is not expected.

## Instrumentation

Vehicle performance.- The sixth-stage radio tracking beacon previously mentioned was used in conjunction with several ground receiving stations to determine vehicle trajectories by a Doppler method described in reference 8. Numerous radars also served to track the vehicle flights, and an S-band radar tracking beacon was installed in the velocity-package nose. A four-channel telemeter was installed in the third-stage separation-mechanism housing to provide information on longitudinal, normal, and transverse acceleration and to provide an indication of velocity-package separation. A spinsonde telemeter was installed on the fifth stage to provide vehicle spin-rate information.

Reentry monitoring.- All the reentry monitoring instrumentation was ground based and consisted of special radar and optical equipment. Some of the tracking radars were provided with special instrumentation to obtain radar cross-section data throughout the flight. A photograph of the two principal radars used for these measurements is presented as figure 21. The radars are located on the mainland near Wallops Station and were installed and operated by the Massachusetts

Institute of Technology - Lincoln Laboratory. A detailed description of the radar equipment is presented in references 9 and 10.

Numerous types of optical equipment at several locations were utilized to obtain data such as streak photographs, time-chopped streak photographs, and spectrographs in the visible range. Photographs of typical optical site arrangements and some of the optical equipment utilized are shown in figure 22.

## RESULTS OF FLIGHT TESTS

The actual trajectories flown by all the vehicles reported herein are compared with the nominal vehicle trajectories in figure 23. For those flights from which reentry trajectory data were obtained, these data are also shown in the figures as side displacement from the plane of the ascending trajectory plotted against both horizontal range and altitude. Radar enhancement data and optical reentry photographs with sketches of the star backgrounds are presented for those vehicles from which reentry data were obtained. Temperature calculations were made for some of the reentry payloads, and these data are also presented. Data on the vehicle spin rate during third-stage burning are shown in figure 24. The data were obtained from measurements of the third-stage telemeter signal strength which varies with the roll angle because of polarized antenna patterns. Spin-rate data during fourth and fifth-stage burning as obtained from the fifth-stage spinsonde telemeter are shown in figure 25. The differences in the spin rates will be discussed in the subsequent section entitled "Description of Flights."

### Description of Flights

Trailblazer Iα.- The first vehicle flight test was made for the purpose of checking out the vehicle design concept and instrumentation system, and the results of the test were considered satisfactory for this purpose, even though some equipment failures were experienced. The Trailblazer Iα booster system functioned satisfactorily throughout its flight, as determined by radar tracking and by the third-stage telemeter instruments. The vehicle spin rate produced by the third-stage fins is shown in figure 24 and was quite satisfactory. During third-stage burning, however, the normal and transverse accelerometers indicated that the vehicle was experiencing considerable wobble motion, which was thought to be caused principally by third-stage fin misalinement. The radar beacon in the nose of the velocity package failed to function satisfactorily, and the tracking radars lost track at an altitude of about 500,000 feet. (See fig. 23(a).) Ground receiving stations failed to receive data of sufficient quality from the sixth-stage radio beacon to allow determination of the trajectory by the Doppler method; however, the radio-beacon data did show ignition and burning of the fourth and fifth stages at the expected times. At the time of sixth-stage ignition the beacon signal was lost completely. Subsequently, an expected faint visible trail produced by reentry of the fifth-stage motor was observed by numerous personnel on the ground and by the crew of an aircraft flying in the vicinity of the expected reentry event. No reentry of the sixth-stage motor was observed or photographed.

The available radar tracking data are shown in figure 23(a) and indicate that the ascending trajectory was slightly higher than intended. At the time of this test the large cross-section measurement radars, which are capable of skin tracking throughout the entire flight, were not available.

The results of the flight test showed that the vehicle concept was sound, although there were some problems apparent, and that the instrumentation system required major changes and advances. On the basis of difficulties experienced during development of an igniter for the sixth-stage motor, it was postulated that the motor exploded at ignition and further ground development tests were conducted.

Trailblazer Iβ.- In view of the difficulties experienced in the first flight it was considered advisable to conduct a second test, even though the then available radars could not track the complete trajectory. The results of this second development test were completely satisfactory in that good trajectory data were obtained and the sixth stage was observed to reenter and was photographed in the proper location and at the expected time. The Trailblazer Iβ booster system functioned properly throughout its flight as determined by radar tracking and by the third-stage telemeter instrumentation. The vehicle spin rate produced by the third-stage fins is shown in figure 24 and was quite satisfactory. During the third-stage burning, the telemeter indicated that very little wobble motion was experienced by the vehicle. Again, it was believed that the fin misalinement had previously caused the wobble in the flight of Trailblazer Iα. The radio beacon in the nose of the sixth stage functioned satisfactorily, and the MIT radar tracked the vehicle to apogee, an altitude of about 875,000 feet. (See fig. 23(b).) Ground receiving stations recorded sufficient data to allow determination of the trajectory by the Doppler method of reference 8. The remaining reentry trajectory, shown in figure 23(b), was computed by using this method. This side displacement shown in figure 23(b) is the measured distance from the plane of the outgoing trajectory in this and each subsequent trajectory and shows how much the vehicle deviated from the outgoing trajectory in the two side views. Optical cameras located at Coquina Beach, N.C., photographed the reentry of the sixth stage, and a photograph of the reentry is shown in figure 26 together with an accompanying sketch of the star background.

The available radar tracking data, shown in figure 23(b), indicate that the trajectory was slightly higher than intended but did not reach the anticipated altitude at apogee. The incoming trajectory was more nearly vertical than expected, and this again could have been caused by a very small wobble angle existing at fourth-stage ignition. No cross-sectional measuring radars capable of skin tracking the vehicle were available.

The results of the flight test indicated a successful flight, and it appeared that some of the problems had been eliminated.

Trailblazer Iγ.- Several changes to the vehicle were made before the flight test of Trailblazer Iγ. Spin rockets (four Honest John spin motors) were added to the first stage and a cant angle of $0.5^{\circ}$ was incorporated in each first-stage fin to aid in the reduction of dispersions due to thrust misalinements. Prior to the flight test of Trailblazer Iγ, very little evidence existed that indicated any serious problems due to the first-stage thrust misalinements; therefore, the

addition of spin motors and fin cant was a precautionary step. Reflectors were added to the S-band beacon of the vehicle to increase the signal strength for tracking.

In order to give the radars a hemispherical target to track, the spike radio transmitter was eliminated from the sixth stage and was rebuilt to fit into a torus shell around the 5-inch-diameter spherical rocket motor. The adapter joining the fifth and sixth stages was redesigned and made of a material capable of radiating the telemetry signal. The hemispherical shape permitted the use of several different materials of known chemical composition and thickness as reentering objects. In addition to the already tested sixth-stage radio beacon transmitter, a similar beacon of different frequency was added to the fifth stage to give spin data through fifth-stage firing.

The trajectory of the flight through apogee is shown in figure 23(c). The spin rate produced by the third-stage fins is shown in figure 24 and was satisfactory for spin stability. Shortly after third-stage burnout the third-stage telemeter showed a gradual increase in normal and transverse accelerations to the 5g stops. It is thought that the vehicle diverged and that this divergence prevented the final three stages from igniting. No optical data were obtained for this flight.

Trailblazer Ia.- As a result of the failure of Trailblazer Iγ, several modifications were incorporated in the vehicle hardware. Prior to the flight test of Trailblazer Ia, a vibration test was conducted to determine the structural stiffness of the third stage and velocity package. During the vibration tests, several mechanical joints showed signs of loosening. Locking screws and other mechanical locking devices were added to the vehicle to insure that all joints remained tight during flight. During the buildup of the vehicle, alinement of the vehicle was checked by using a theodolite to insure that the thrust axis and vehicle center line were as near the same as manufacturing tolerances would allow. Separation of the third stage and velocity package was reset to occur earlier in flight than for the previous vehicles. (See table III.) This adjustment was made to reduce the time for divergence to build up within the vehicle. In addition to these improvements, tip flares were added to the second stage for use as visual acquisition and tracking aids by the radars. These flares were successful in aiding the radars during acquisition and were used on all subsequent vehicles.

The trajectory for Trailblazer Ia is shown in figure 23(d). The vehicle was tracked by radars to fifth-stage ignition. As may be seen in figure 23(d), the trajectory for Trailblazer Ia was very close to the preflight predicted trajectory. The spin rate produced by the third-stage fins is shown in figure 24 and was satisfactory for velocity-package spin stability. The telemeter records for Trailblazer Ia (fig. 27(a)) shows that the divergence problem had not been completely solved because the normal and transverse accelerations were gradually approaching the 5g stops. Although preventing the joints from loosening had improved the stiffness and early separation of the velocity package had prevented any further breakups, additional stiffness was necessary.

Temperature calculations made during the design study showed that the aft section of the velocity package would reach 300° F to 400° F during flight. Although this temperature rise was not considered serious, possible loss of

stiffness could have resulted as the vehicle traversed the atmosphere. The fifth-stage radio beacon indicated a spin rate of 40 to 42 cycles per second shortly after fourth-stage burnout. The quality of the record after this time was not good enough to determine any further spin rates. There were some indications that a breakup occurred at fifth-stage ignition. The tracking radars also indicated a failure near this time, as several targets were observed by the radars. Calculations of the stiffness of the final three stages showed that both the minimum section of the fifth-stage rocket-motor nozzle and the adapter joining the fifth and sixth stages had marginal structural strength. Since the reentry payload did not obtain the necessary velocity, no optical data were obtained for this vehicle.

Trailblazer Ib.- As a result of a postflight analysis of Trailblazer Ia, several modifications were made to increase the vehicle stiffness. Metal stiffeners were added to the inside of the velocity package at the fiber-glass antenna section. These stiffeners could carry almost as much load as the original fiber-glass section and would not be subjected to the aerodynamic heating. Also, a coat of ablative material was applied to the rear half of the velocity package. Photographs of the velocity package before and after the application of the ablative material are shown in figure 28. The thickness of the ablative material varied from 0.010 inch at the middle of the velocity package to 0.100 inch at the fiber-glass section.

In order to increase the stiffness of the downward-firing stages, a metal sleeve was inserted over the fifth-stage nozzle and glued into place. This modification resulted in a rigid rocket motor capable of withstanding the loads applied by the fourth-stage rocket motor, since the strength was needed only until the fifth stage was ignited. Redesign of the adapter joining the fifth and sixth stages was also necessary to increase the stiffness of the adapter used on Trailblazers Iγ and Ia. In order to increase the rigidity of the stages within the velocity package, six hollow-column-type gauze-coated phenolic stiffeners were glued to the inside of the velocity package and at the juncture of the fifth and sixth stages within the velocity package. These columns would prevent the cantilever portion of the incoming stages from vibrating while in the velocity package. These columns would be ruptured when the fourth stage separated the incoming stages from the velocity package.

The trajectory of Trailblazer Ib is shown in figure 23(e). The vehicle was tracked by radars through apogee (approximately 965,000 feet), and the incoming stages were tracked to reentry. As may be seen in figure 23(e), the trajectory for Trailblazer Ib was very close to the preflight predicted trajectory. The spin rate produced by the third stage was 8.2 cycles per second. (See fig. 24.) Although preflight calculations indicated the spin rate should have been 10 cycles per second, the spin rate of 8.2 cycles per second did not appear to affect the spin stability of the velocity package. As mentioned previously, two fixes were included on this vehicle to reduce the divergence of the outgoing third stage and velocity package. Figure 27 shows the third-stage telemeter records for Trailblazers Ia and Ib. As may be noted, Trailblazer Ia showed a steady increase in the normal and transverse accelerations from near burnout of the third stage to separation, whereas the normal and transverse accelerations of Trailblazer Ib

did not increase during the same period. In fact, at separation very little normal or transverse accelerations were noted on any of the subsequent flights.

The fifth-stage telemeter indicated spin rates of 56.5 cycles per second at ignition of the sixth-stage 5-inch-diameter rocket motor. (See fig. 25.) Very little, if any, burning of the sixth-stage rocket motor was observed. It is believed that the high spin rate of the sixth-stage rocket affected the rocket performance. Two targets were observed on radar at sixth-stage ignition. It is believed that the igniter functioned properly and the grain failed to ignite. The sixth stage did not obtain the proper velocity, and no optical data were obtained for this vehicle.

Trailblazer Ic.- Several changes were included in Trailblazer Ic before the vehicle was flight tested. The velocity package and internal stages were dynamically balanced in part and together. Fin misalinements were measured, and if they exceeded manufacturing tolerance, alterations were made to remedy this excessive misalinement. Several tests performed at the NASA Langley Research Center and at several rocket-motor companies indicated that excessive spin rates could affect both the ignition qualities and burning characteristics of the rocket-motor grain. In view of this, the fourth-stage torque nozzle (fig. 10) was recut to reduce the spin of the final three stages to approximately 30 cycles per second instead of the present 40 to 60 cycles per second. The igniter for the sixth stage was rebuilt to include a slower burning, higher temperature propellant material to insure a positive ignition of the sixth-stage grain.

The trajectory for Trailblazer Ic is shown in figure 23(f). The vehicle was tracked by radars through apogee (980,000 feet), and the incoming stages were tracked through fourth-stage burning only. At this time the third-stage rocket motor entered the beam of the radar, and subsequently, the radar locked on the third stage. After tracking this stage for a few seconds, the mistake was realized, but acquisition of the incoming stages could not be obtained. The reentering trajectory shown in figure 23(f) was computed by using the Doppler method of reference 8. The trajectory was slightly higher than preflight predictions, and the incoming trajectory was more nearly vertical than predicted. The spin rate produced by the third stage was approximately 8.6 cycles per second. (See fig. 24.) The spin rate of the fifth and sixth stages at fifth-stage burnout was 34.8 cycles per second. (See fig. 25.) Optical cameras located at Coquina Beach, N.C., and Wallops Station, Va., photographed the reentry configuration, and some of the photographs are shown in figure 29 together with a sketch of the star background for each camera. The material used for the Trailblazer Ic sixth stage was titanium, and the bright flareup in the photograph shows ignition of the titanium due to aerodynamic heating. Figures 29(e) and 29(f) show a chopped photograph and sketch of the star background from Coquina Beach that when used in conjunction with other radar or optical data, will provide the reentry velocity of the sixth stage.

Although the radars did not track the reentering stages, optical data were of sufficient quality and quantity for good data reduction. Trailblazer Ic flight test results were satisfactory for all phases of the test and indicated that most of the problem areas had been eliminated.

Trailblazer Id.- After the flight test of Trailblazer Ic, it was decided to conduct further flight tests with a vehicle which was similar to Ic with only minor exceptions. For Trailblazer Id, care was taken to insure that the fin alinements were held to small tolerances, and dynamic balancing of each combination of stages was considered necessary. Some of the combinations that were balanced were (1) fifth and sixth stages, (2) fourth, fifth, and sixth stages, and (3) velocity package with fourth, fifth, and sixth stages in their rearward position. The third-stage telemeter record of Trailblazer Ic showed normal and transverse acceleration traces similar to those of Trailblazer Ib. Therefore, it was decided to increase the separation time between the third stage and velocity package from 47 seconds to 90 seconds after launch. (See table III.) The fifth-stage telemeter on Trailblazer Ic indicated that the spin rate produced by the fourth stage was near the desired value; hence, the nozzle of Trailblazer Id had the same torque angle as did that of Ic.

The trajectory for Trailblazer Id is shown in figure 23(g). The outgoing stages were tracked by radar to apogee, and at this time the radar lost track of the vehicle because of an alinement problem of the radar mount. The trajectory was higher than the nominal, and the vehicle exceeded the nominal apogee by nearly 80,000 feet. The spin rate produced by the third-stage fin was approximately 9.4 cycles per second. (See fig. 24.) The incoming trajectory could not be obtained by the Doppler method of reference 8 because only one receiving station was successful in tracking the sixth-stage beacon. The fifth-stage spin rate was 32.2 cycles per second at ignition of the sixth stage. (See fig. 25.) Time of ignition of the sixth stage (as determined from a disturbance indicated by the fifth-stage telemeter) was very close to preflight estimates, and performance of the sixth stage was normal because reentry occurred on schedule as determined from optical data.

The reentry body for Trailblazer Id had a phenolic-nylon-coated aluminum case and is shown in figure 19(c). This phenolic nylon was expected to ablate and decrease the temperature of the trailing gases. It was also expected that the intensity of the reentry streak would be quite dim and that it might not be possible to obtain a photograph of the reentry; however, several photographs were obtained, but because of the dimness of the reentry, only one photograph is included. This photograph is presented in figure 30 together with a sketch of the star background for the camera. Examination of the photograph and star background showed that two objects were visible upon reentry. It was believed that the heating of the rocket motor during burning had expanded the motor case thereby cracking the phenolic nylon and permitting two pieces to reenter. Both pieces reentered at approximately the same velocity. In order to substantiate this belief, a similarly coated rocket motor was static fired; cracking of the phenolic nylon and subsequent parting from the rocket motor near the equator resulted.

Although the reentry was less than desired because of failure of the radars to obtain a good track, the vehicle performance was satisfactory. Although equipment failure, both onboard and ground based, prevented a completely successful flight, much useful information was obtained from this vehicle.

Trailblazer Ie.- The performance of Trailblazers Ic and Id was of such success that no major design changes were necessary for Trailblazer Ie. The fourth-stage torque nozzle used on Trailblazers Ic and Id was also used on Ie.

Separation time for the third stage and velocity package of Trailblazer Ie was also the same as that of Id.

The trajectory for Trailblazer Ie is shown in figure 23(h) and the ascent trajectory was lower than the preflight nominal although the apogee was higher than predicted. The lower flight-path angle resulted in an increased horizontal range for the reentering portion of the trajectory. The spin rate produced by the third stage was 9.4 cycles per second. (See fig. 24.) The radar tracked the vehicle until the sixth stage (fig. 19(b)) broke into two pieces at a low altitude. The fifth stage was tracked, and a spin rate of 44.5 cycles per second was measured at sixth-stage ignition. (See fig. 25.) Ignition and burning of the sixth stage were satisfactory, and plots of the variation of reentry velocity with time and altitude are shown in figure 31. Some radar cross-section data were obtained for the first time on this flight, and one such curve is shown in figure 32 for the MIT S-band radar. Figure 32 shows that radar enhancement - that is, an increase in the returned signal strength which gives the appearance that a larger target is present than would be expected from geometrical measurements - occurred as the reentry object reached 155,000 feet and remained large until the altitude of the reentry object became 115,000 feet. The velocity had decreased from 19,000 feet per second to 11,000 feet per second during the enhancement.

The reentering sixth stage was photographed at Wallops Station, Va., and Coquina Beach, N.C. Some of the photographs are shown in figure 33 together with a sketch of the star background for each camera. One such photograph is a chopped trace from Wallops Station for measurement of velocity.

Trailblazer Ie did not follow the planned nominal trajectory, but much useful information, both optical and radar, was obtained.

Trailblazer If.- Prior to flight testing Trailblazer If, the same balance procedure was followed as for Id and Ie. The fourth-stage nozzle used on Trailblazer If was the same as that used on Ie, and the separation times for the two configurations were the same. The reentry stage had a copper shield, and a sketch of the reentry stage is shown in figure 19(d).

The outgoing trajectory for Trailblazer If was higher than the preflight nominal. (See fig. 23(i).) As the incoming stages burned, a disturbance was experienced by the vehicle which resulted in a side displacement from the nominal. Near an altitude of 200,000 feet, the incoming stages were at the nearest point to the tracking radars directly offshore. Spin rate produced by the third-stage fins was only 7.6 cycles per second (fig. 24), and it is believed that the low spin rate of the third-stage fins, together with the high winds throughout the wind-compensating altitude and a possible unsymmetrical loading of the rupture diaphragm, could have caused the reentering stages to deviate from the nominal trajectory more than had been experienced in previous flights. The fifth-stage telemeter was tracked, and a spin rate of 39.8 cycles per second was measured at sixth-stage ignition. (See fig. 25.)

The reentering trajectory with the large side displacement did not prevent the radars from obtaining an excellent track of the reentering stages. The

variation of the velocity with time and altitude is presented in figure 34. The maximum velocity for Trailblazer If was 19,300 feet per second just prior to reentry. Cross-sectional data were obtained for both the MIT S-band and UHF-band radars and are presented in figures 35 and 36 as a function of altitude and velocity. Enhancement occurred approximately 20,000 feet higher in altitude for the UHF-band radar than for the S-band radar. Both radars gave large enhancements during reentry.

The reentering sixth stage (fig. 19(d)) for this shot was photographed from only one location because of the side dispersion of the reentry. This photograph together with the accompanying star background is shown in figure 37. Very little optical data were obtained for this shot although the radar data obtained were of considerable interest.

### Dispersion Summary

The dispersion of the reentry stages for five of the vehicles flight tested has been summarized and is presented in figure 38 as the deviation in flight-path angle from the nominal reentry trajectory. In the upper portion of figure 38, the sign convention for the displacement from the nominal reentry trajectory is shown. The reentry flight-path angle used was the average flight-path angle measured from a point shortly after sixth-stage burnout to an altitude of 300,000 feet. The displacement presented in figure 38 is the difference between this measured flight-path angle and the nominal.

Data for only five vehicles are presented because of the inability in some cases of the radar or radio beacon to produce a trajectory down to an altitude of 300,000 feet. As may be noted in figure 38, reentry dispersion for one of the vehicles, Trailblazer If, was quite large in both pitch and yaw. Possible reasons for this large dispersion have been discussed in the section concerning Trailblazer If. The maximum dispersion of the other vehicles was approximately $10^{\circ}$ in yaw and $15^{\circ}$ in pitch.

## TEMPERATURE CALCULATIONS

The heating rates at the stagnation point were calculated for the reentry bodies of Trailblazers Ic, Ie, and If by using the method of reference 11. No heating rates were computed for Trailblazer Id since the multiple reentry trails suggested that the sixth stage did not reenter as a single integral unit. By using these calculated heating rates, it was possible to compute a time history of the reentry-body wall temperature taking into account the thermal conductivity of the structural material. The variations of the stagnation-point heating rate and wall temperature with altitude are presented in figures 39, 40, and 41. The wall temperature of the copper reentry body (Trailblazer If) is the same for the inner and outer faces because of the high thermal conductivity of copper and the thinness of the material. The temperature difference between the inside and outside faces is quite apparent, however, in the case of the steel and titanium reentry bodies.

If the reentry body is at an angle of attack and spinning, the stagnation point, instead of being at the pole, would have an angular displacement equal to the angle of attack. If, in addition, the reentry body is precessing, the stagnation point would cover the area included by a lateral spherical segment. It is also obvious that the heat input to any given point on the spinning precessing sphere would be appreciably less than the heat input to the stagnation point of a nonmoving sphere. The ratio of the heating rate at the stagnation point to that at some other point may be determined from reference 12. In general, the heat input was less near the pole and greater near the equator for the case of the spinning precessing sphere than for the case of the nonmoving sphere. In most cases, the net result is a longer survival time for the wobbling sphere for the particular sphere design used.

By averaging the heating rate over each cycle, it was possible to calculate the average heating rate for any point on the forward surface of the rotating and precessing sphere. Presented in figures 39, 40, and 41 are calculations for the heating rate and wall temperature at the stagnation point when located at the pole of the nonprecessing sphere at $\alpha = 0^\circ$ and also when located at points $30^\circ$ from the pole of the sphere at $\alpha = 30^\circ$ and precessing through an angle of $30^\circ$. The use of this latter motion was quite arbitrary, but it was felt that this represented a rather extreme condition for the wobbling motion and that the actual flight case lay between the $30^\circ$ wobbling case and the $0^\circ$ case.

Since the radar did not track the reentry body for Trailblazer Ic, the initial reentry velocity and angle were calculated from the optical data. Figure 39 shows that the titanium reentry body started to melt at about 146,000 feet for the no-wobble condition and at about 117,000 feet for the $30^\circ$ wobble condition. Titanium will ignite at about $1,200^\circ$ F at atmospheric pressure. It is interesting to note that the start of the large flare in the visible trail of figures 29(a), (c), and (e) is at about 152,000 feet where, according to the calculations, the maximum wall temperature was about $3,000^\circ$ F for the no-wobble condition or about $2,400^\circ$ F for the wobble condition. The stagnation pressure at this altitude was about 0.5 atmosphere. At 123,000 feet, which is about the center of the flare, the wall temperature at the stagnation point is above the melting point ($3,140^\circ$ F) for the no-wobble condition and very close to the melting point for the wobble condition with a stagnation pressure of about 1.25 atmospheres.

Figure 40 shows that the steel reentry body of Trailblazer Ie started to melt at 172,000 feet for the no-wobble condition or 156,000 feet for a $30^\circ$ wobble angle. The reentry body first became visible from the ground at about 149,000 feet.

Figure 41 shows that the copper reentry body of Trailblazer If started to melt at 233,000 feet for the no-wobble condition, or 219,000 feet for a $30^\circ$ wobble angle. Destruction of the reentry body probably occurred quite rapidly once melting started, since melting started well below the maximum heating rate. This altitude was higher than the altitude at which the sixth stage first became visible from the ground (184,000 feet) or the altitude at which radar enhancement started (195,000 feet).

No attempt has been made herein to analyze the optical or radar data received from the Trailblazer I vehicles. Rather, this report has been an attempt to

describe the vehicle and to present some of the basic trajectory data together with some of the problems encountered in the vehicle design development.

## CONCLUDING REMARKS

Preliminary results obtained from flight tests of nine Trailblazer I vehicles indicated that the design concept of a rearward-firing reentry rocket research vehicle was valid. This unique six-stage solid-fuel rocket system was designed for the sole purpose of performing experimental reentry physics research in such a manner that a test object is caused to reenter the atmosphere at ICBM speeds at a location which is near the launching site.

This unique system resulted in placing a small reentry body of hemispherical shape and of different materials close enough to ground-based optical and radar stations that good reentry data were obtained on six of nine vehicles. Some problems with the vehicle became evident during the initial phase of the program but were eliminated as the program progressed.

Langley Research Center,
National Aeronautics and Space Administration
Langley Station, Hampton, Va., November 8, 1963.

## REFERENCES


1. Robinson, Ross B.: Effects of Body and Fin Deflections on the Aerodynamic Characteristics in Pitch of a 0.065-Scale Model of a Four-Stage Rocket Configuration at Mach Numbers of 1.41 and 1.82. NASA TN D-37, 1959.

2. Gregory, Donald T., and Carraway, Ausley B.: Investigation of the Static Longitudinal Stability and Roll Characteristics of a Three-Stage Missile Configuration at Mach Numbers From 1.77 to 2.87. NASA TM X-124, 1959.

3. Schippell, Herbert R.: Trailblazer I Reentry-Body Wind-Tunnel Tests at a Mach Number of 6.7 With Theoretical Aerodynamics and a Limited Dynamic Analysis. NASA TN D-1936, 1963.

4. Gungle, Robert L., Brosier, Williams S., and Leonard, H. Wayne: An Experimental Technique for the Investigation of Tipoff Forces Associated With Stage Separation of Multistage Rocket Vehicles. NASA TN D-1030, 1962.

5. Henning, Allen B., Lundstrom, Reginald R., and Keating, Jean C.: A Wind-Compensation Method and Results of Its Application to Flight Tests of Twelve Trailblazer Rocket Vehicles. NASA TN D-2053, 1963.

6. Martz, C. William: Method for Approximating the Vacuum Motions of Spinning Symmetrical Bodies With Nonconstant Spin Rates. NASA TR R-115, 1961.

7. Brown, Clarence A., Jr.: Performance Analysis of Six Solid-Fuel Rocket-Motor Boost Systems With Payloads of 300 to 2,000 Pounds. NASA TM X-131, 1959.

8. Henning, Allen B.: Some Experimental Results for a Doppler Tracking Method Using a Simple CW Beacon. NASA TN D-2188, 1963.

9. Anon.: Reentry Physics Program Semiannual Technical Summary Report to the Advanced Research Projects Agency - October 1, 1958 - June 30, 1959. Contract AF 19(604)-4559, Lincoln Lab., M.I.T., Oct. 8, 1959.

10. Anon.: Reentry Physics Program Semiannual Technical Summary Report to the Advanced Research Projects Agency - July 1, 1959 - December 31, 1959. Contract AF 19(604)-5200, Lincoln Lab., M.I.T., Mar. 23, 1960.

11. Kemp, N. H., and Riddell, F. R.: Heat Transfer to Satellite Vehicles Re-Entering the Atmosphere. Jet Propulsion, vol. 27, no. 2, pt. 1, Feb. 1957, pp. 132-137, 147.

12. Lees, Lester: Laminar Heat Transfer Over Blunt-Nosed Bodies at Hypersonic Flight Speeds. Jet Propulsion, vol. 26, no. 4, Apr. 1956, pp. 259-269, 274.

TABLE I

REENTRY TEST CONDITIONS

| Trailblazer | Reentry-body material | Reentry weight, lb | Nominal reentry velocity, ft/sec |
|---|---|---|---|
| Iα | Aluminum | 0.77 | 24,600 |
| Iβ | Aluminum | .80 | 24,400 |
| Iγ | Titanium | 2.06 | 18,800 |
| Ia | Steel | 2.28 | 18,300 |
| Ib | Aluminum | 2.15 | 18,600 |
| Ic | Titanium | 2.10 | 18,700 |
| Id | Phenolic nylon | 2.17 | 18,500 |
| Ie | Steel | 2.33 | 18,200 |
| If | Copper | 2.03 | 18,900 |

TABLE II

COMPARISON OF WEIGHTS FOR TRAILBLAZER I VEHICLES

| | Weight, lb, of Trailblazer - | | | | | | | | |
|---|---|---|---|---|---|---|---|---|---|
| | Iα | Iβ | Iγ | Ia | Ib | Ic | Id | Ie | If |
| Outer skin of velocity package: | | | | | | | | | |
| Nose | 6.81 | 8.5625 | 8.56 | 37.3125 | 37.700 | 28.82 | 11.00 | 29.25 | 29.625 |
| Beacon section | 14.88 | 18.3125 | 12.38 | | | | 18.501 | | |
| Upper skin | 14.25 | 15.75 | 15.88 | 15.3125 | 15.375 | 17.00 | 16.063 | 14.500 | 14.375 |
| Lower skin | 35.88 | 35.3125 | 35.75 | 36.8125 | 42.500 | 46.75 | 47.75 | 46.500 | 47.500 |
| Total | 71.82 | 77.94 | 72.57 | 89.4375 | 95.575 | 92.57 | 93.314 | 90.25 | 91.500 |
| Sixth stage: | | | | | | | | | |
| Rocket-motor case | ------- | 0.21 | -------- | -------- | ------- | ------- | ------- | 1.04 | 0.894 |
| Case and liner | ------- | .24 | -------- | -------- | ------- | ------- | ------- | 1.07 | .924 |
| Propellant | ------- | 3.74 | -------- | -------- | ------- | ------- | ------- | 3.77 | 3.770 |
| Nozzle | ------- | .208 | -------- | -------- | ------- | ------- | ------- | .27 | .270 |
| Total: 5" motor | 4.210 | 4.188 | 5.17 | 5.125 | 5.062 | 5.000 | 5.000 | 5.11 | 4.964 |
| Spike radio beacon | .298 | .352 | | | | | | | |
| Torus radio beacon | | | .63 | .899 | .827 | .840 | .906 | .96 | .807 |
| Igniter assembly | .154 | .110 | .10 | .125 | .125 | .110 | .126 | .123 | .130 |
| Diaphragm | .031 | .027 | .06 | .062 | .026 | .030 | .026 | .026 | .027 |
| Sixth-stage total | 4.693 | 4.677 | 5.96 | 6.211 | 6.040 | 5.980 | 6.058 | 6.219 | 5.928 |
| 5" motor grain | 3.74 | 3.74 | 3.74 | 3.74 | 3.74 | 3.74 | 3.74 | 3.77 | 3.77 |
| Reentry weight | .77 | .80 | 2.06 | 2.28 | 2.15 | 2.10 | 2.17 | 2.30 | 1.99 |
| Fifth stage: | | | | | | | | | |
| Adapter (5" to T55) | 0.357 | 0.688 | 1.81 | 1.563 | 2.625 | 2.69 | 2.813 | 2.69 | 2.970 |
| Loaded T55 with nozzle and headcap | 47.50 | 47.125 | 47.440 | 46.875 | 49.729 | 50.00 | 48.915 | 49.375 | 49.66 |
| Igniter assembly | .82 | .638 | .810 | .636 | .688 | .56 | .625 | .725 | .690 |
| Telemeter | | 1.020 | 1.060 | 1.108 | 1.269 | 1.08 | 1.181 | 1.108 | 1.120 |
| Fifth-stage total | 48.677 | 49.471 | 51.120 | 50.182 | 54.311 | 54.33 | 53.534 | 53.898 | 54.440 |
| Fourth stage: | | | | | | | | | |
| T55 diaphragm | 0.38 | 0.438 | 0.44 | 0.375 | 0.375 | 0.42 | 0.688 | 0.416 | 0.46 |
| Adapter (T40 to T55) | 1.25 | 1.062 | 1.13 | 1.188 | 1.250 | 1.22 | 1.688 | 1.190 | 1.33 |
| Loaded T40 without nozzle | 126.75 | 126.75 | 127.50 | 127.25 | 126.30 | 127.13 | 126.688 | 126.25 | 126.25 |
| Nozzle | 6.75 | 6.75 | 6.63 | 6.75 | 6.813 | 6.62 | 6.700 | 6.75 | 6.75 |
| Igniter assembly | .72 | .628 | .88 | .628 | .688 | .71 | .625 | .781 | .75 |
| Diaphragm (T40 to package) | .44 | .875 | .38 | .438 | .625 | .46 | .438 | .461 | .46 |
| Fourth-stage total | 136.29 | 136.503 | 136.96 | 136.629 | 135.938 | 136.56 | 136.940 | 135.848 | 136.00 |
| Package total | 261.48 | 268.591 | 266.61 | 282.459 | 291.864 | 289.44 | 289.845 | 286.215 | 287.868 |
| Package c.g., in. from nose . . . . . | ------- | -------- | 57.84 | 54.05 | 58.009 | 58.62 | 58.56 | 58.06 | 58.09 |

TABLE II.- Concluded

COMPARISON OF WEIGHTS FOR TRAILBLAZER I VEHICLES

| | Weight, lb, of Trailblazer - | | | | | | | | |
|---|---|---|---|---|---|---|---|---|---|
| | Iα | Iβ | Iγ | Ia | Ib | Ic | Id | Ie | If |
| Velocity-package separation mechanism: | | | | | | | | | |
| Push plate and piston section | 36.19 | 34.5625 | 72.31 | 74.0625 | 76.8125 | 78.38 | 75.38 | 76.250 | 97.125 |
| Retainer and bolts | .88 | 1.375 | | | | | | | |
| Telemeter, battery, antenna, and extension housing | 33.26 | 36.795 | | | | | | | |
| Timer assembly | 2.13 | 2.6875 | 3.06 | 3.0625 | 3.46 | 3.78 | 3.38 | 3.4375 | 3.125 |
| Total | 72.46 | 75.42 | 75.37 | 77.125 | 80.2725 | 82.16 | 78.76 | 79.6875 | 100.25 |
| Third stage: | | | | | | | | | |
| TX 77 rocket motor | 1,778.0 | 1,705.2 | 1,701.8 | 1,712.0 | 1,735.5 | 1,735.81 | 1,724.4 | 1,648.5 | 1,737.25 |
| 2.0-sq-ft fin panel and shroud | | 75.0 | 75.0 | | | | | 74.5 | |
| Third-stage total | 1,778.0 | 1,780.2 | 1,776.8 | 1,712.0 | 1,735.5 | 1,735.81 | 1,724.4 | 1,723.0 | 1,737.25 |
| Third-stage c.g., in. aft thrust face . . . . . | | 86.67 | 86.47 | 87.438 | 86.81 | 82.41 | 86.87 | 86.69 | 85.87 |
| Second stage: | | | | | | | | | |
| Nike motor, adapter, 2.5-sq-ft fin panel, and shroud | 1,298.0 | 1,308.56 | 1,312.19 | 1,275.56 | 1,315.56 | 1,299.0 | 1,310.7 | 1,303.56 | 1,302.7 |
| Flares | | | | | 1.5 | 1.38 | 1.38 | 1.38 | 1.4 |
| Second-stage total | 1,298.0 | 1,308.56 | 1,312.19 | 1,275.56 | 1,317.06 | 1,300.38 | 1,312.08 | 1,304.94 | 1,304.1 |
| Second-stage c.g., in. aft thrust face . . . . . | -------- | 60.62 | 60.82 | 60.75 | 60.30 | 60.44 | 60.50 | 60.69 | 60.625 |
| First stage: | | | | | | | | | |
| Honest John motor, 7.5-sq-ft fin panel, adapter, spin rockets, and housing | 4,153.0 | 4,166.0 | 4,328.0 | 4,217.0 | 4,250.0 | 4,204.75 | 4,156.75 | 4,237.0 | 4,272.5 |
| Igniter | 4.37 | 4.44 | 4.37 | 4.44 | 4.3 | 4.25 | 4.25 | 4.44 | 4.44 |
| First-stage total | 4,157.37 | 4,170.44 | 4,332.37 | 4,221.44 | 4,254.3 | 4,209.0 | 4,161.0 | 4,241.44 | 4,276.9 |
| First-stage c.g., in. aft thrust face . . . . . | -------- | 88.5 | 87.69 | 87.125 | 87.50 | 87.62 | 87.62 | 86.31 | 87.0 |
| Total at launch | 7,567.31 | 7,603.21 | 7,763.34 | 7,568.58 | 7,678.99 | 7,616.78 | 7,566.08 | 7,635.28 | 7,706.4 |

TABLE III

GENERAL INFORMATION

(a) Vehicle description

| Trailblazer | Reentry body | Nominal launch angle, deg | Spin rate at package separation, cps | Total cant angle of third-stage fins |
|---|---|---|---|---|
| Iα | Thin aluminum case | 80 | 10.6 | 3°55' |
| Iβ | Thin aluminum case | 80 | 10.5 | 3°55' |
| Iγ | Thick titanium case | 80 | 10.4 | 3°50' |
| Ia | Thick steel case | 82 | 10.6 | 3°40' |
| Ib | Thick aluminum case | 82 | 8.2 | 3°31' |
| Ic | Thick titanium case | 82 | 8.8 | 3°18' |
| Id | Thin aluminum case with phenolic-nylon shield | 82 | 9.4 | 3°35' |
| Ie | Thick steel case | 82 | 9.4 | 3°17' |
| If | Thin aluminum case with copper shield | 82 | 7.6 | 3°24' |

(b) Time history

| Trailblazer | Time, sec, at - | | | | | | | | | |
|---|---|---|---|---|---|---|---|---|---|---|
| | First-stage ignition | First-stage burnout | Second-stage ignition | Second-stage burnout | Third-stage ignition | Third-stage burnout | Separation | Fourth-stage ignition | Fifth-stage ignition | Sixth-stage ignition |
| Iα | 0 | 4.80 | 12.90 | 16.16 | 34.56 | 40.70 | 149.31 | 328.4 | 339.9 | 343.9 |
| Iβ | 0 | 4.81 | 12.53 | 16.02 | 33.42 | 42.24 | 149.42 | 300.6 | 311.8 | 318.8 |
| Iγ | 0 | 4.98 | 13.53 | 17.04 | 33.16 | 40.95 | 150.02 | ------ | ------ | ------ |
| Ia | 0 | 4.87 | 11.36 | 14.81 | 32.47 | 40.40 | 45.85 | ------ | ------ | ------ |
| Ib | 0 | 4.84 | 10.98 | 14.45 | 33.92 | 41.54 | 47.04 | 301.99 | 310.35 | 315.81 |
| Ic | 0 | 4.57 | 10.71 | 14.14 | 34.63 | 42.03 | 46.91 | 300.84 | 309.47 | 313.57 |
| Id | 0 | 4.68 | 10.40 | 13.81 | 33.62 | 41.36 | 59.38 | 300.5 | 309.3 | 316.67 |
| Ie | 0 | 4.75 | 11.19 | 14.74 | 33.92 | 42.10 | 90.00 | 302.93 | 309.63 | 323.39 |
| If | 0 | 4.82 | 10.53 | 14.01 | 34.09 | 42.10 | 91.11 | 301.15 | 309.33 | 315.24 |

TABLE IV

TRAILBLAZER I MASS PARAMETERS

| Time after launch, sec | Weight, lb | Center of gravity, in. aft of nose | Moment of inertia, $I_X$ (roll), slug-ft$^2$ | Moment of inertia, $I_Y$ (pitch), slug-ft$^2$ |
|---|---|---|---|---|
| First stage, second stage, third stage, and velocity package | | | | |
| 0 | 7562.9 | 425.6 | 156.5 | 43,240 |
| 5.2 | 5516.9 | 384.0 | 128.0 | 34,626 |
| Second stage, third stage, and velocity package | | | | |
| 5.2 | 3410.0 | 269.2 | 32.35 | 8,902 |
| 34.4 | 2675.0 | 239.8 | 27.30 | 6,544 |
| Third stage and velocity package | | | | |
| 34.4 | 2110.0 | 202.9 | 18.80 | 2,193 |
| 45.0 | 872.6 | 173.4 | 8.70 | 1,542 |
| Velocity package | | | | |
| 90.0 | 288.75 | 58.1 | 0.89 | 61.2 |
| 300.0 | 288.75 | 58.1 | .89 | 61.2 |
| Time after launch, sec | Weight, lb | Center of gravity, in. forward of rocket nozzle | Moment of inertia, $I_X$ (roll), slug-ft$^2$ | Moment of inertia, $I_Y$ (pitch), slug-ft$^2$ |
| Fourth stage, fifth stage, and sixth stage | | | | |
| 302.0 | 195.16 | 36.10 | 0.353 | 26.74 |
| 310.0 | 89.17 | 50.75 | .147 | 15.17 |
| Fifth stage and sixth stage | | | | |
| 310.0 | 59.63 | 25.19 | 0.065 | 2.29 |
| 315.0 | 26.13 | 26.80 | .028 | 1.30 |
| Sixth stage | | | | |
| 316.0 | 5.77 | 4.46 | 0.0032 | 0.0061 |
| 320.0 | 1.93 | 3.41 | .0015 | .0031 |

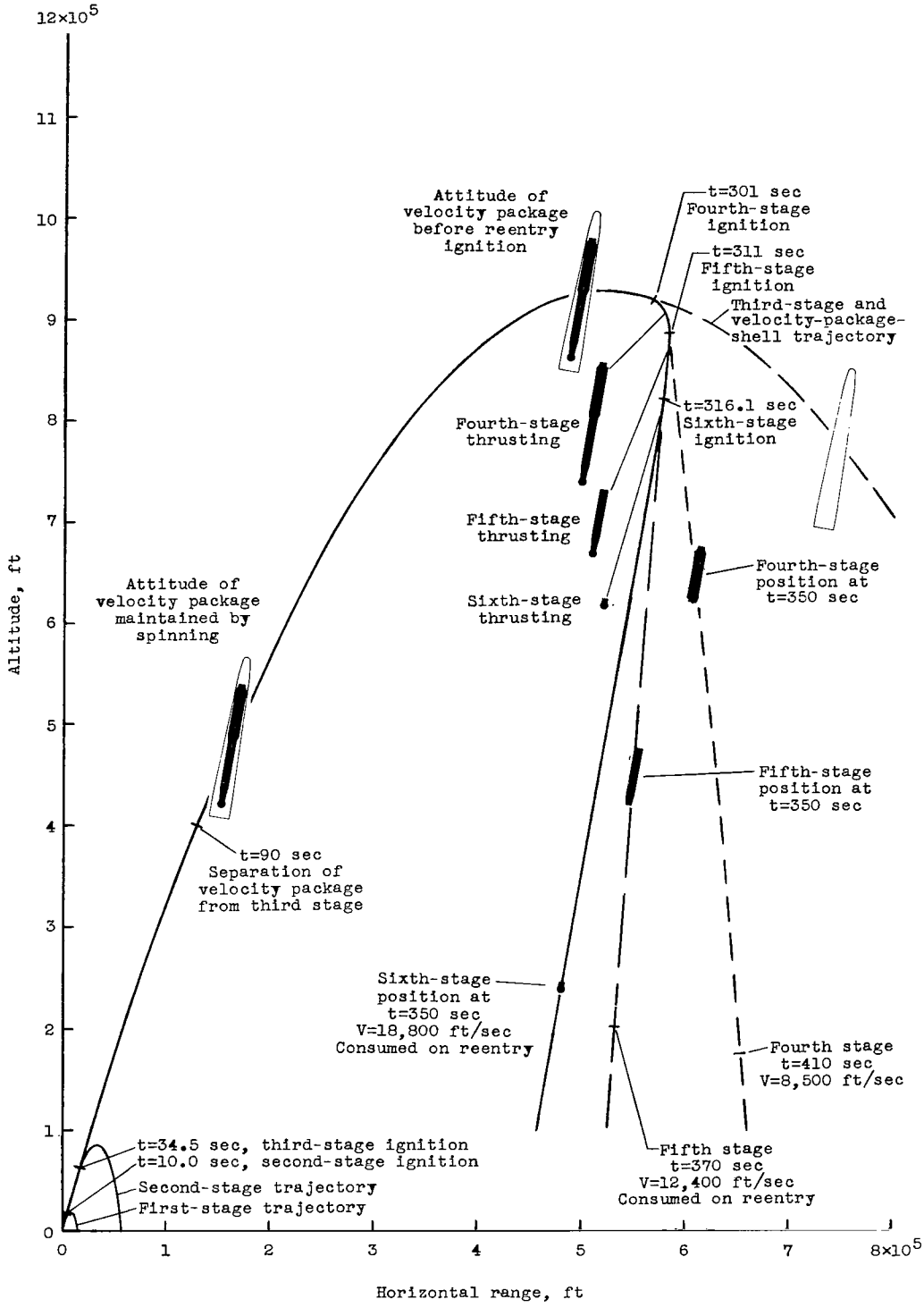


Figure 1.- Schematic representation of a typical Trailblazer I trajectory.

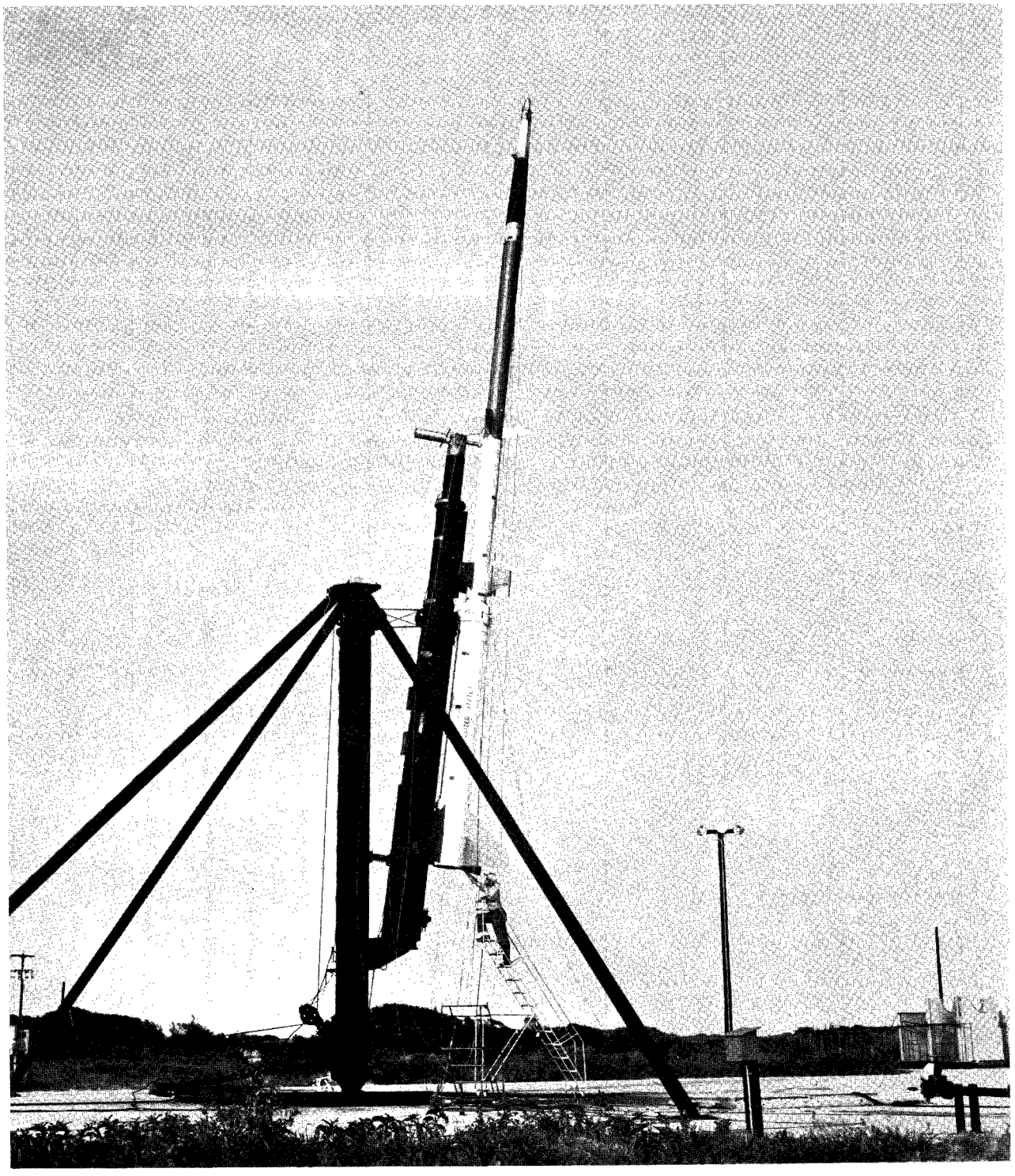

Figure 2.- Photograph of reentry vehicle on launcher. L-60-5153

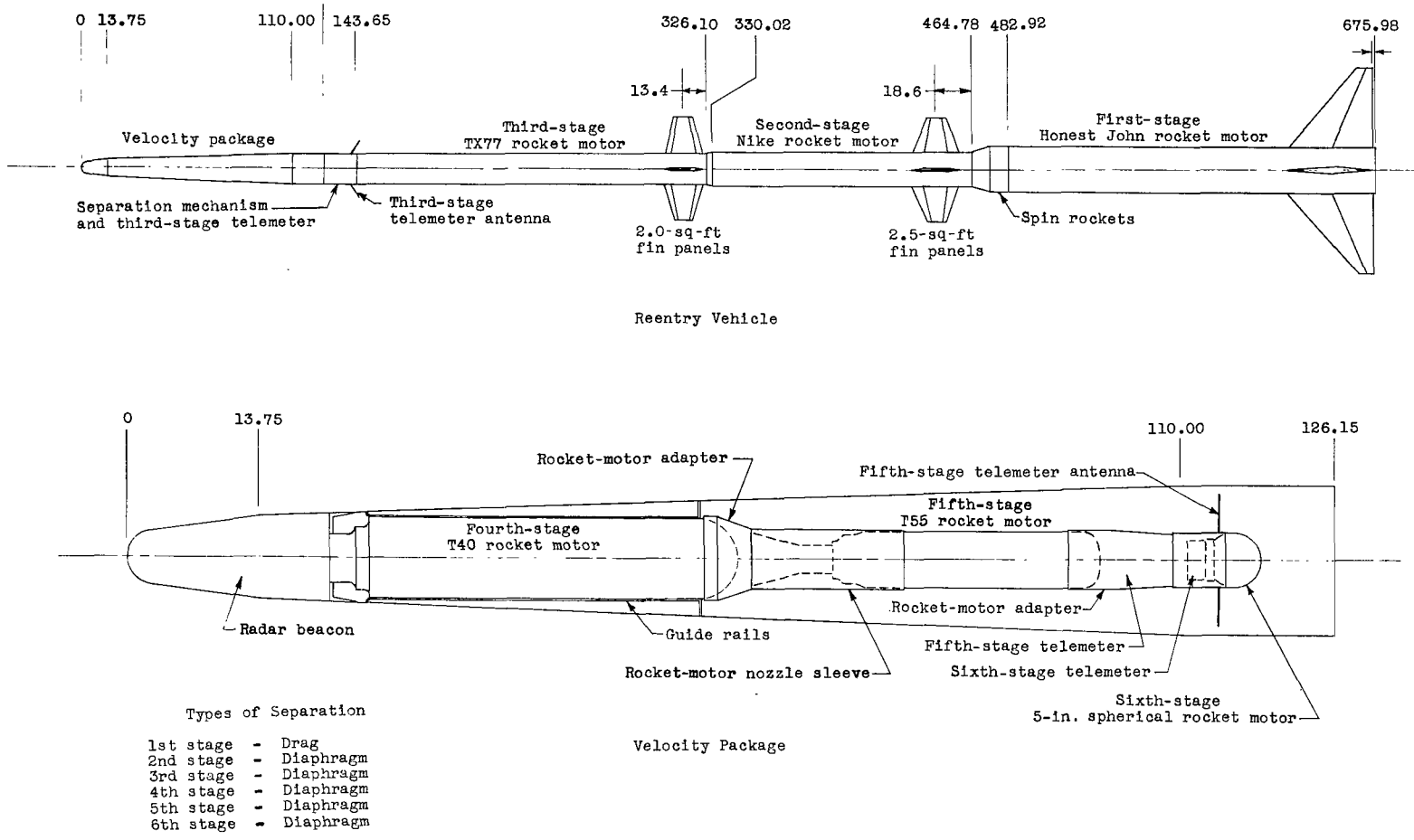


Types of Separation

1st stage - Drag
2nd stage - Diaphragm
3rd stage - Diaphragm
4th stage - Diaphragm
5th stage - Diaphragm
6th stage - Diaphragm

Figure 3.- Sketch of reentry vehicle and velocity package. All dimensions and station locations are in inches.

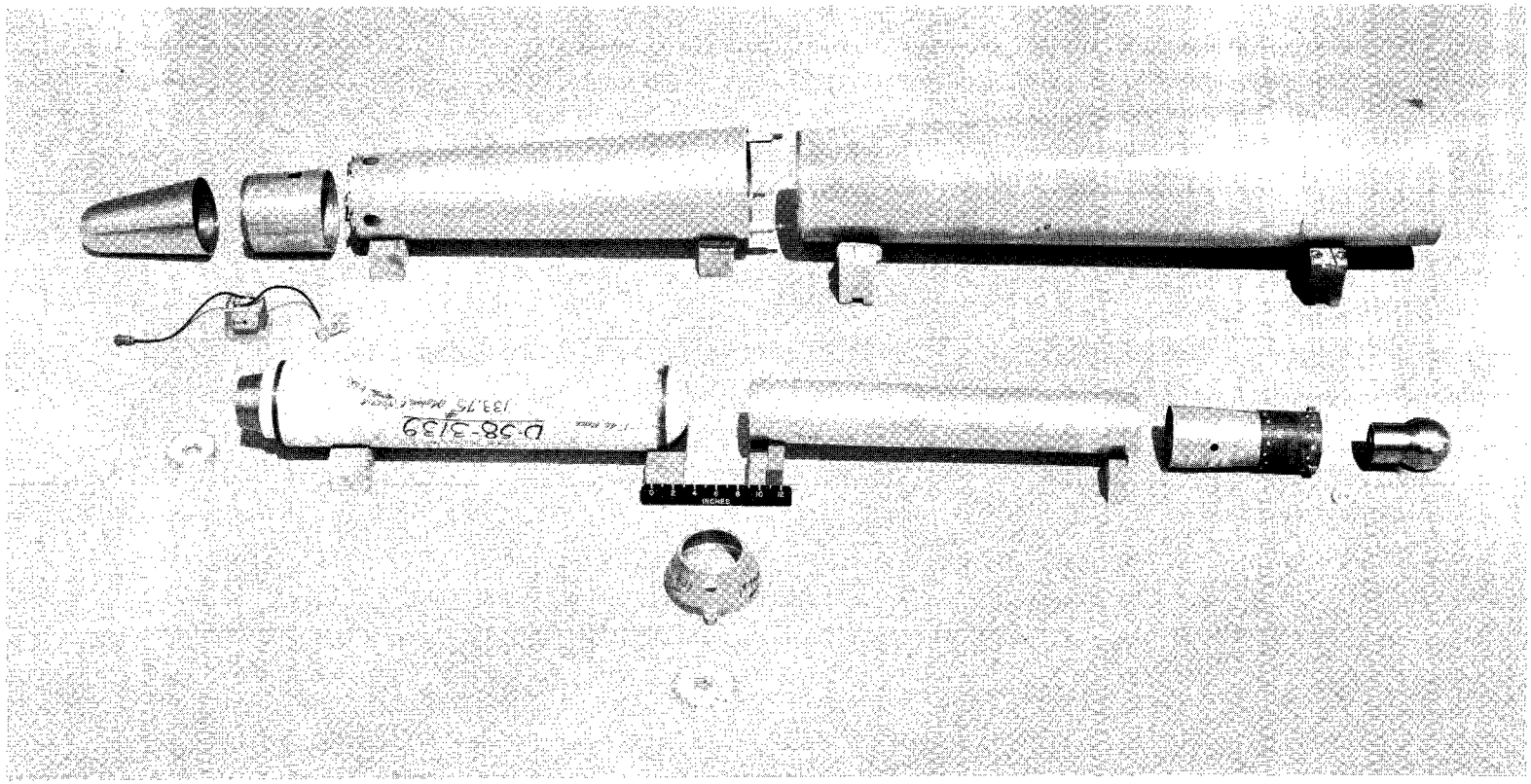

Figure 4.- Exploded view photograph of velocity package. L-61-5939

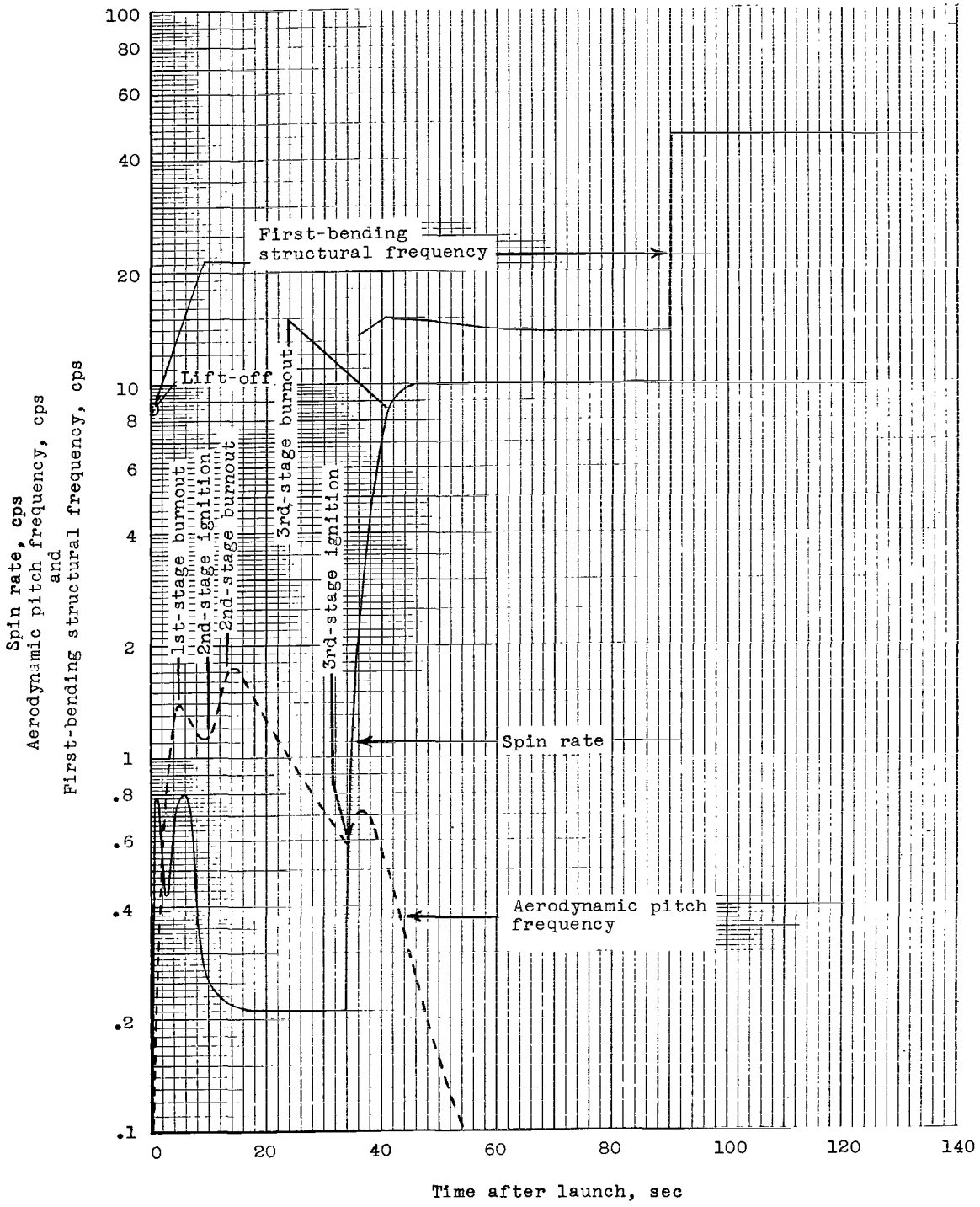


Figure 5.- Variation of theoretical spin rate, aerodynamic pitch frequency, and first-bending structural frequency with time.

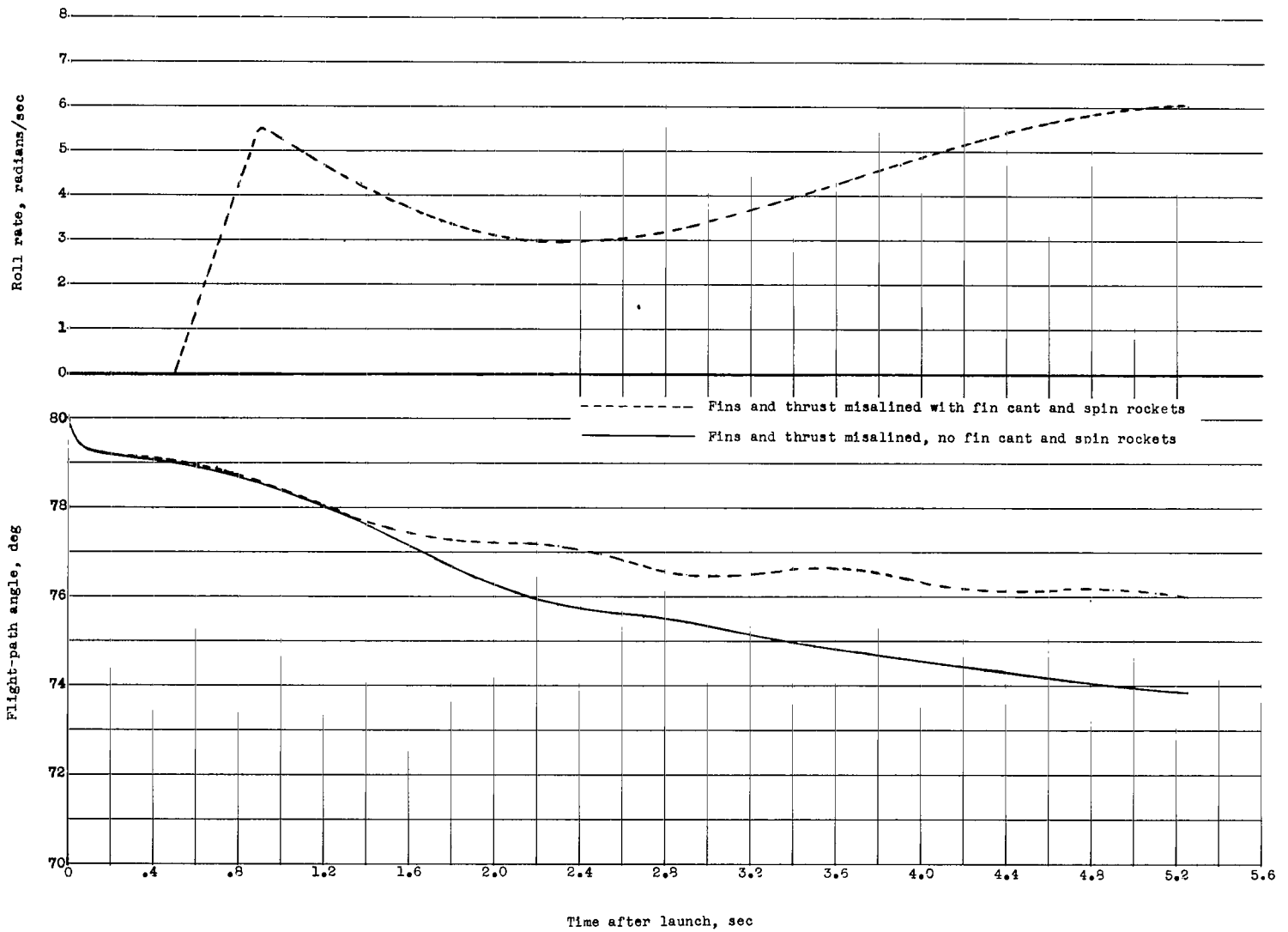


Figure 6.- Time history of roll rate and flight-path angle for first-stage booster with and without fin cant and spin rockets. Fin misalinement, $0.2^{\circ}$; thrust misalinement, $0.1^{\circ}$ nose down.

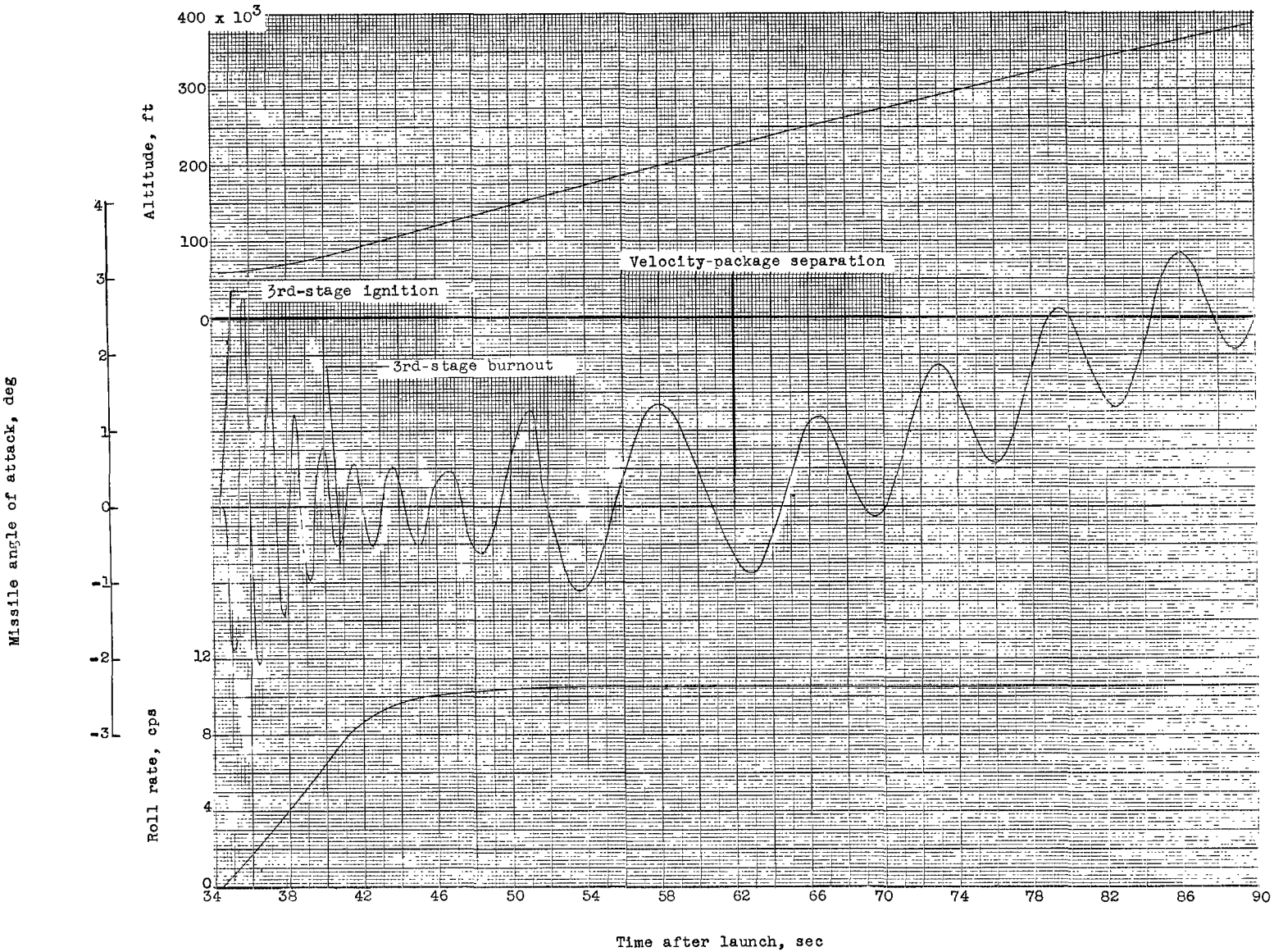


Figure 7.- Time history of angle of attack, as computed from a nonrolling body-axis system, during transition from aerodynamic stability to spin stability.

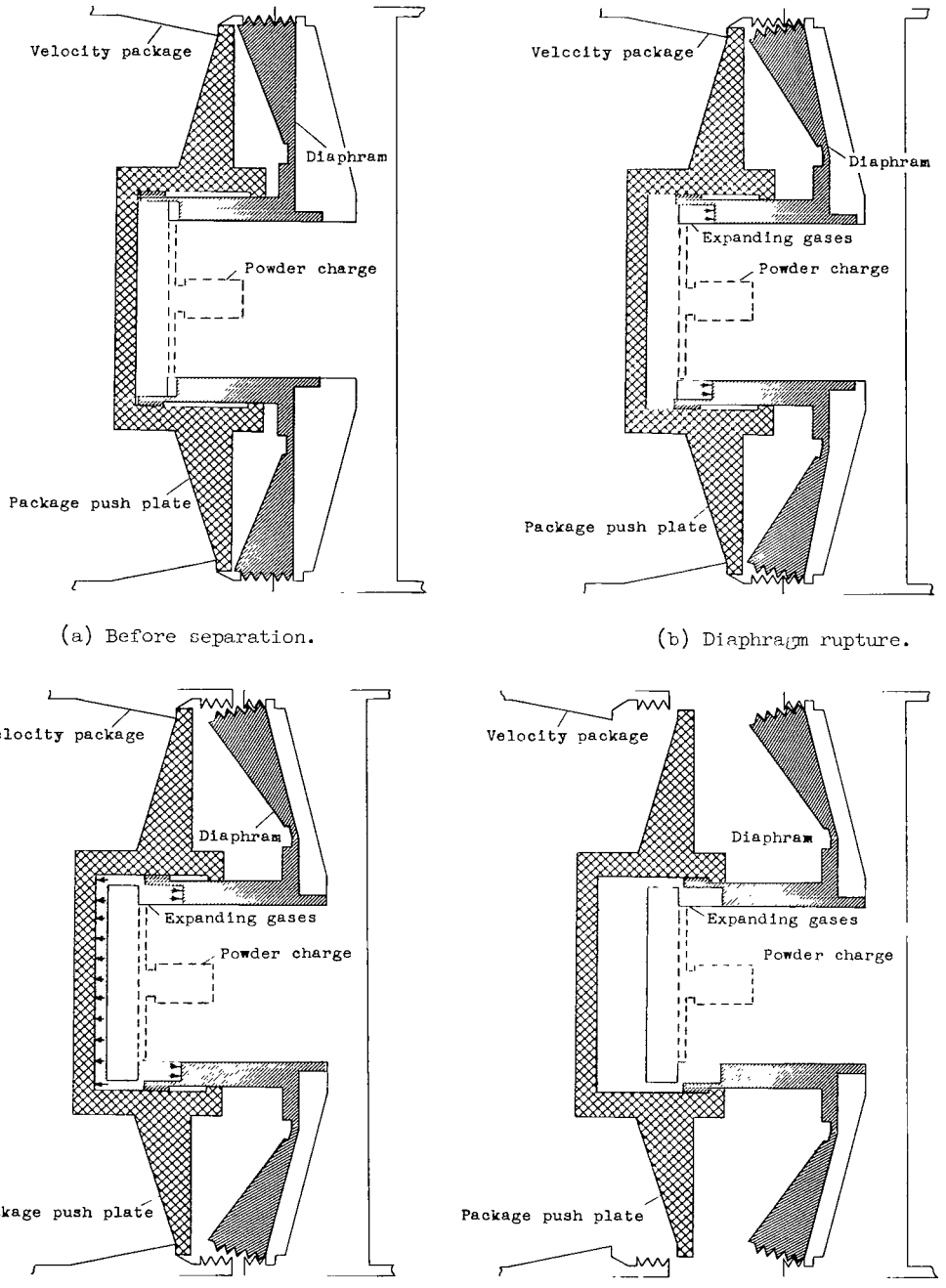


Figure 8.- Schematic drawing of operation of separation mechanism between third-stage rocket motor and velocity package.

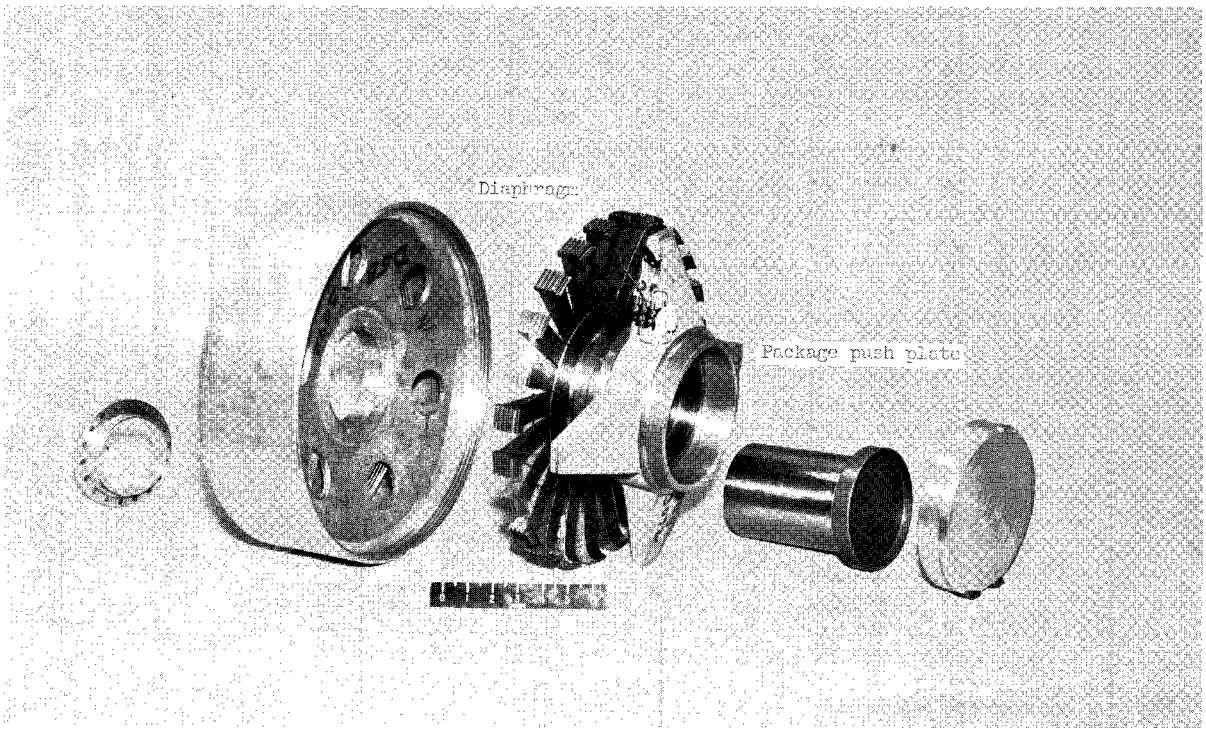


(a) Exploded view showing component parts of separation mechanism. L-60-1237.1

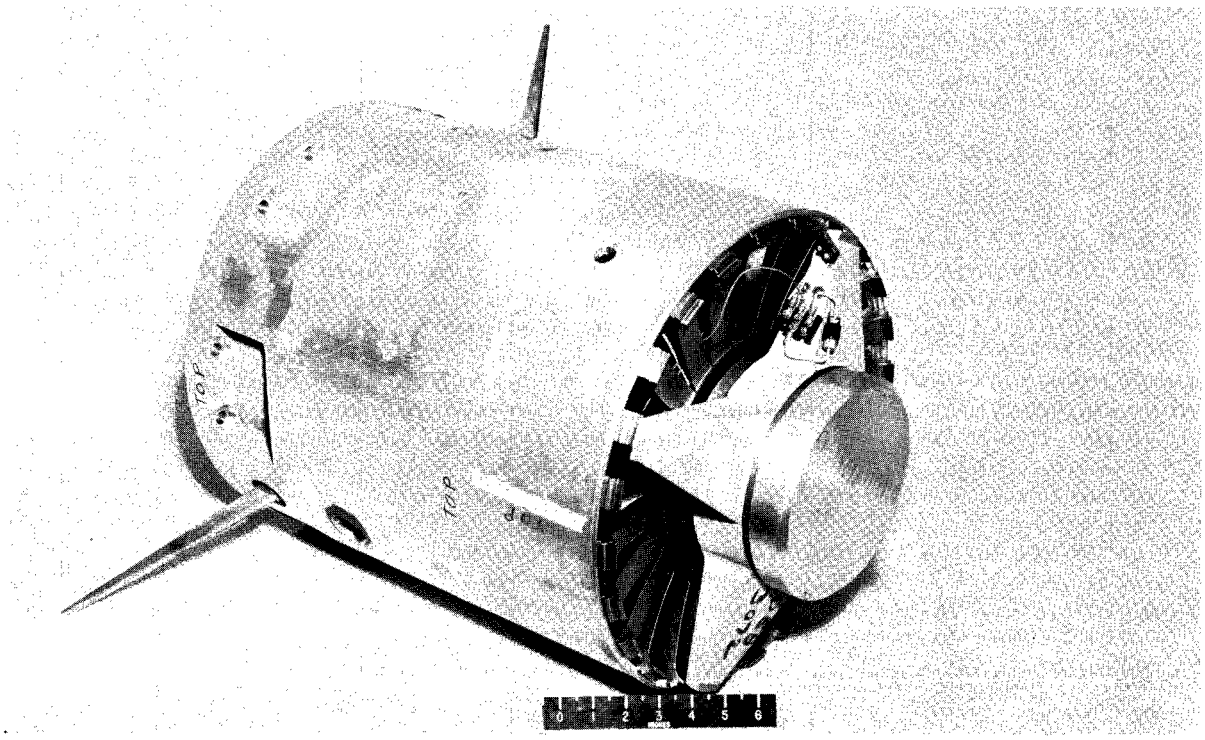

(b) Assembled view of separation mechanism along with third-stage telemeter section. L-60-1238.1

Figure 9.- Photographs of separation mechanism.

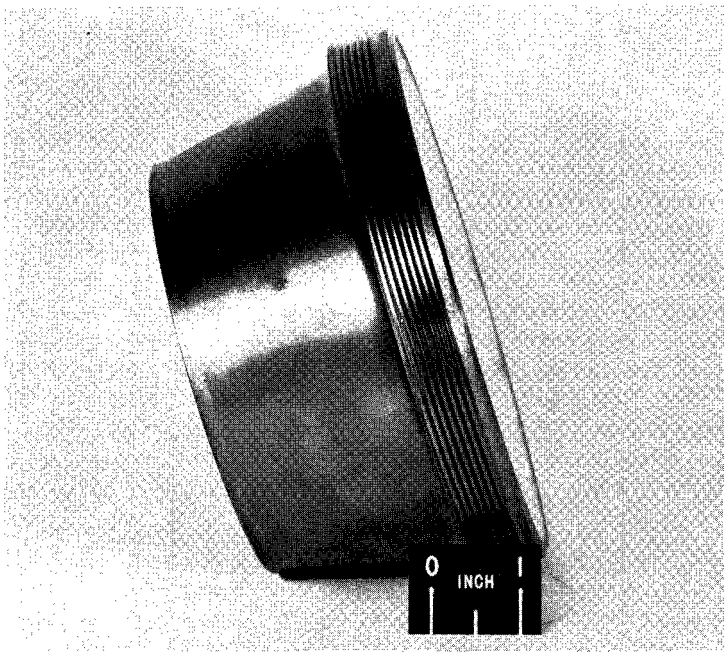


L-62-4891

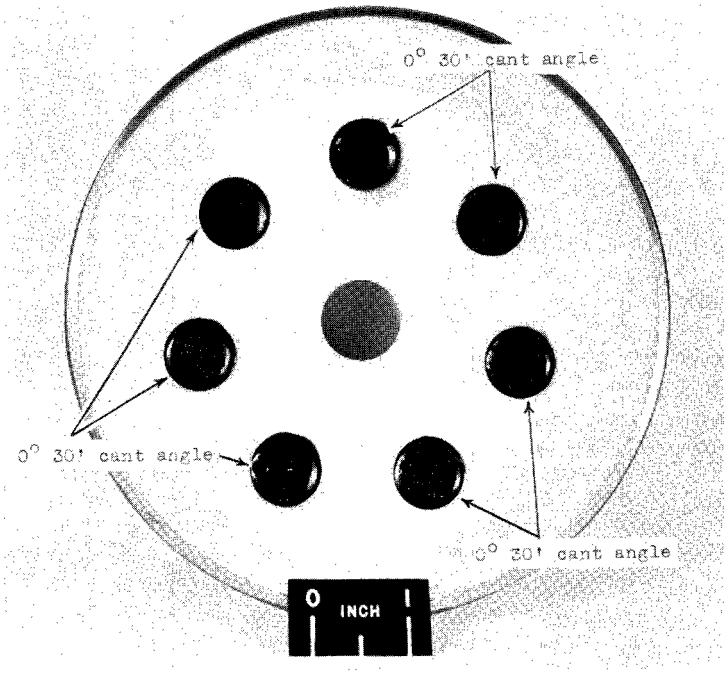


(a) Photographs showing fourth-stage torque nozzle.

Figure 10.- Photographs and sketch of fourth-stage torque nozzle. L-62-4889.1

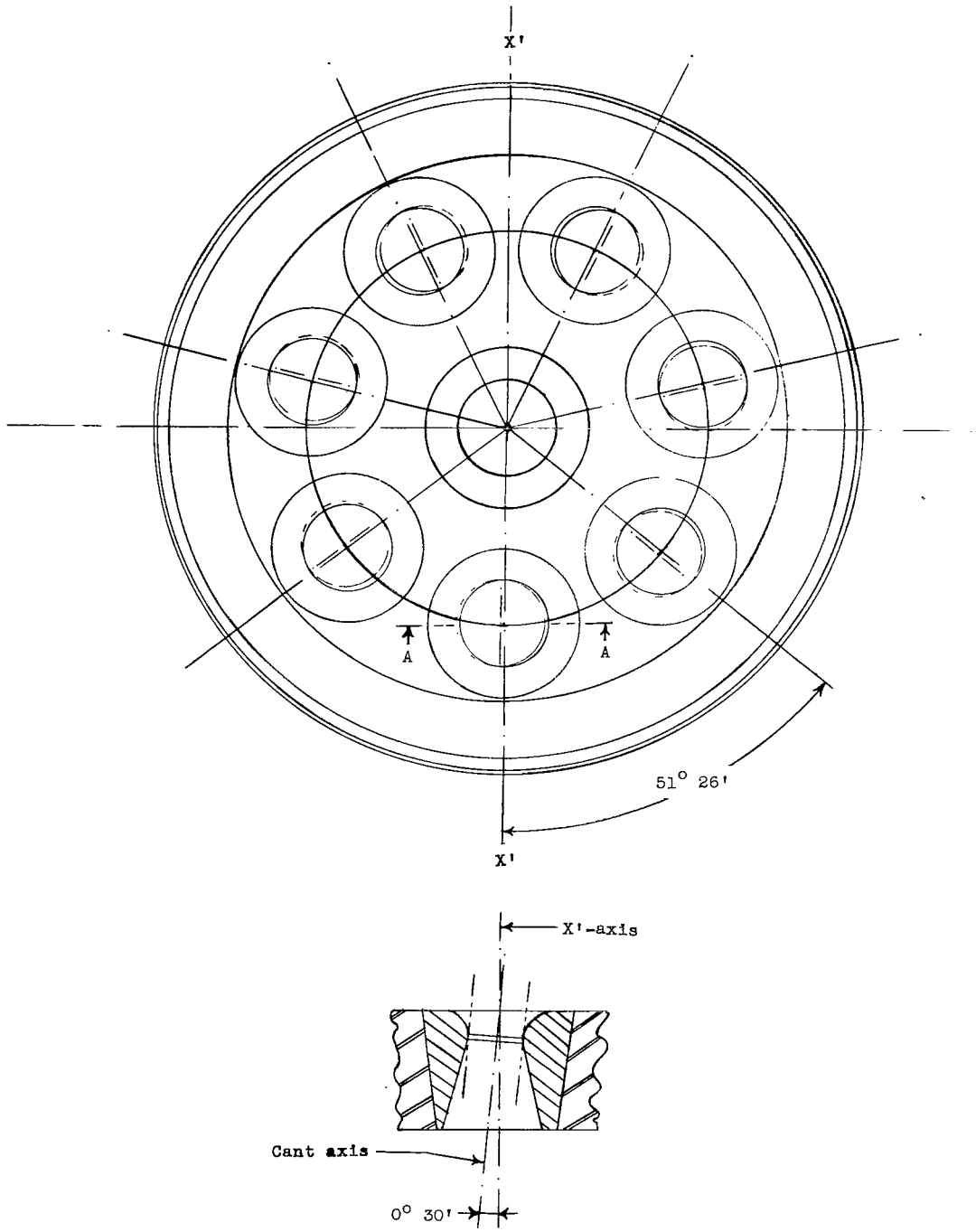


(b) Sketch of fourth-stage torque nozzle.

Figure 10.- Concluded.

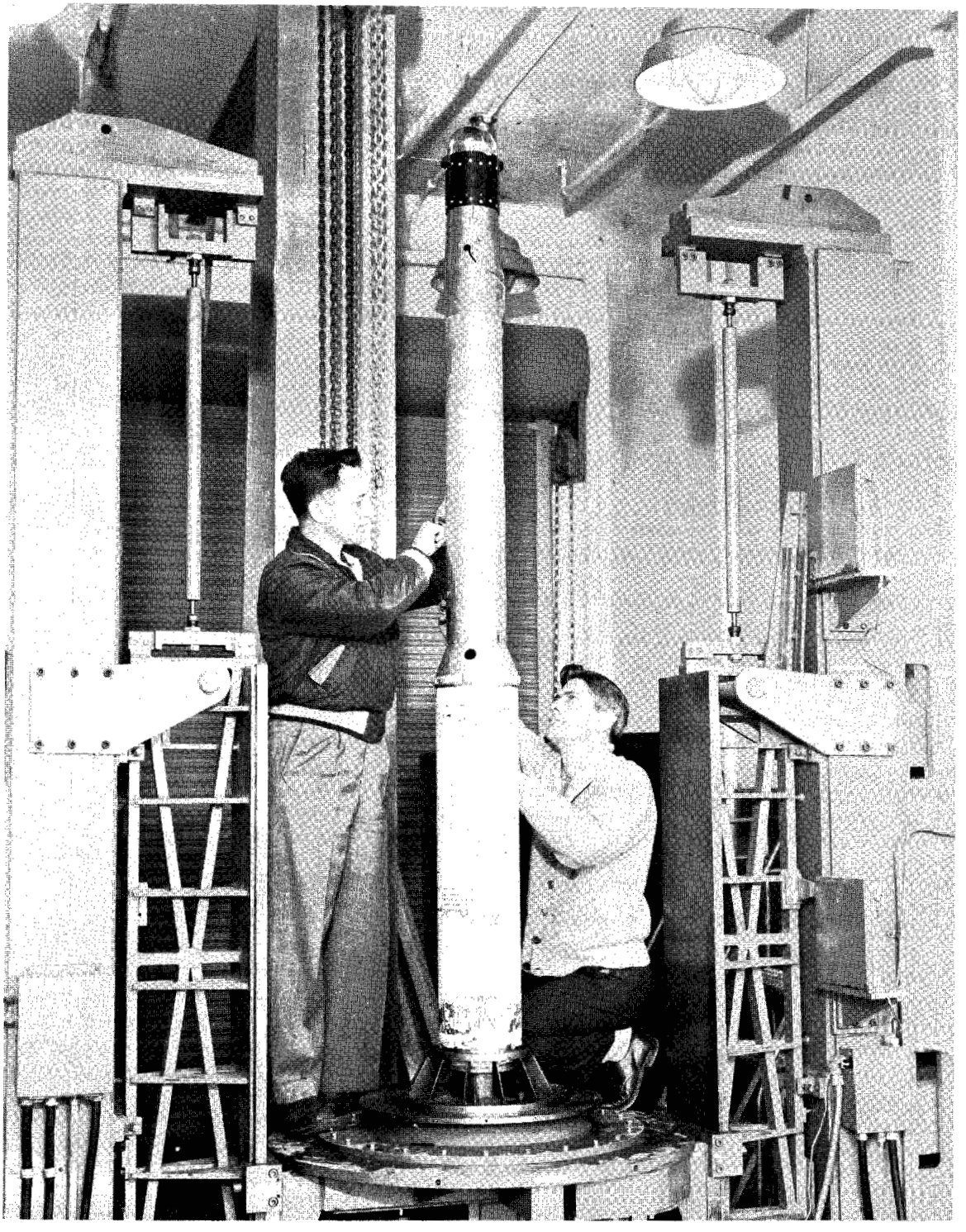

Figure 11.- Photograph of first, second, and third stages mounted on spin table in order to balance this combination in roll. L-61-927

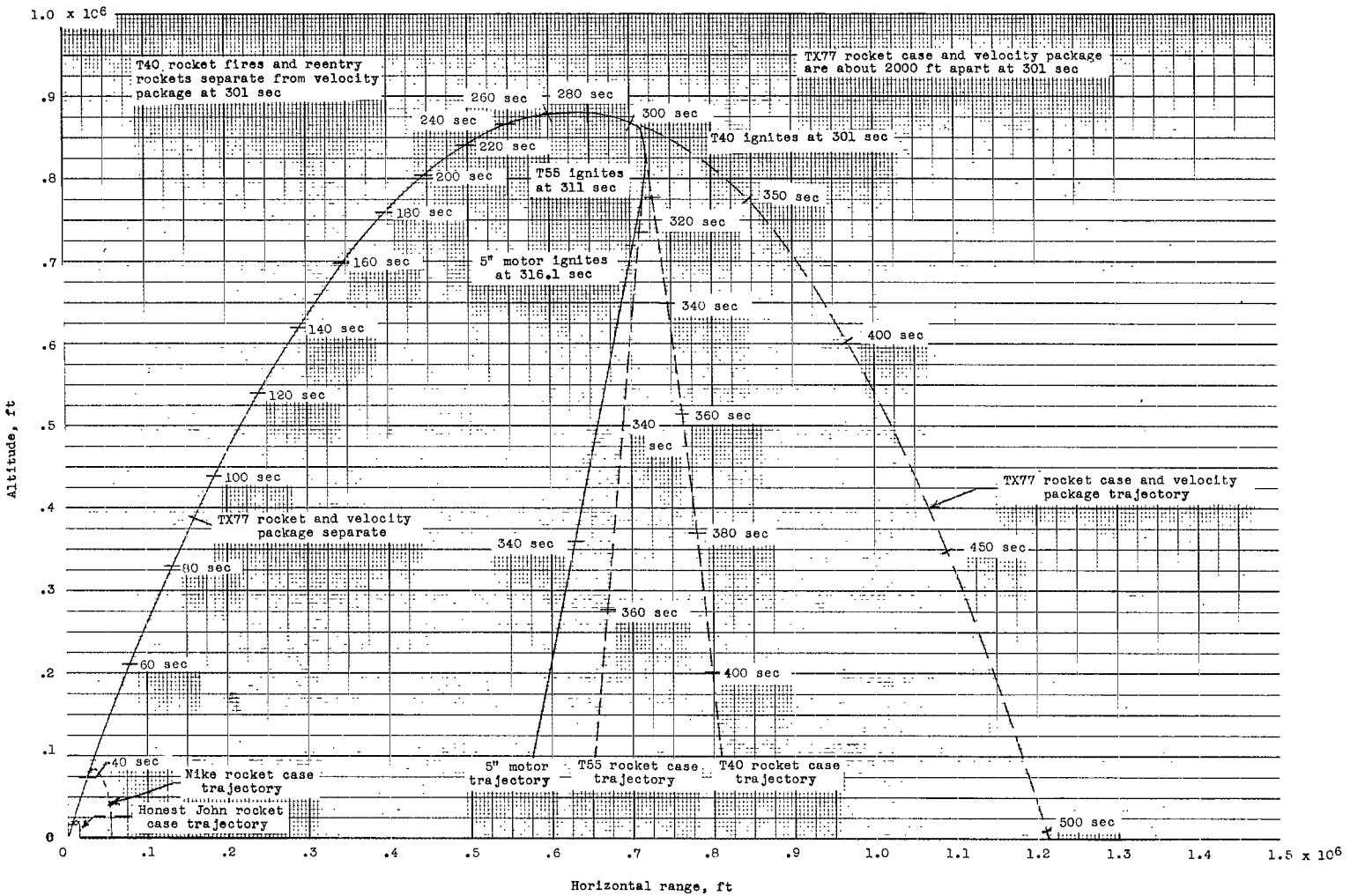


Figure 12.- Nominal computed trajectory of each vehicle stage for 80° launch angle.

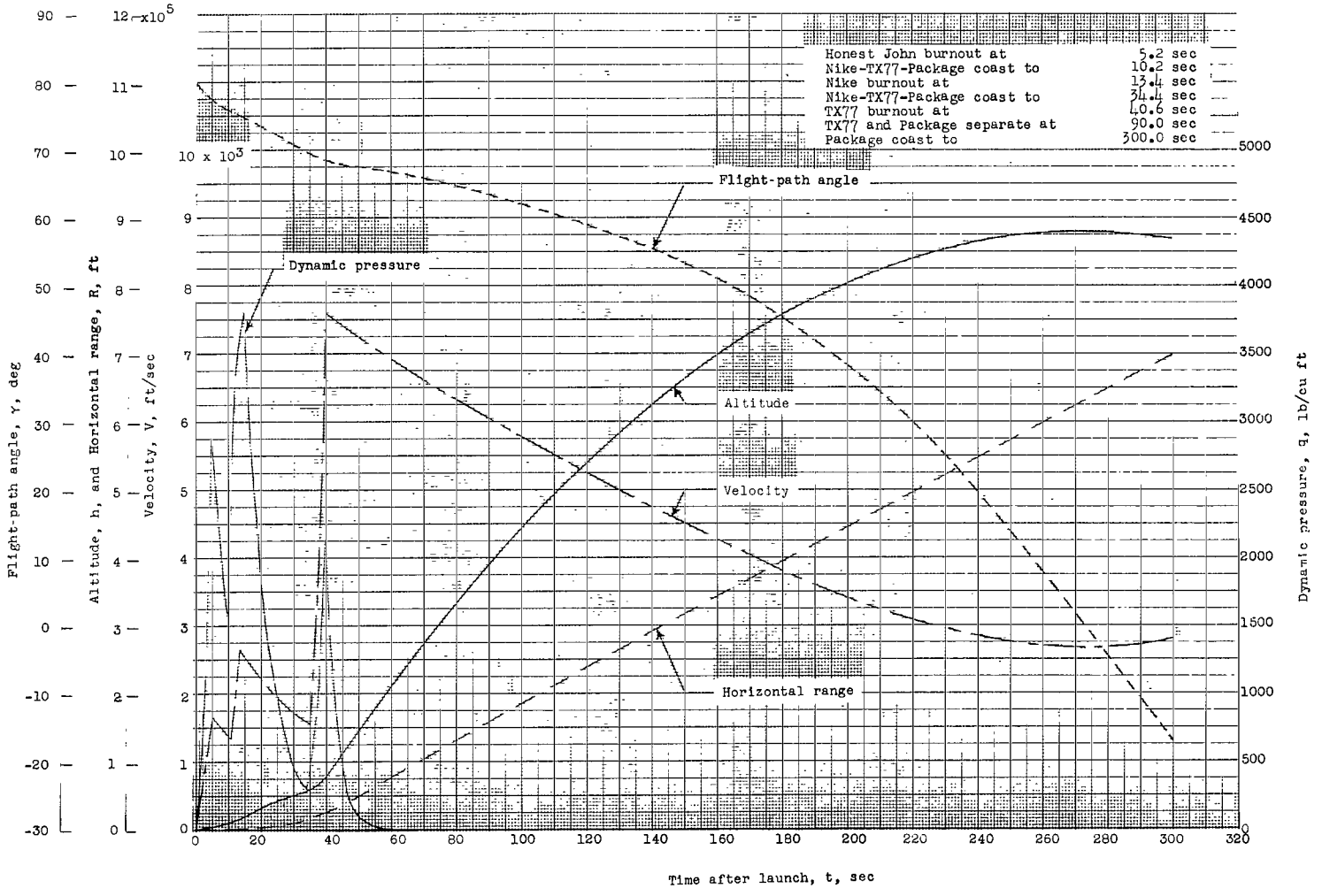


Figure 13.- Time history of flight-path angle, velocity, altitude, and horizontal range for flight time of 300 seconds. 80°, launch angle.

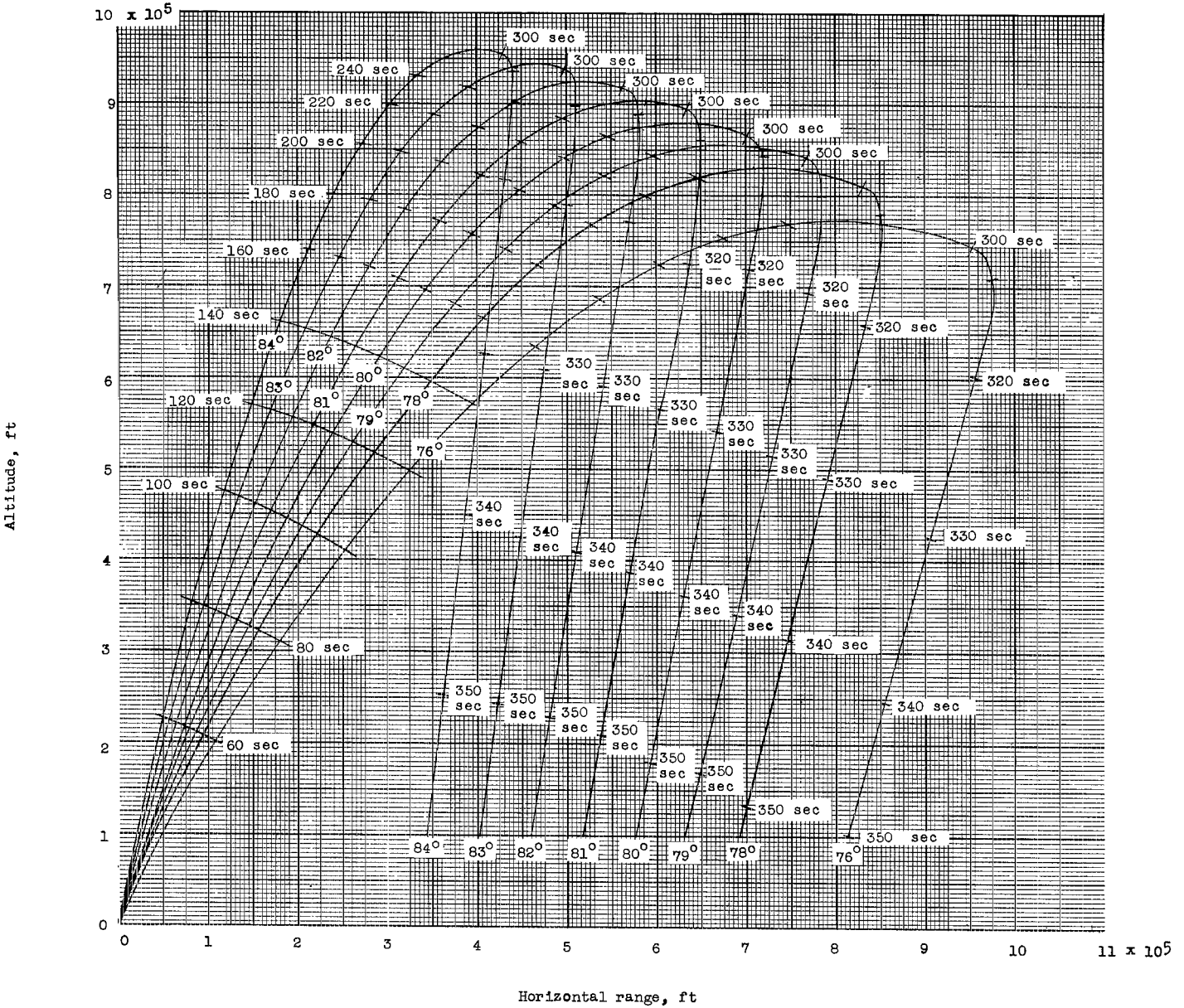


Figure 14.- Family of vehicle ascending trajectories and sixth-stage reentry trajectories for various launch angles.

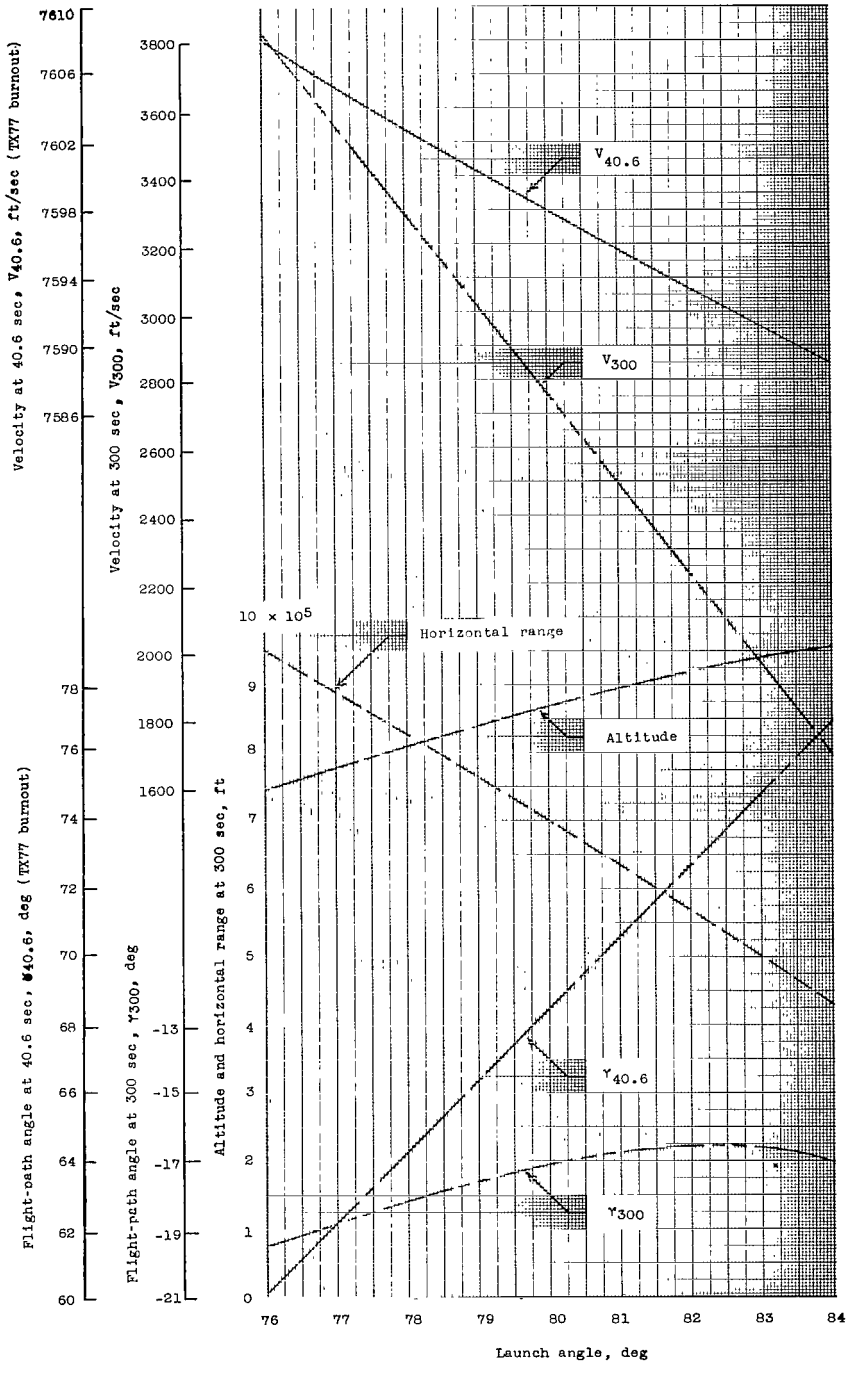


Figure 15.- Variation of velocity and flight-path angle at 40.6 and 300.0 seconds after launch and of altitude and horizontal range at 300.0 seconds after launch with launch angle for nominal trajectories.

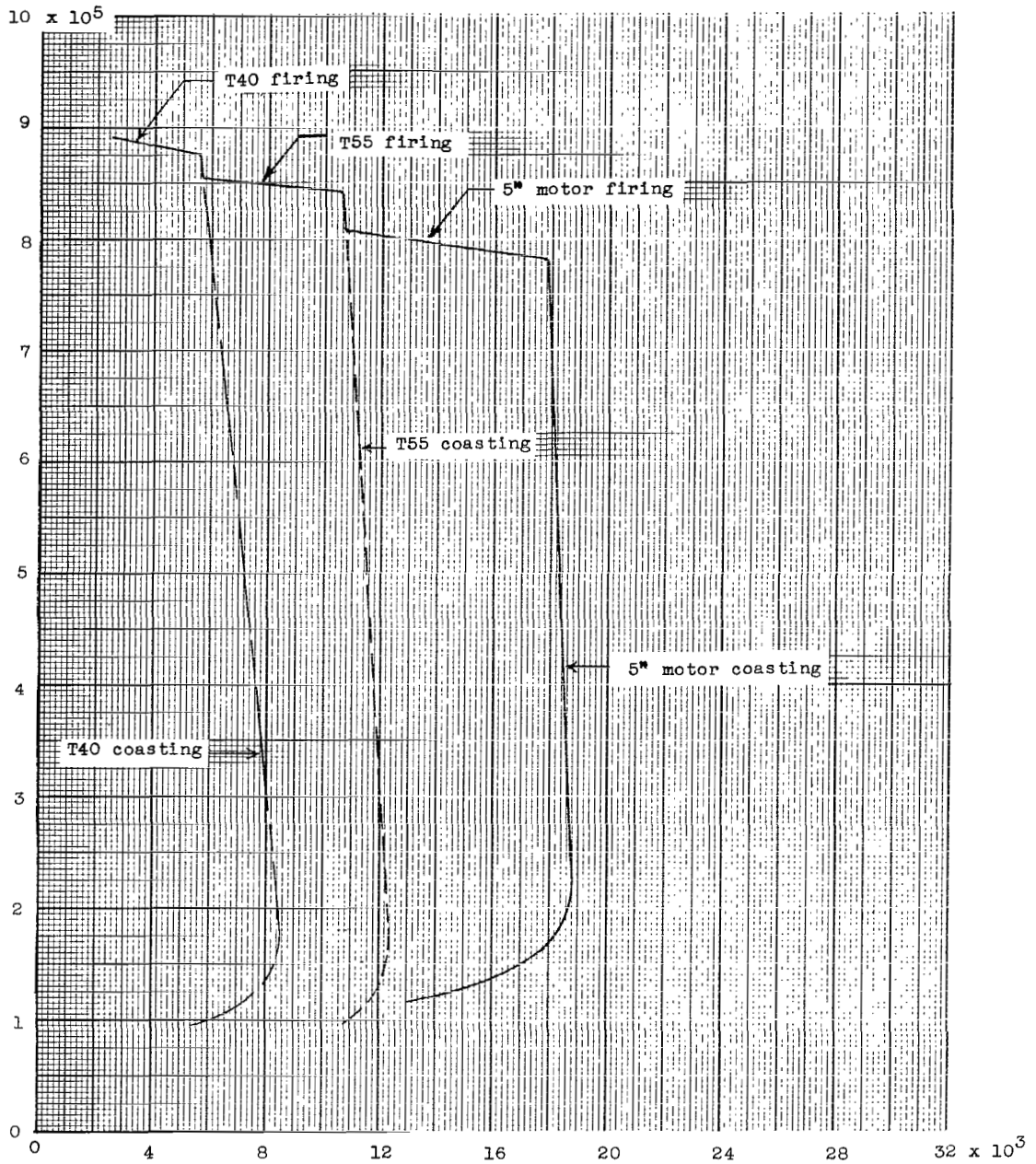


Figure 16.- Typical velocity-altitude relationship for three final stages. Launch angle, 80°; sixth-stage reentry weight, approximately 2 pounds.

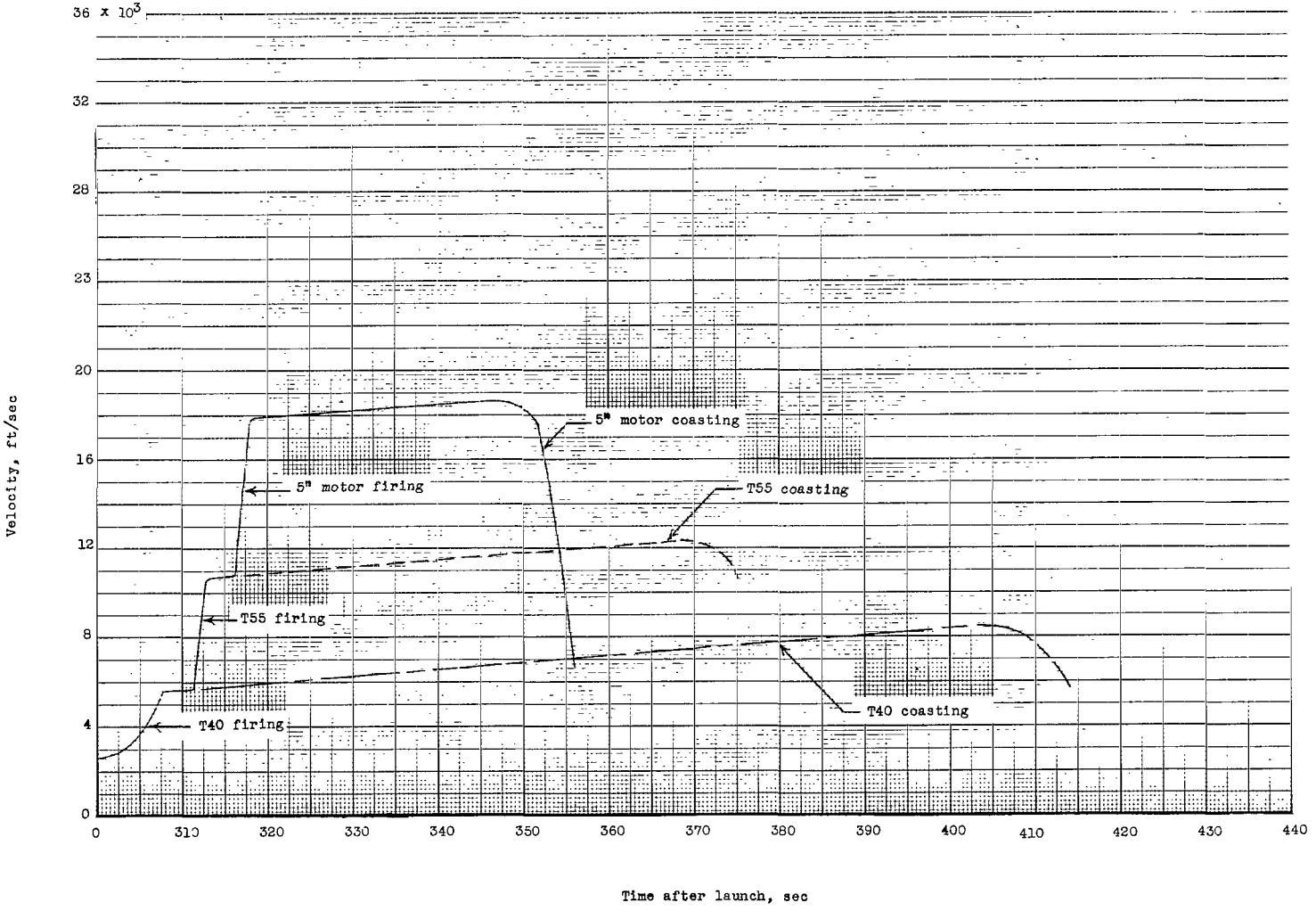


Figure 17.- Velocity time history for three final stages. Launch angle, 80°; sixth-stage reentry weight, approximately 2 pounds.

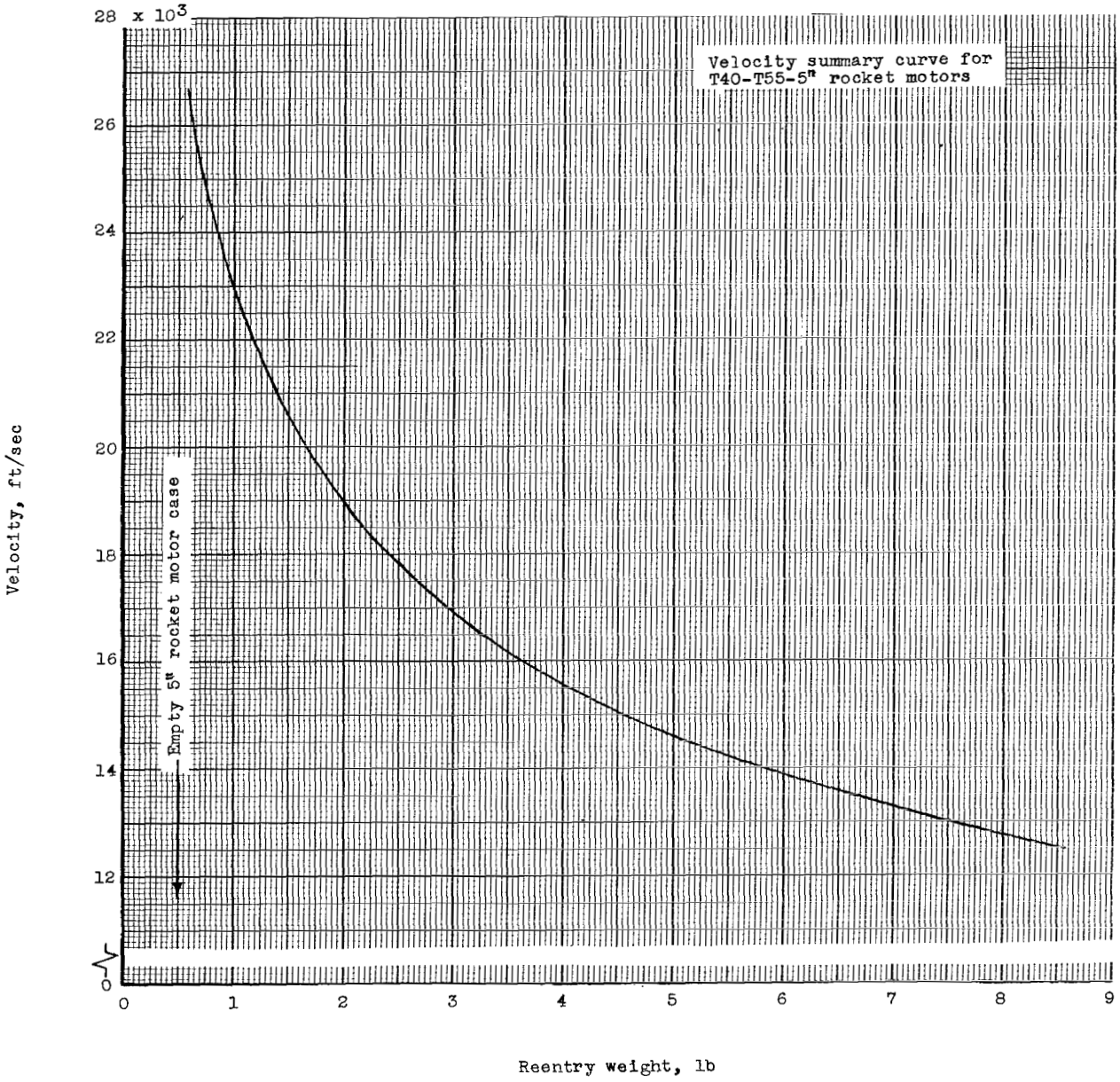


Figure 18.- Variation of reentry velocity with reentry weight assuming no gravity or drag effects.

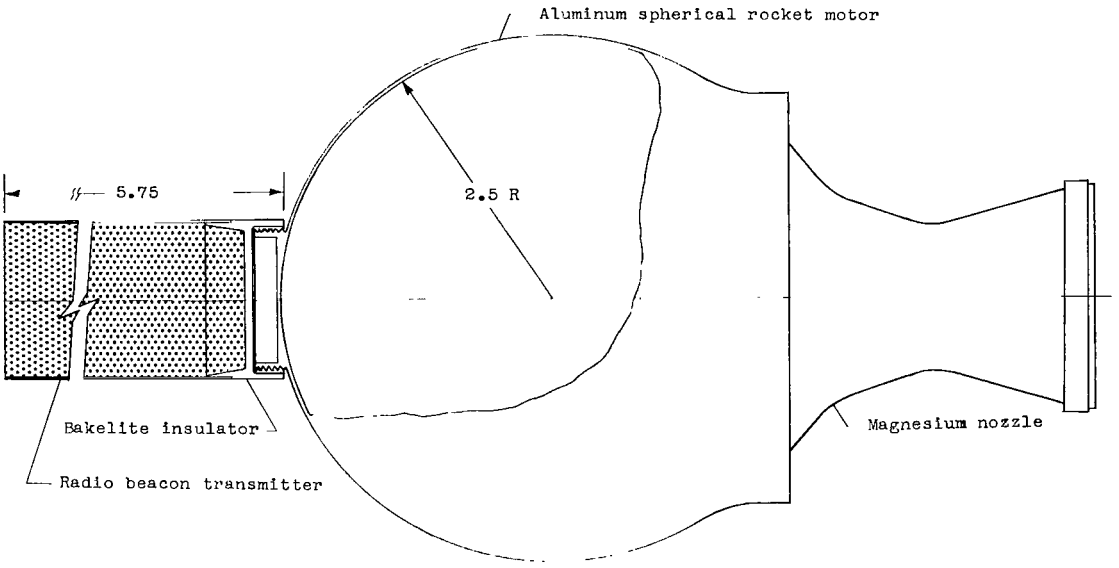


(a) Trailblazer Iα and Iβ, thin aluminum case, spike radio beacon transmitter.

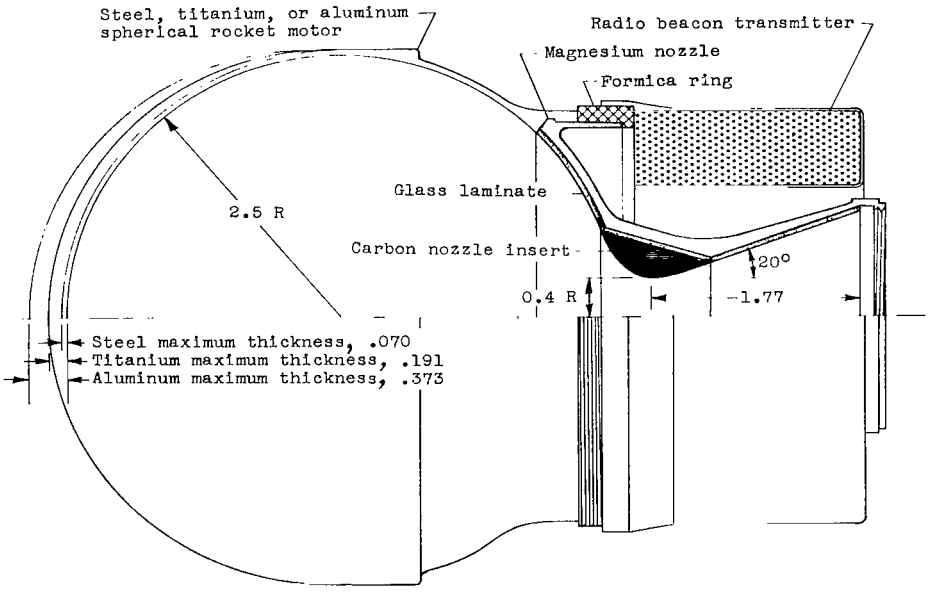


(b) Trailblazer Ia and Ie, steel case; Trailblazer Iγ and Ic, titanium case; Trailblazer Ib, thick aluminum case; all with torus radio beacon transmitter.

Figure 19.- Sketch of 5-inch spherical sixth-stage rocket motor used in flight tests of Trailblazer I. All dimensions are in inches.

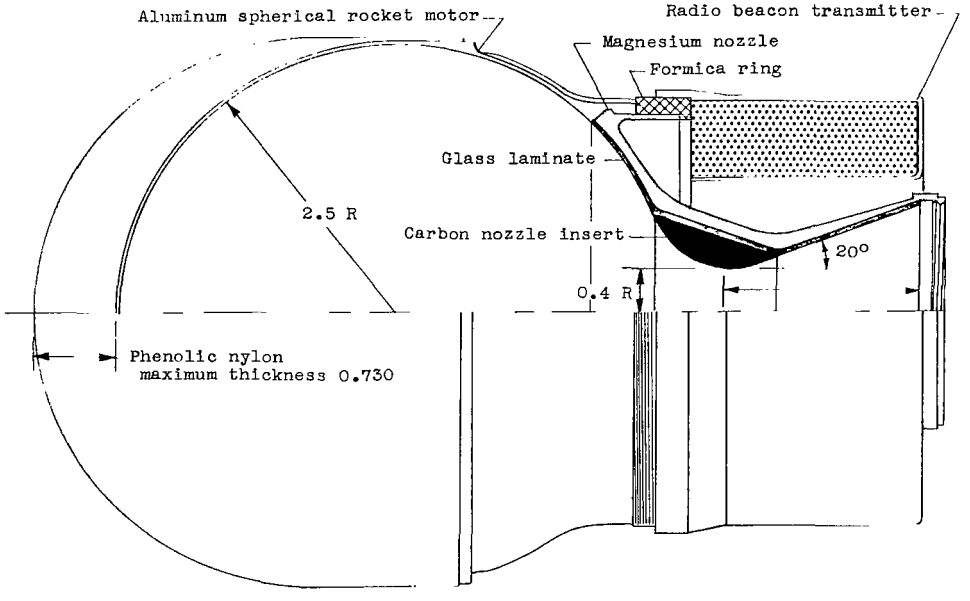


(c) Trailblazer Id, thin aluminum case with phenolic-nylon ablation-material cover, torus radio beacon transmitter.

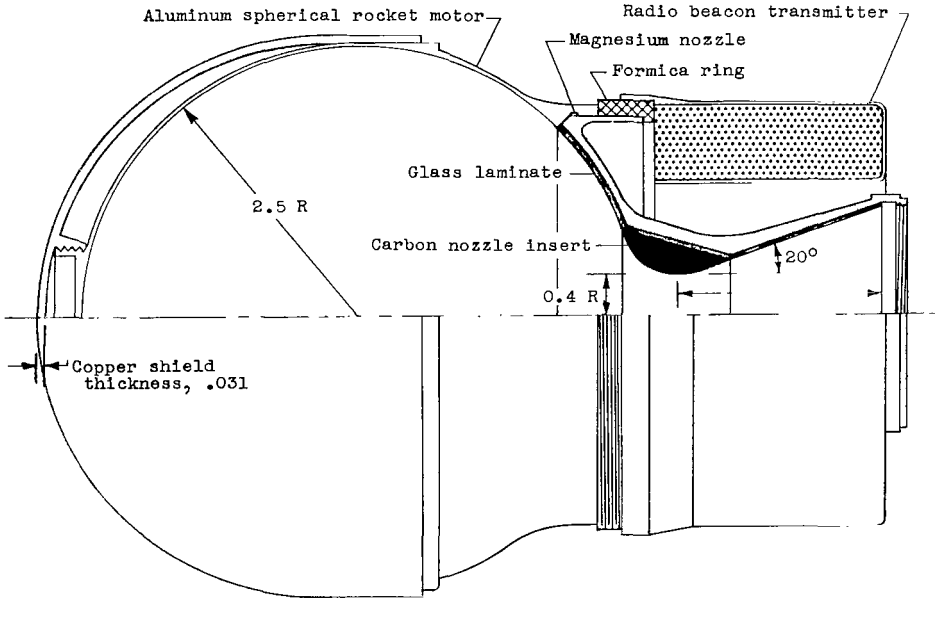


(d) Trailblazer If, thin aluminum case with a copper heat-shield cover, torus radio beacon transmitter.

Figure 19.- Concluded.

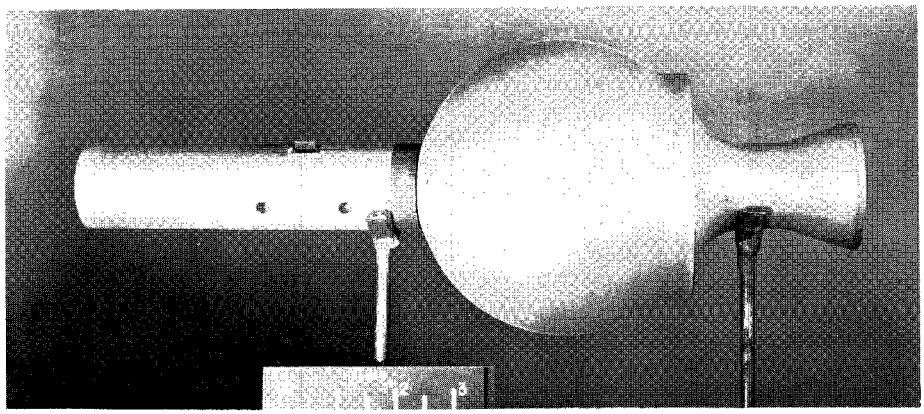

(a) Spherical rocket motor with spike radio beacon transmitter. L-59-309

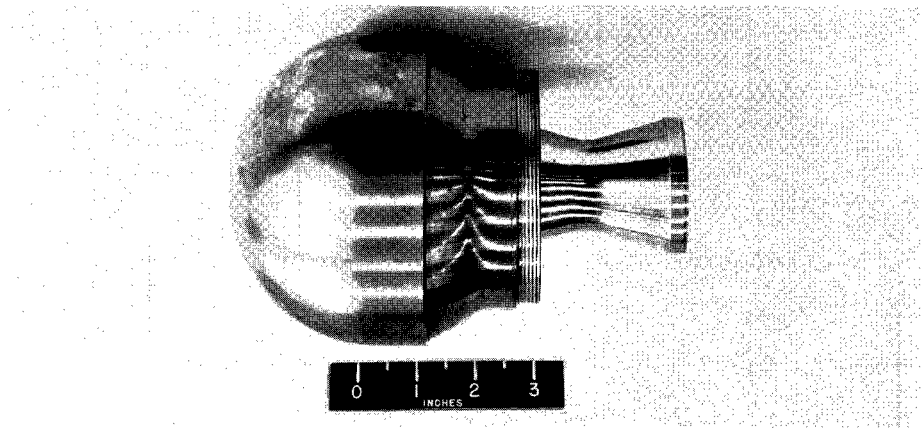


(b) Spherical rocket motor without radio beacon transmitter. L-59-8367

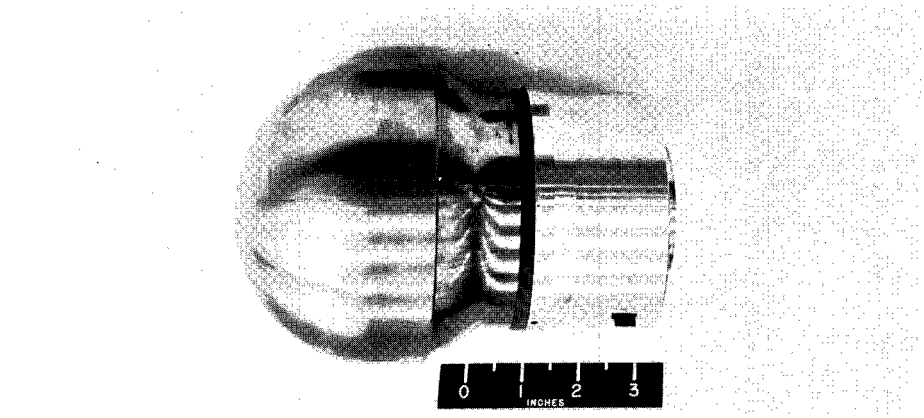


(c) Spherical rocket motor with torus radio beacon transmitter. L-59-8368

Figure 20.- Photographs of 5-inch-diameter spherical rocket motors.

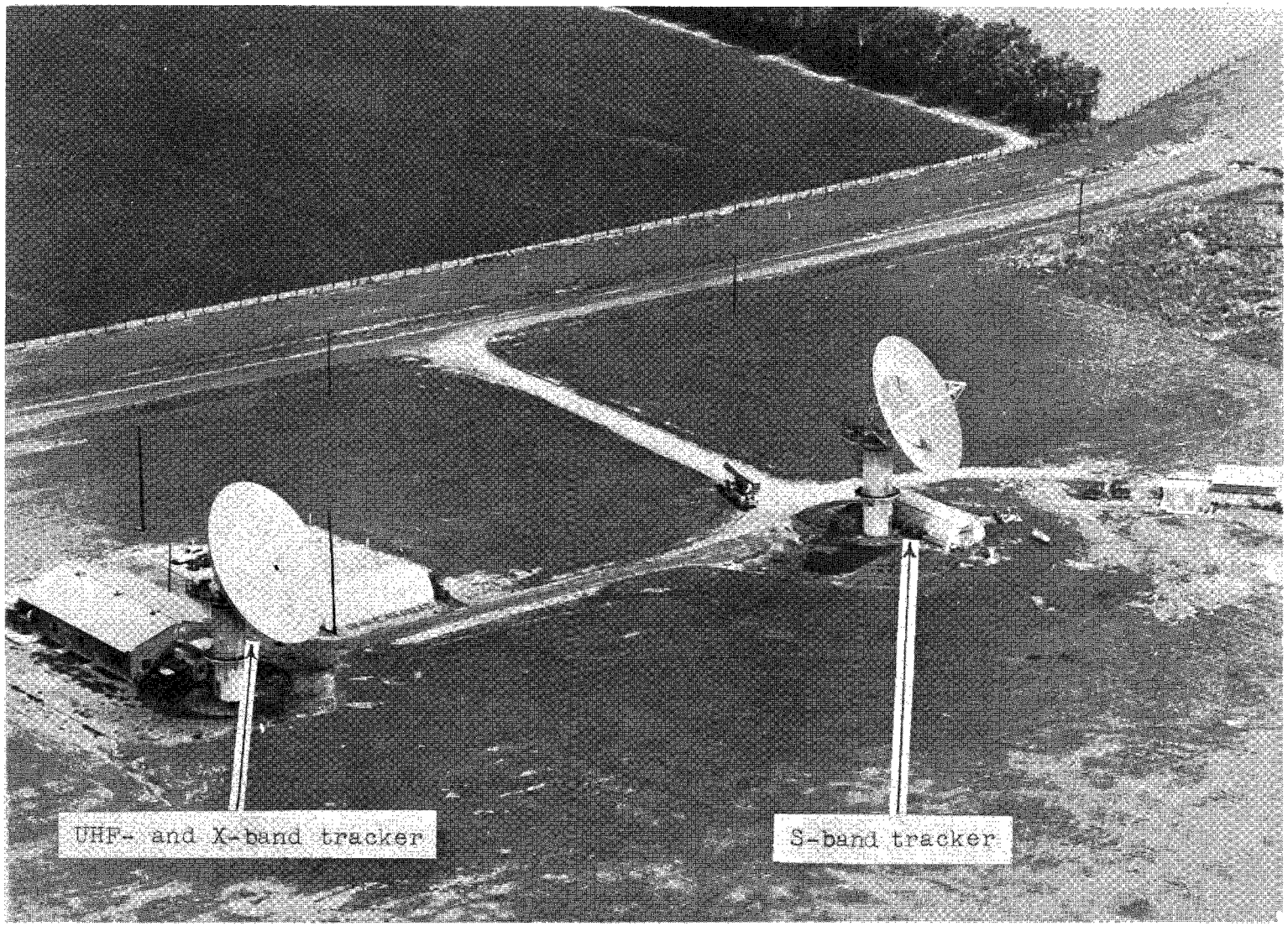


Figure 21.- Photograph of MIT-Lincoln Laboratory radars. L-61-7210.1

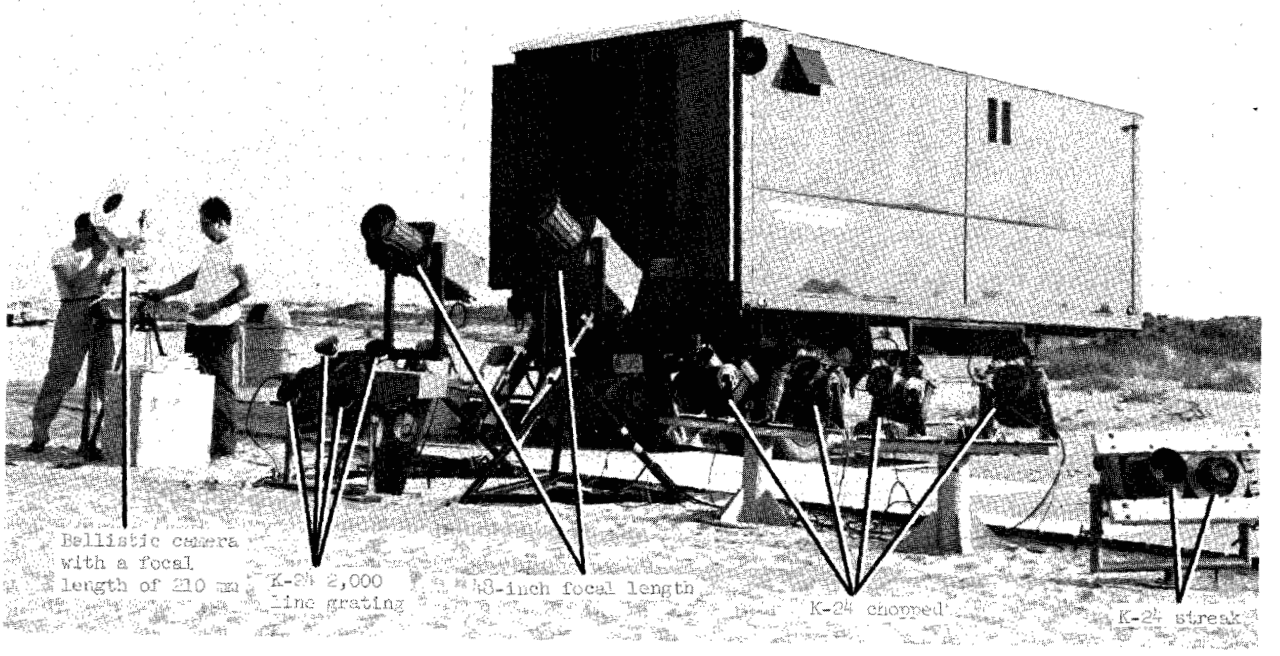


L-60-4475.1

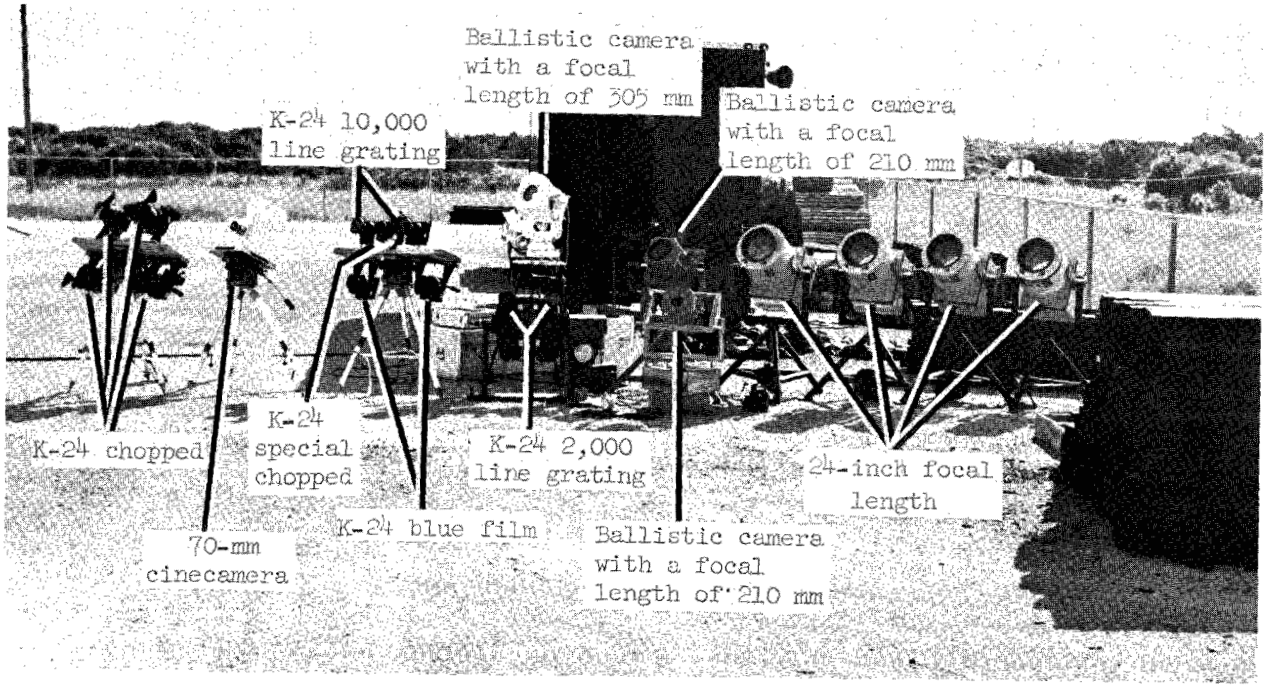


Figure 22.- Photographs showing typical reentry monitoring optical instrumentation. L-61-5217.1

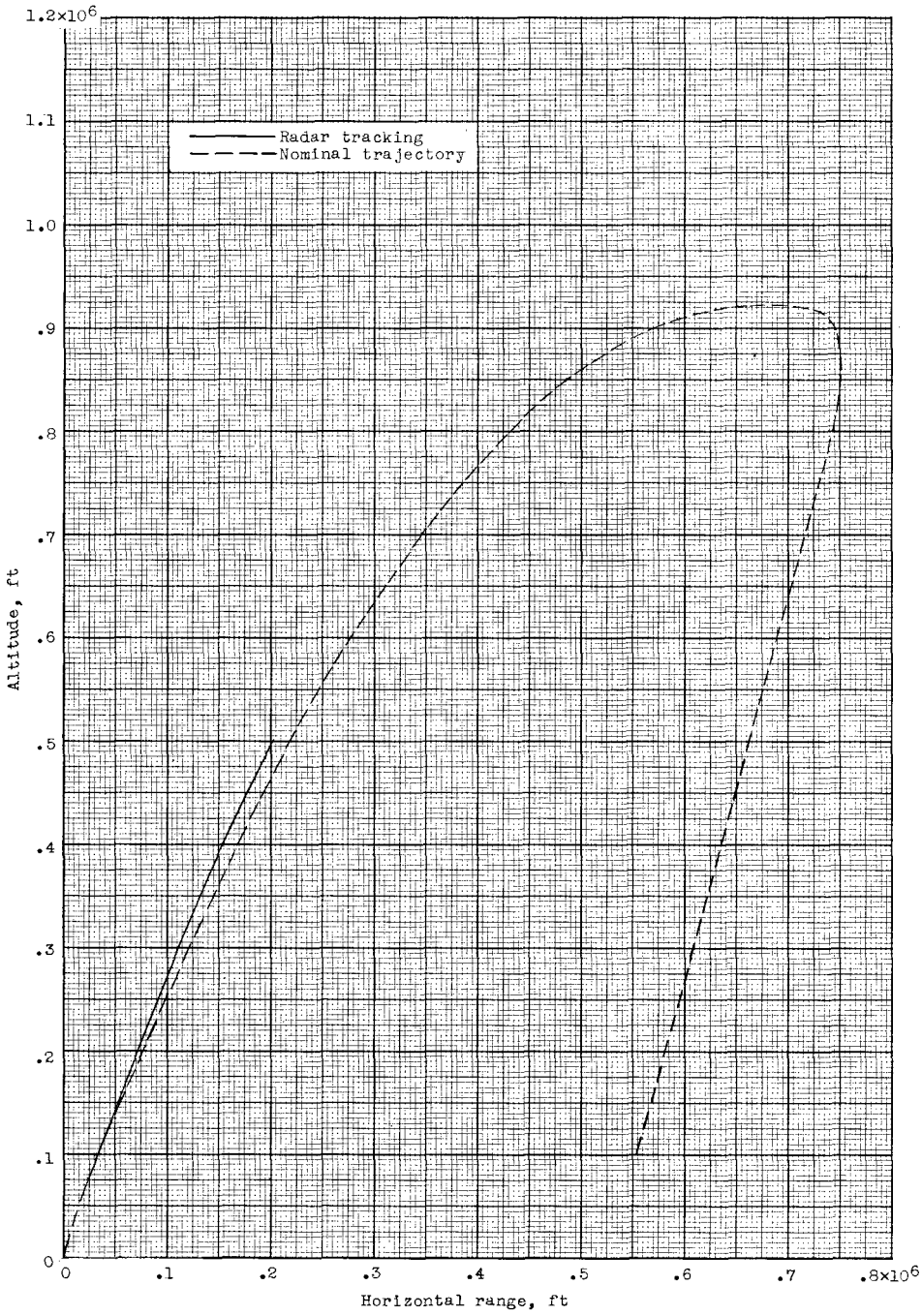


(a) Trailblazer Iα. Launch angle, 80°.

Figure 23.- Trailblazer I flight trajectories, as obtained from the FPS-16, AFMTC Mod II, and/or S-band tracking radars and Doppler tracking, compared with preflight theoretical calculations.

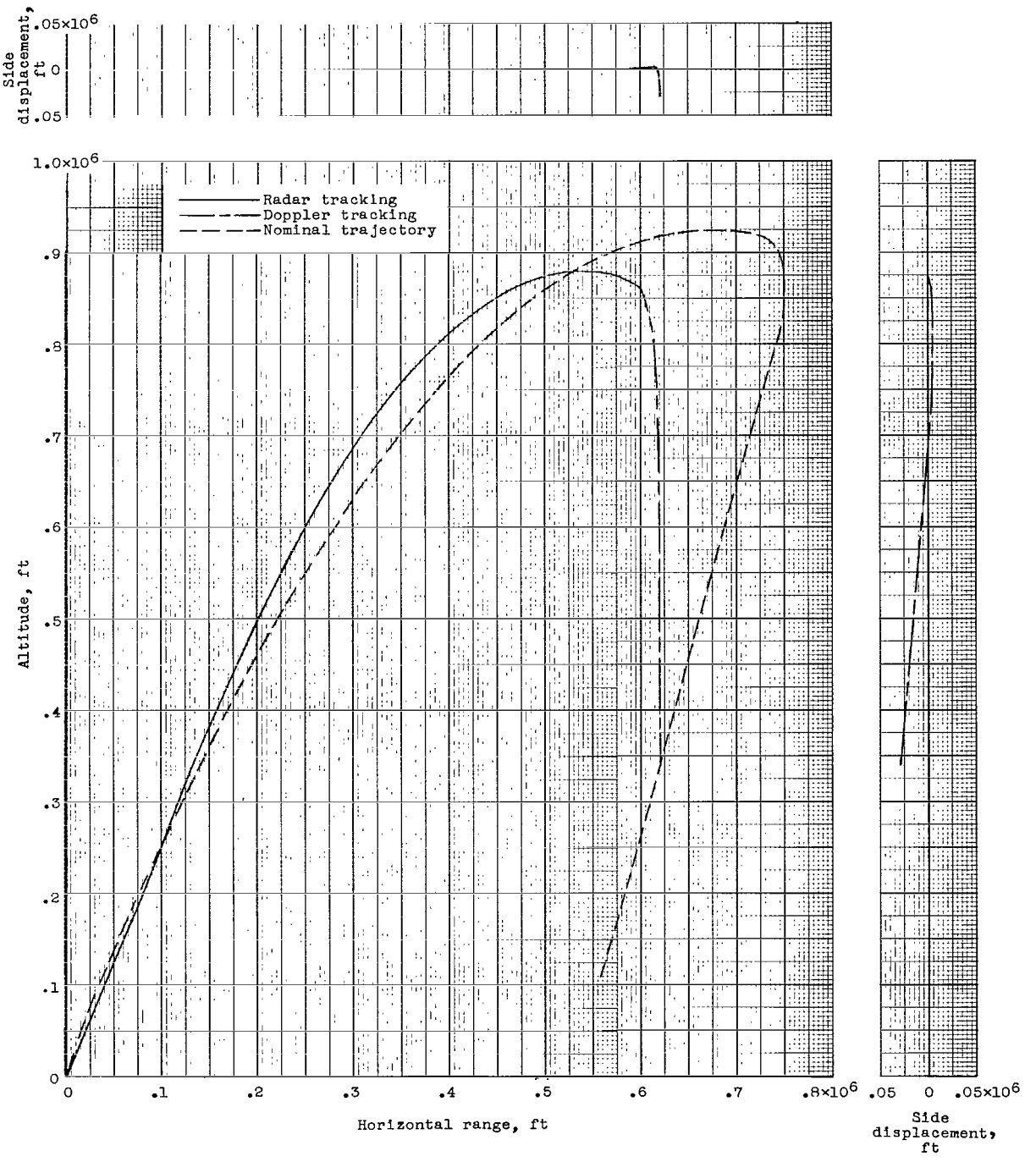


(b) Trailblazer Iβ. Launch angle, 80°.

Figure 23.- Continued.

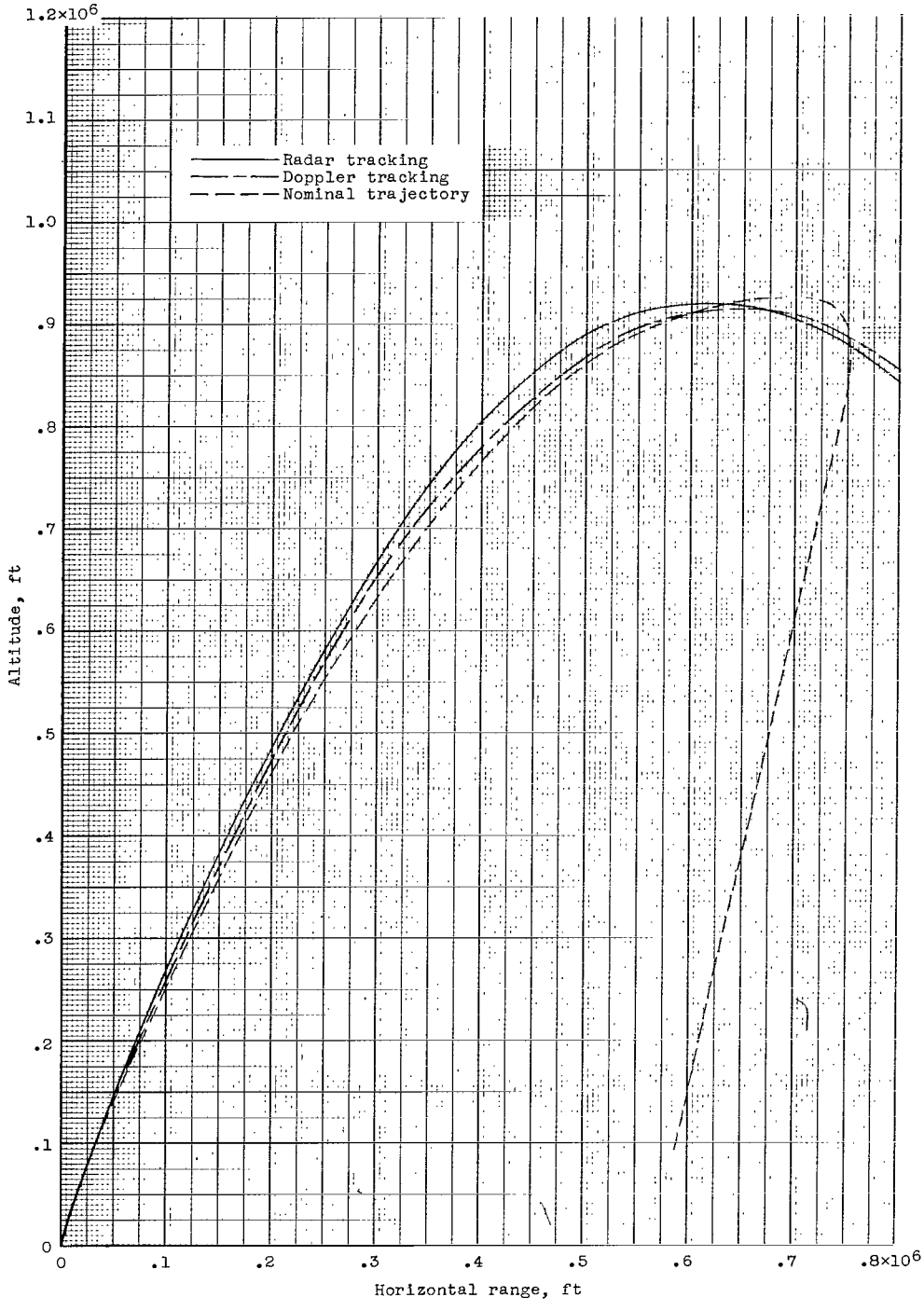


(c) Trailblazer Iγ. Launch angle, 80°.

Figure 23.- Continued.

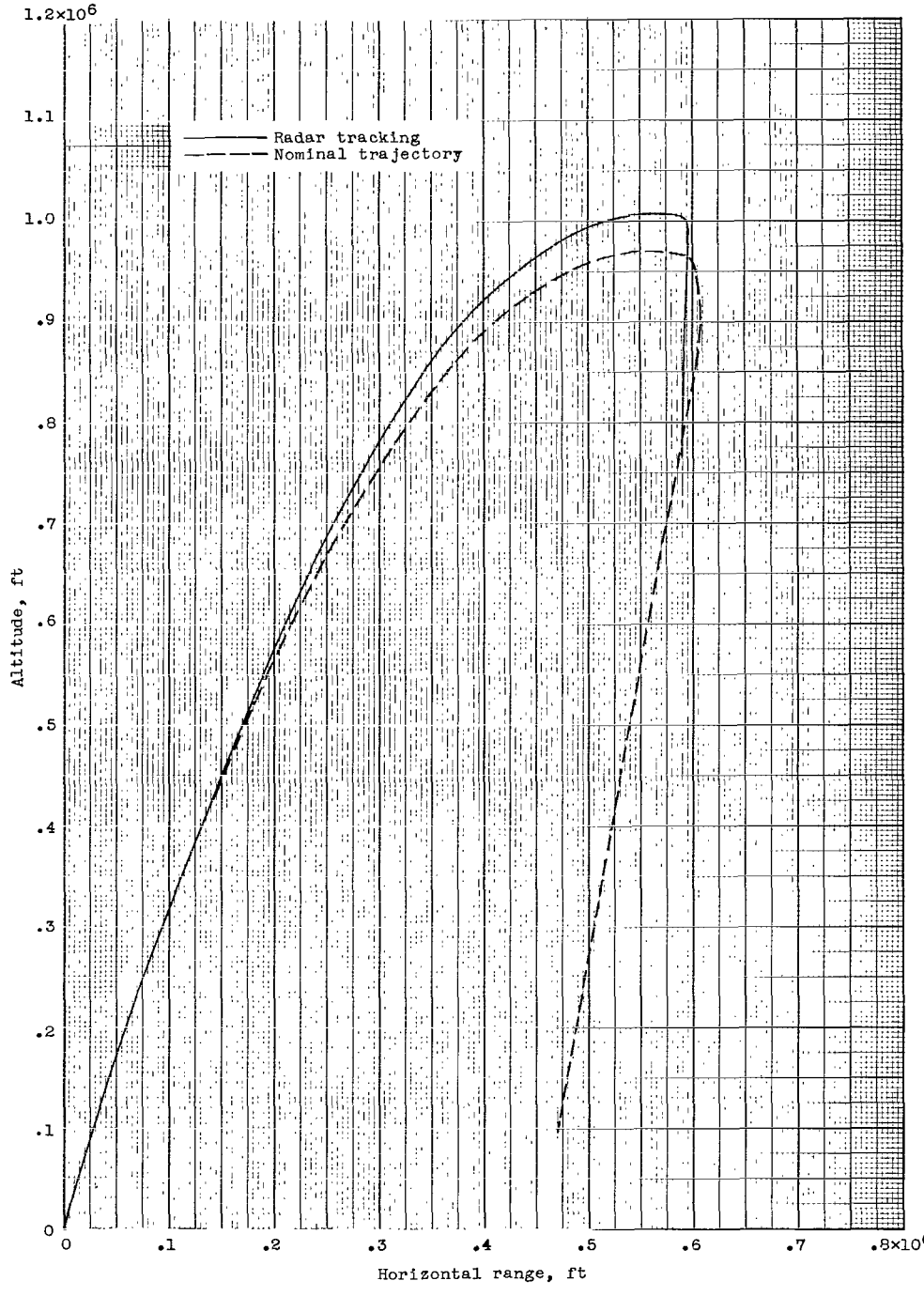


(d) Trailblazer Ia. Launch angle, 82°.

Figure 23.- Continued.

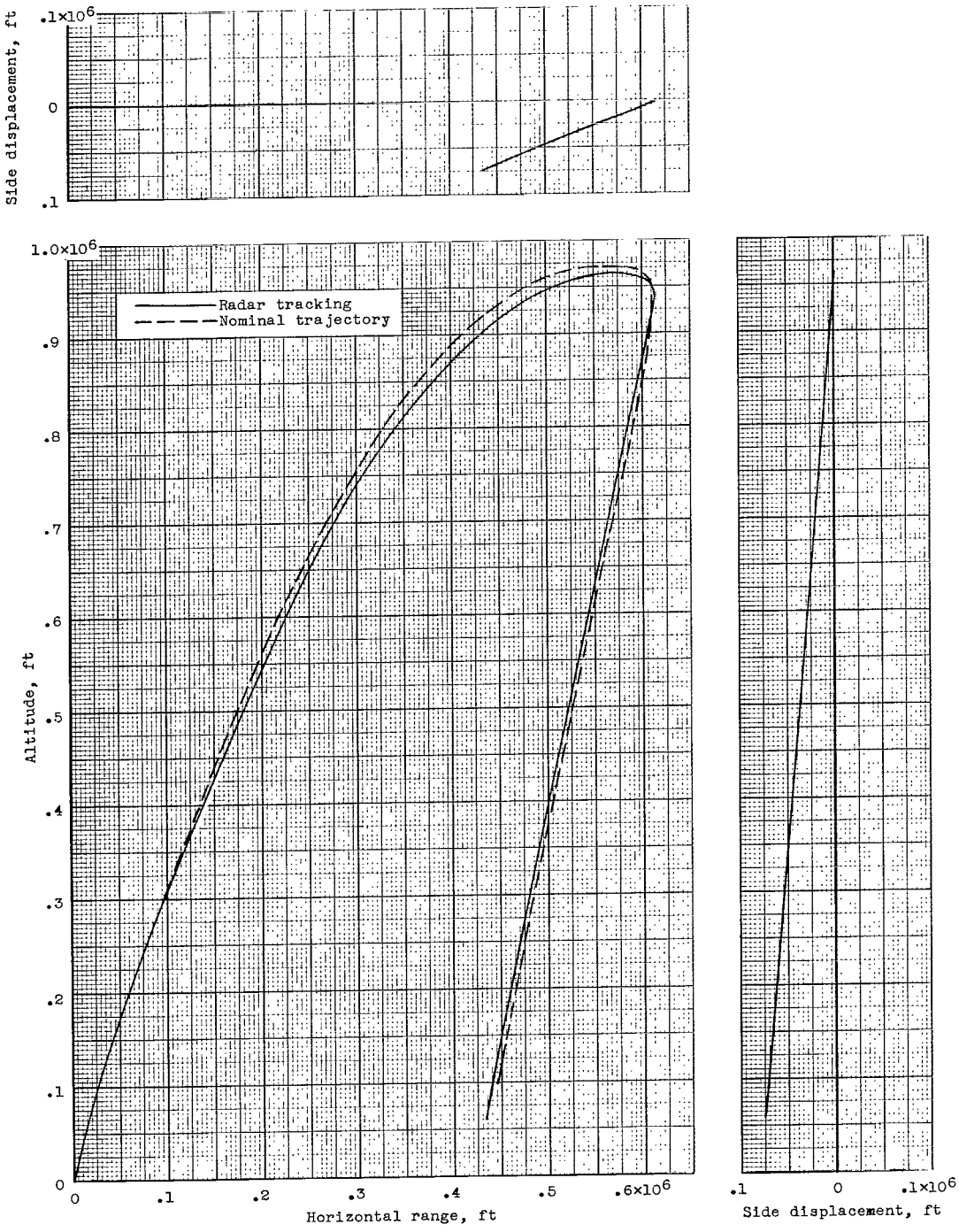


(e) Trailblazer Ib. Launch angle, 82°.

Figure 23.- Continued.

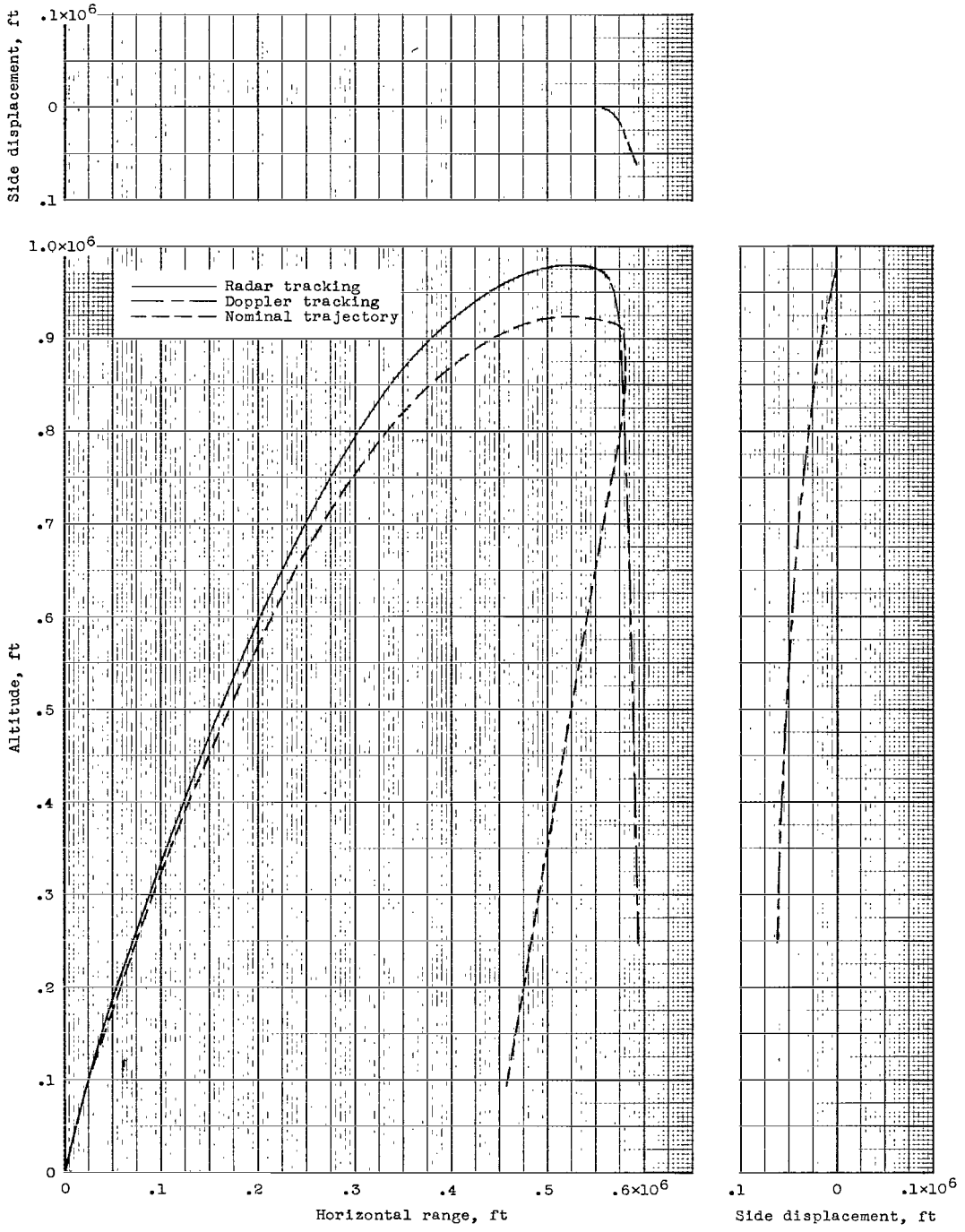


(f) Trailblazer Ic. Launch angle, 82°.

Figure 23.- Continued.

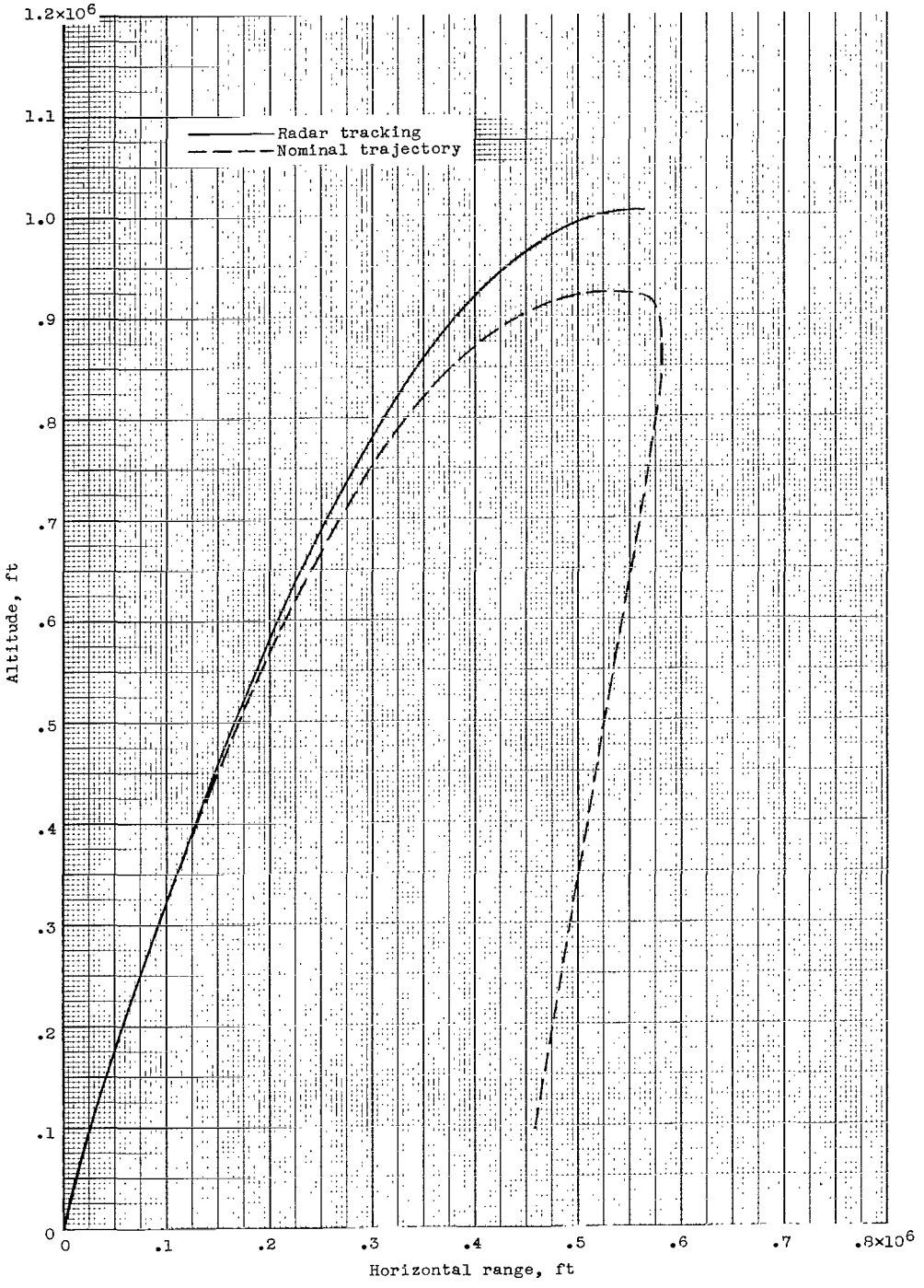


(g) Trailblazer Id. Launch angle, 82°.

Figure 23.- Continued.

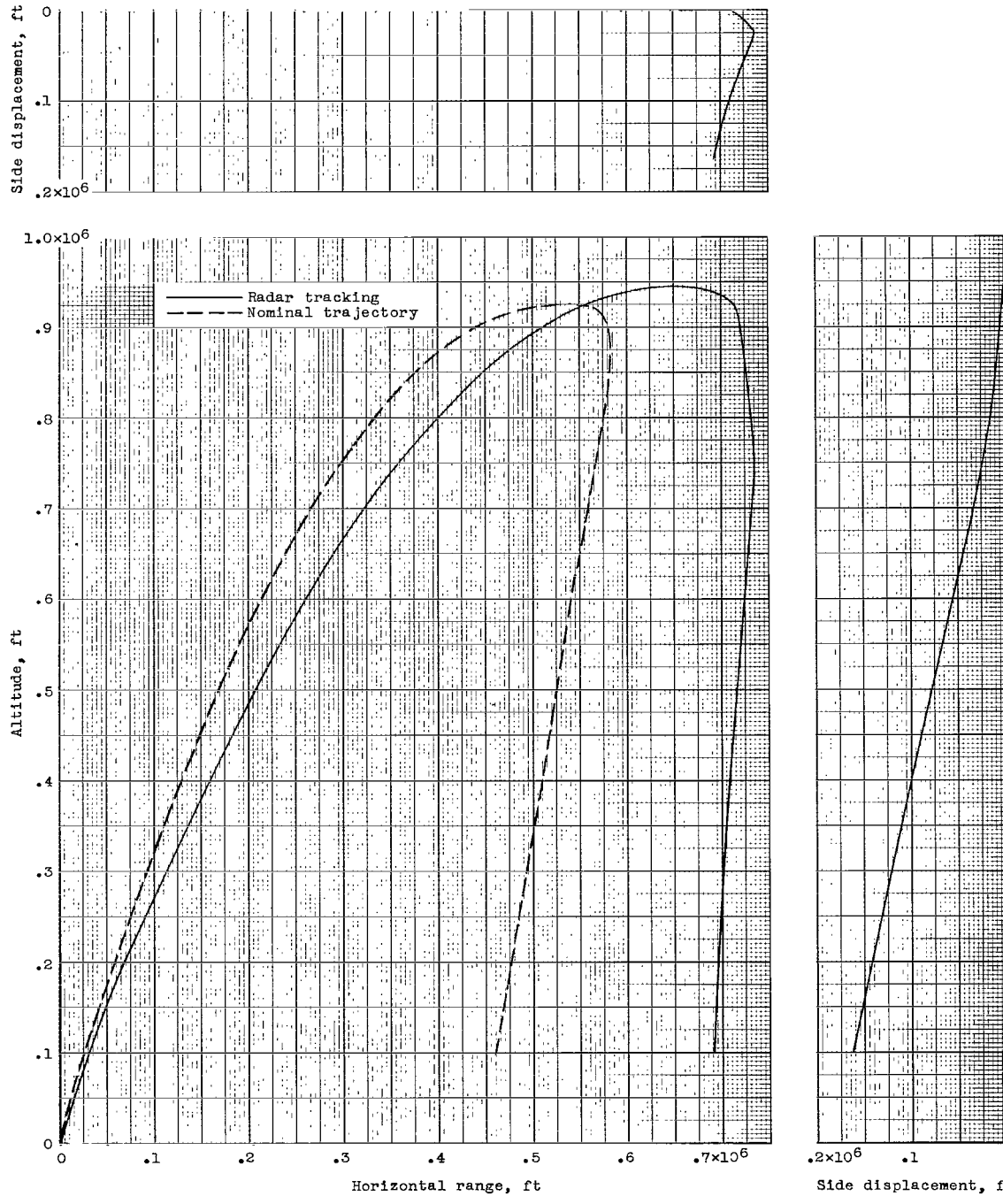


(h) Trailblazer Ie. Launch angle, 82°.

Figure 23.- Continued.

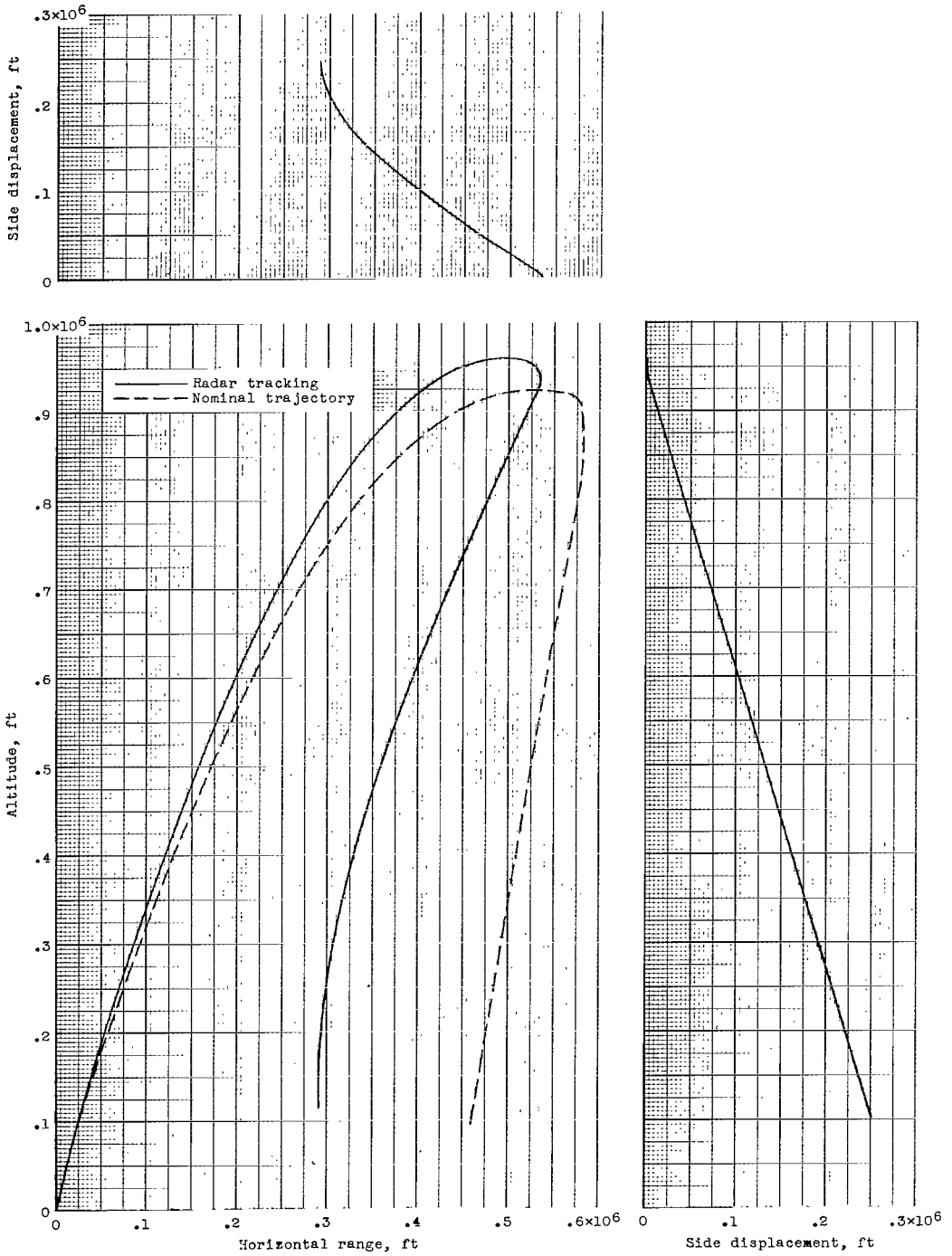


(i) Trailblazer If. Launch angle, 82°.

Figure 23.- Concluded.

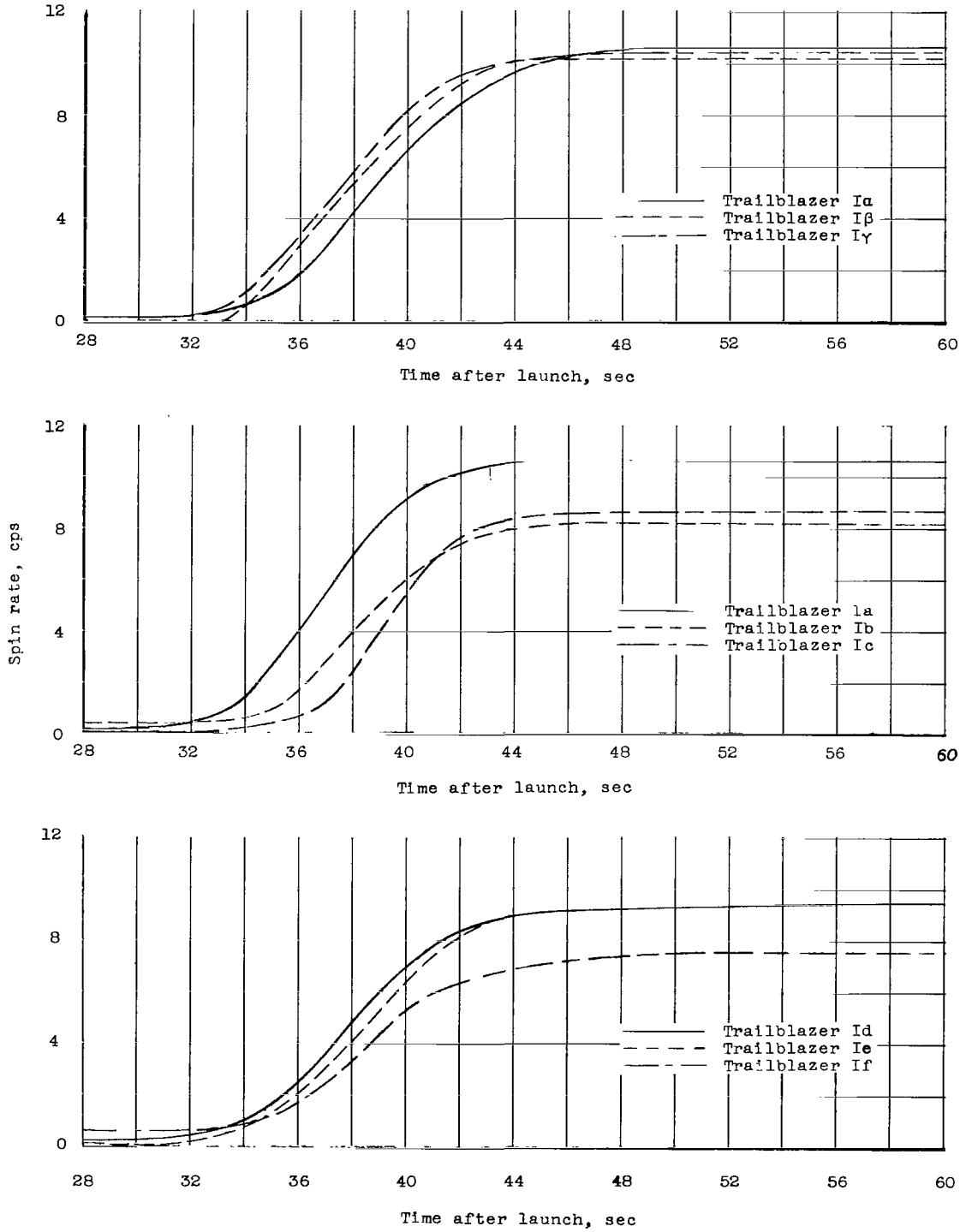


Figure 24.- Variation of vehicle spin rate with time during third-stage burning.

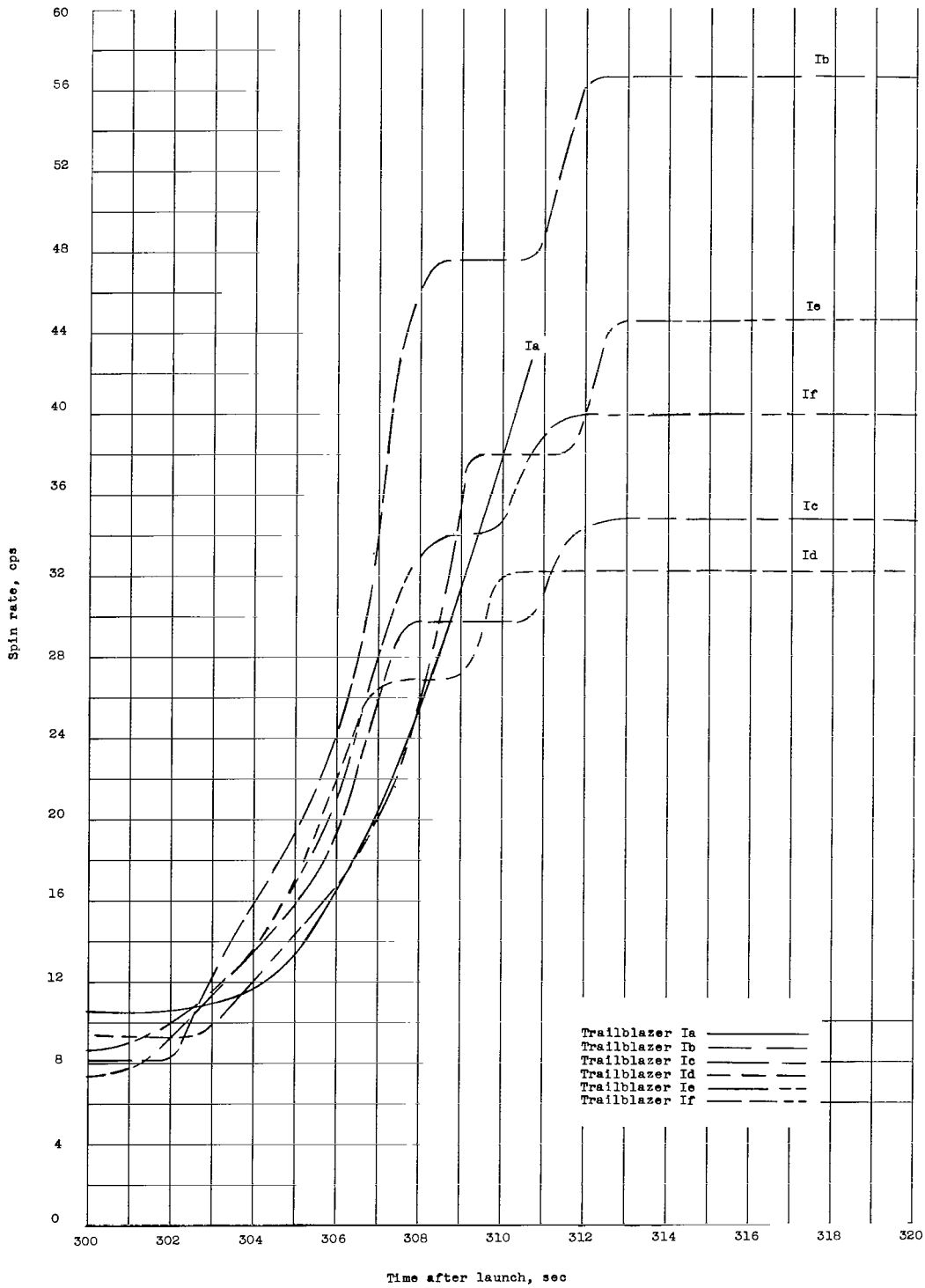


Figure 25.- Variation of vehicle spin rate with time during fourth- and fifth-stage burning.

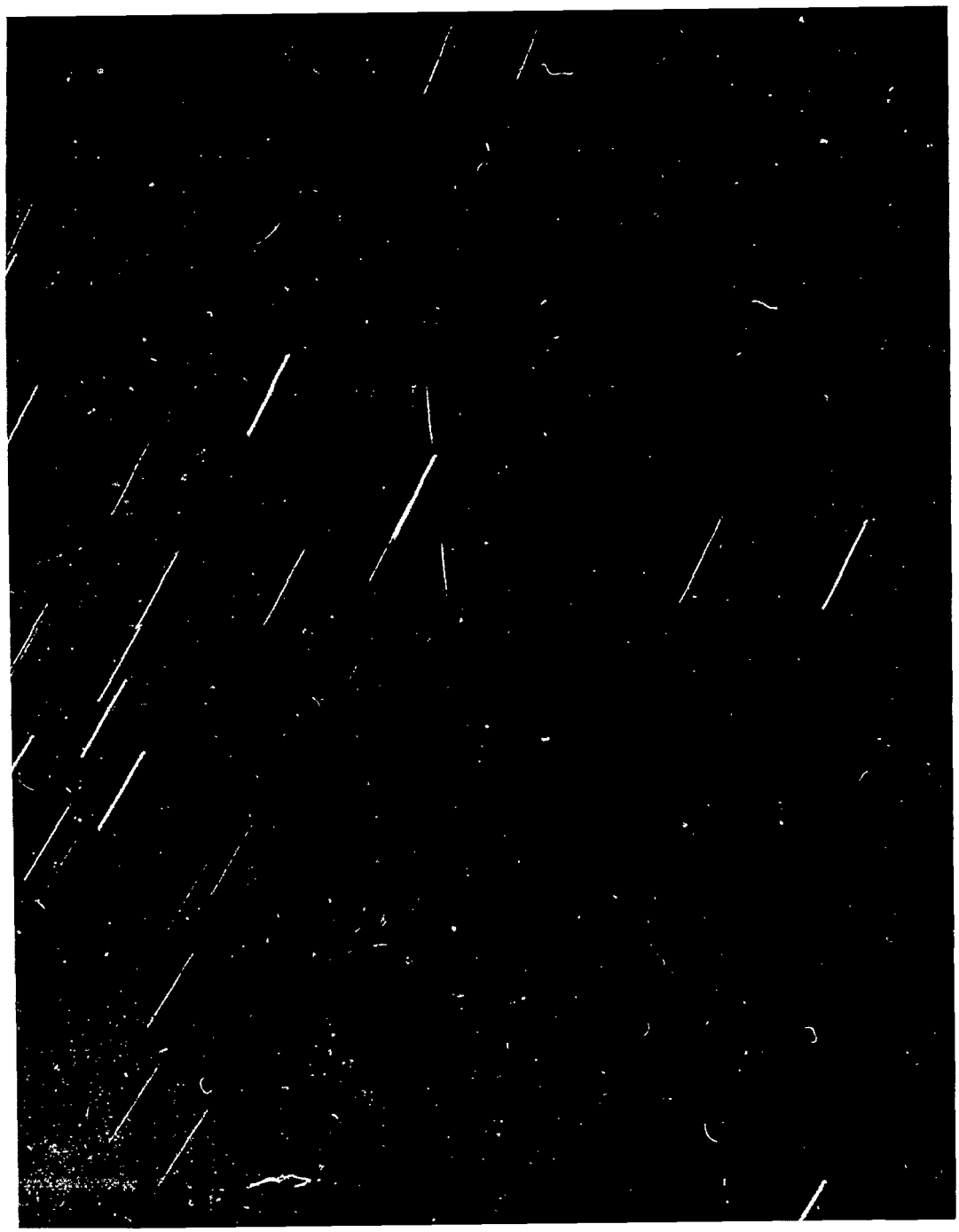

(a) Trailblazer Iβ; camera location: Coquina Beach, N.C. L-59-3948

Figure 26.- Photograph of sixth-stage reentry.

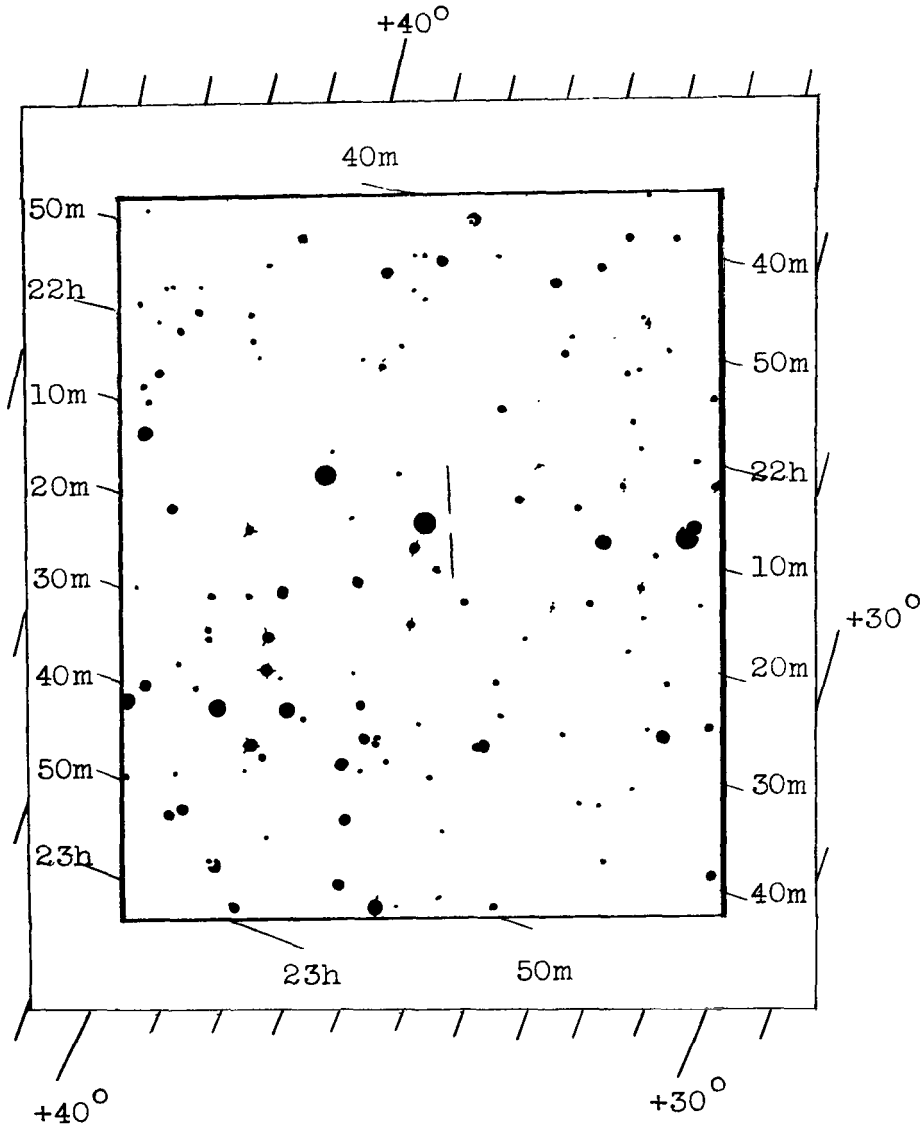


Note: Inner scale - right ascension, hr, min

Outer scale - declination, deg

(b) Sketch of star background for Trailblazer Iβ; camera location: Coquina Beach, N.C.

Figure 26.- Concluded.

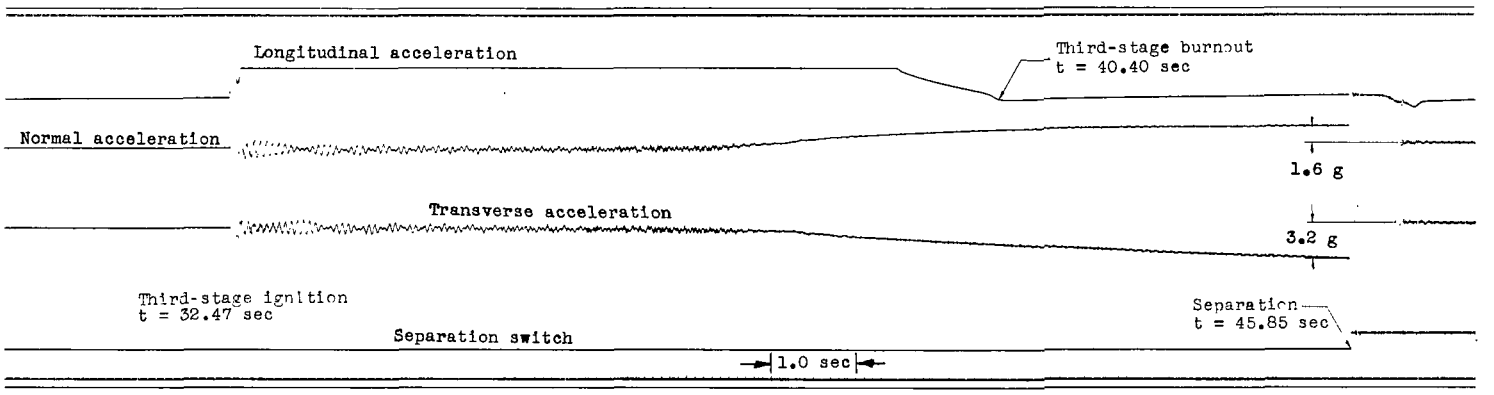


(a) Trailblazer Ia.

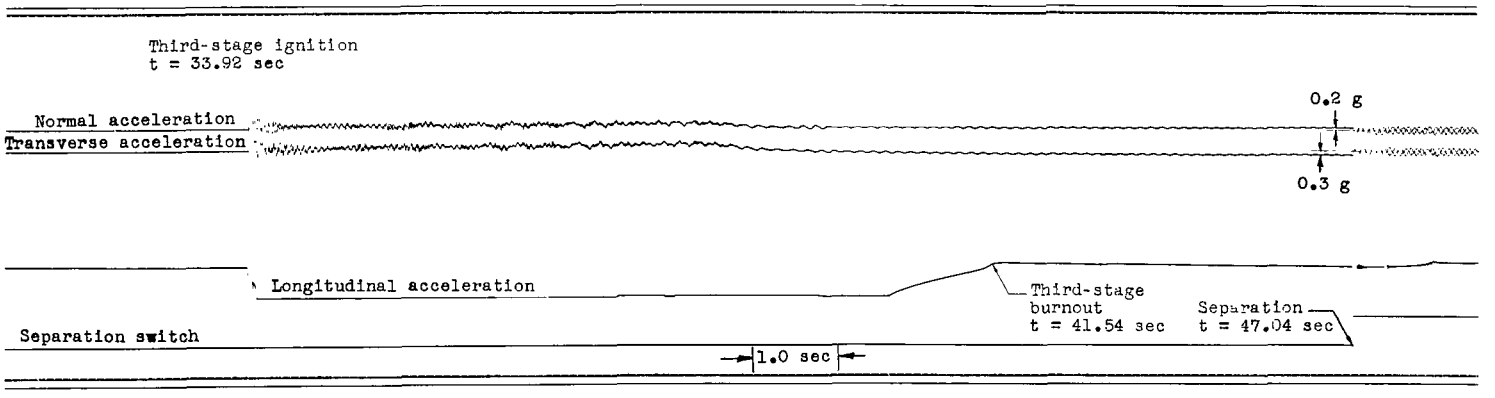


(b) Trailblazer Ib.

Figure 27.- Telemeter records from Trailblazers Ia and Ib test flights showing third-stage burning and velocity-package separation.

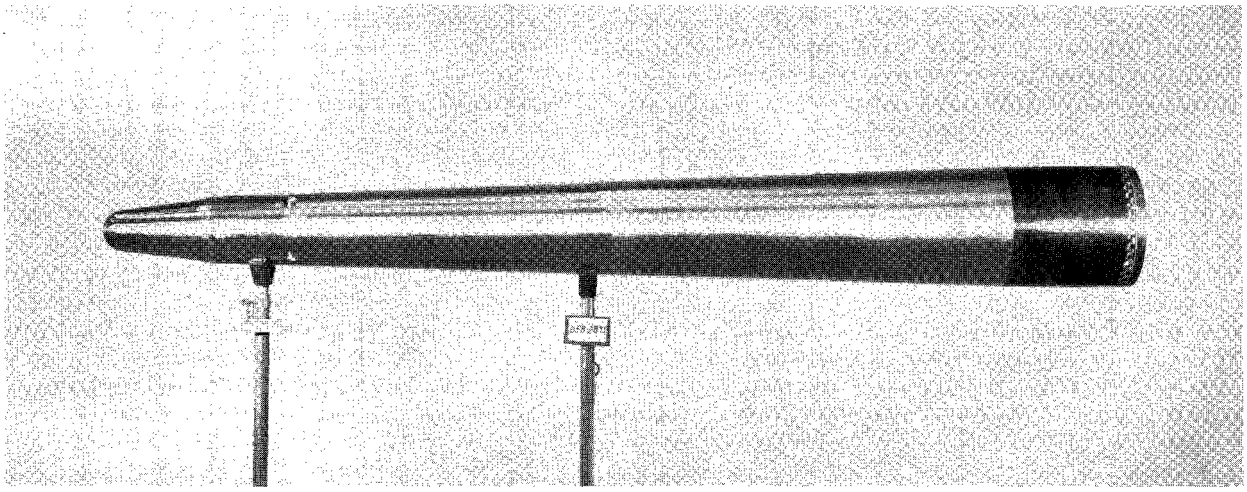

(a) Without ablation coating. L-59-733

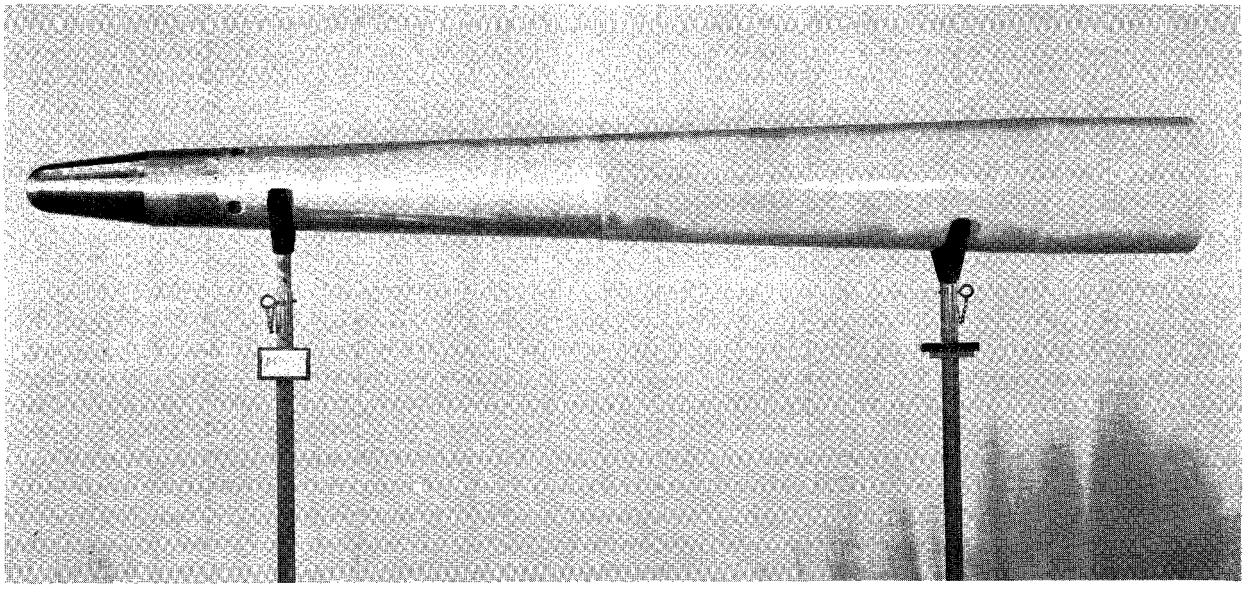

(b) With ablation coating. L-61-3932

Figure 28.- Photographs of velocity package with and without ablation coating on aft section.

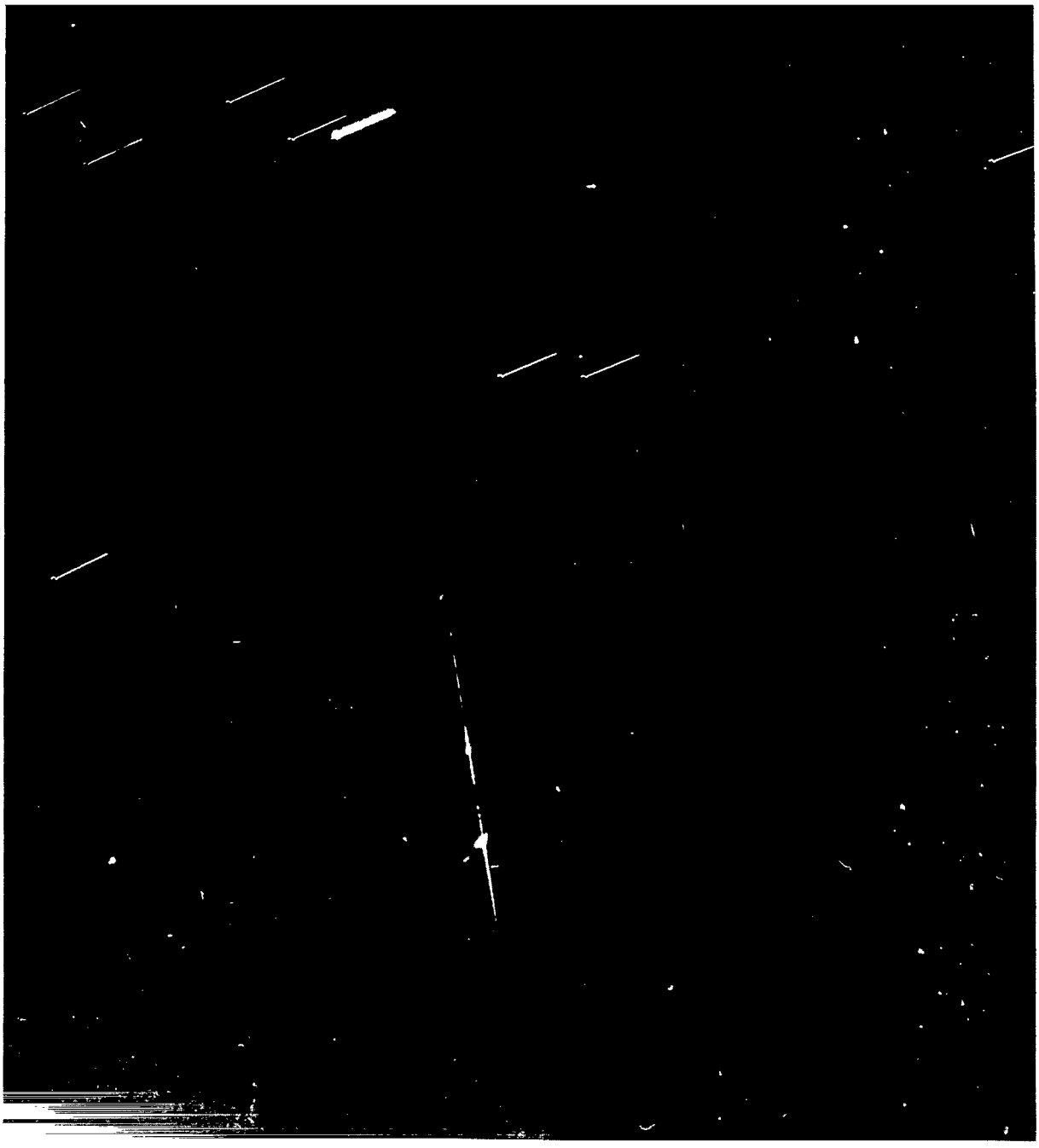

(a) Trailblazer Ic; camera location: Wallops Island, Va.; trace unchopped.

Figure 29.- Photographs of sixth-stage reentry for Trailblazer Ic. L-63-9258

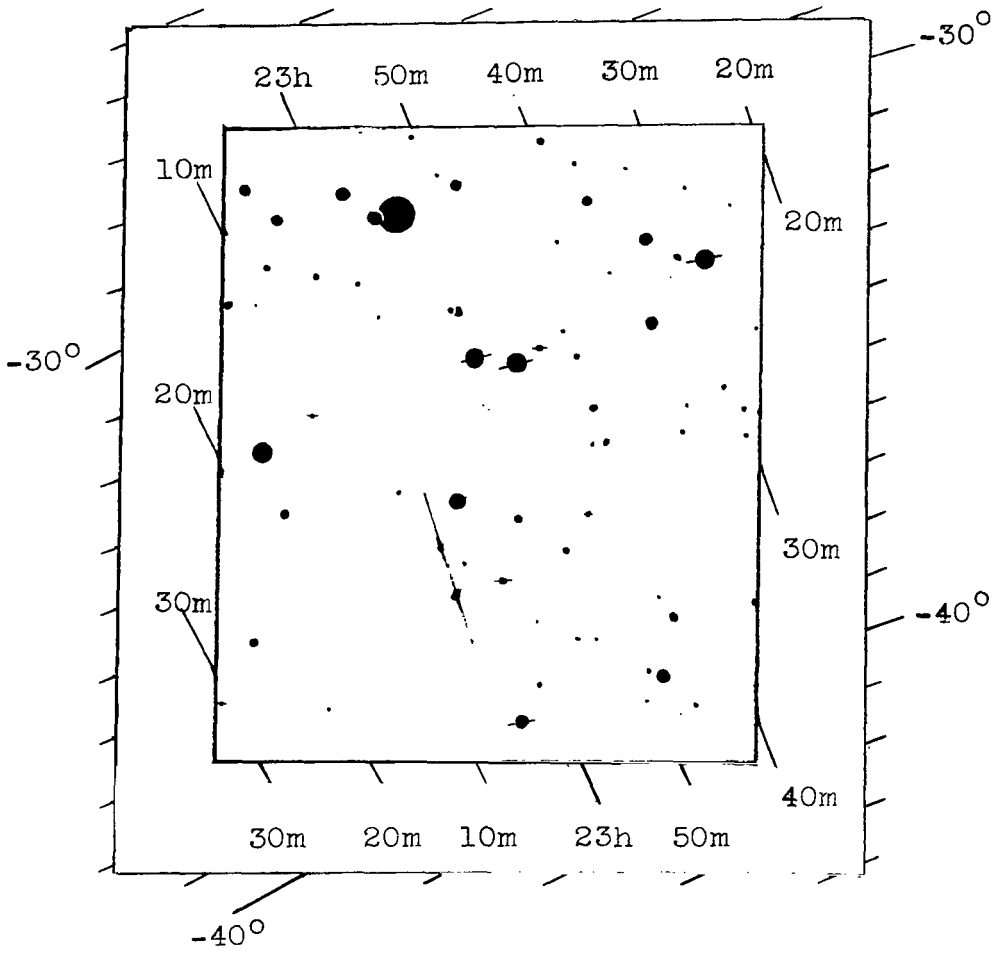


Note: Inner scale - right ascension, hr, min

Outer scale - declination, deg

(b) Sketch of star background for Trailblazer Ic; camera location: Wallops Island, Va.; trace unchopped.

Figure 29.- Continued.

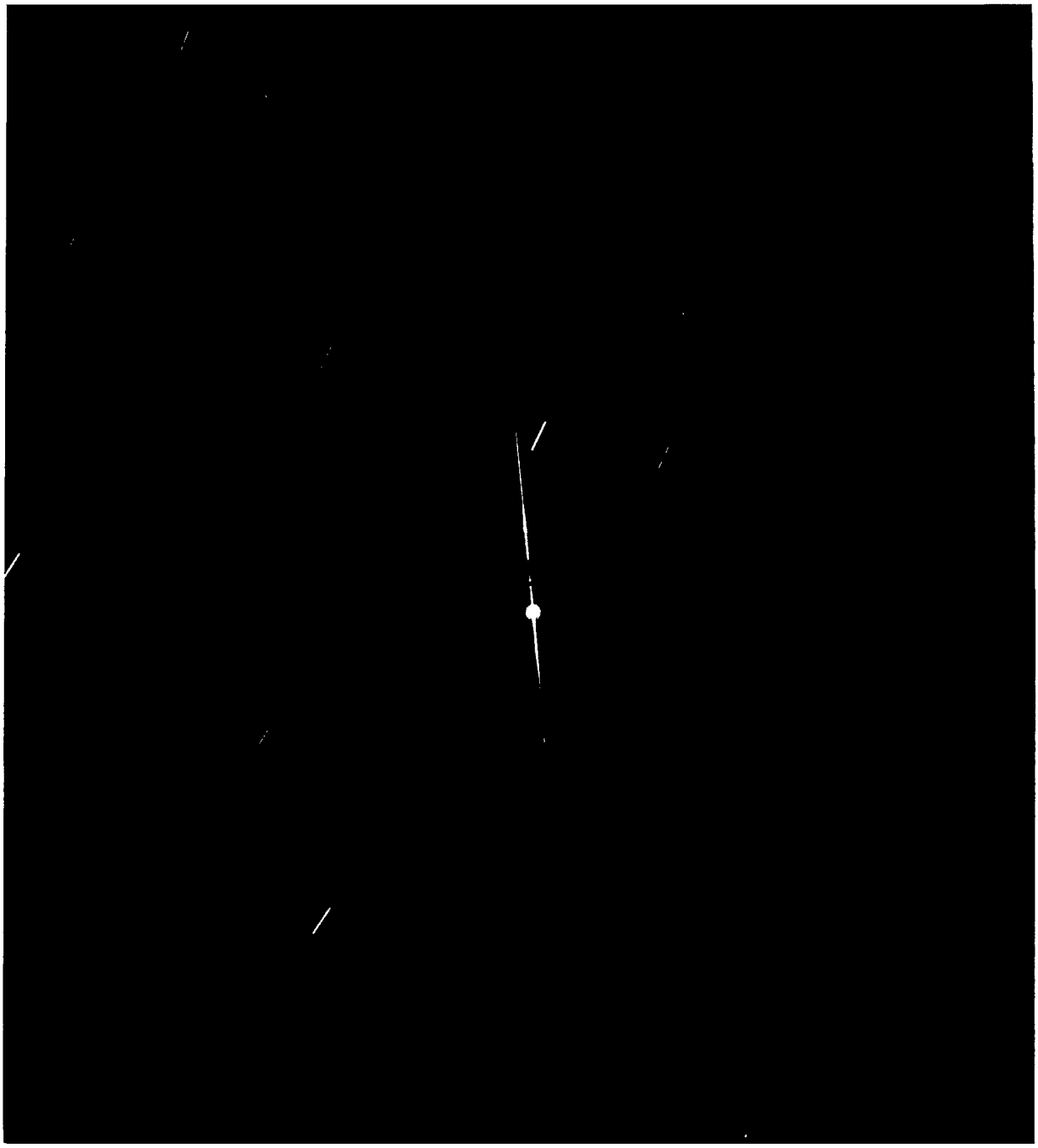

(c) Trailblazer Ic; camera location: Coquina Beach, N.C.; trace unchopped. L-63-9259

Figure 29.- Continued.

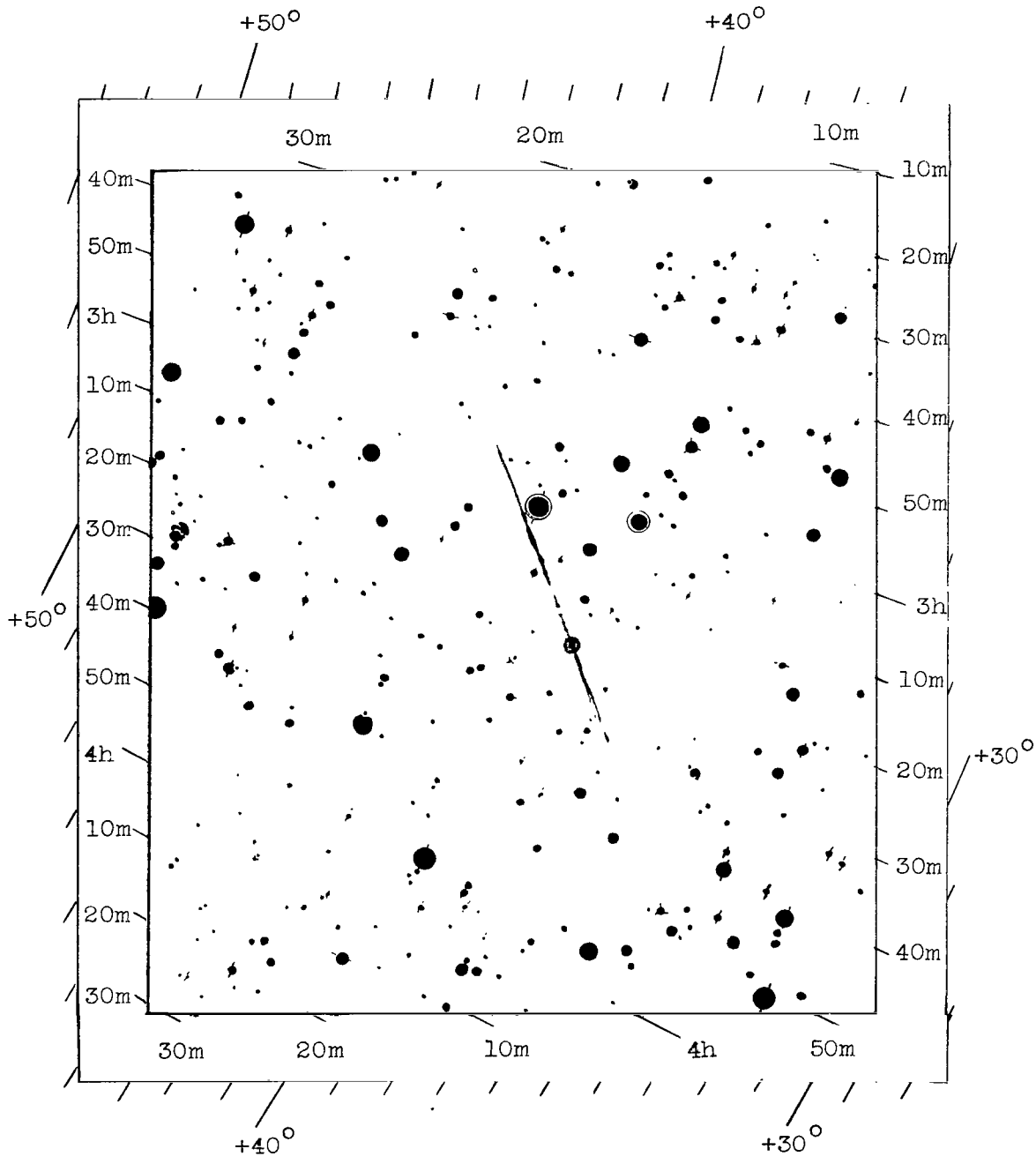


Note: Inner scale - right ascension, hr, min
Outer scale - declination, deg

(d) Sketch of star background for Trailblazer Ic; camera location: Coquina Beach, N.C.; trace unchopped.

Figure 29.- Continued.

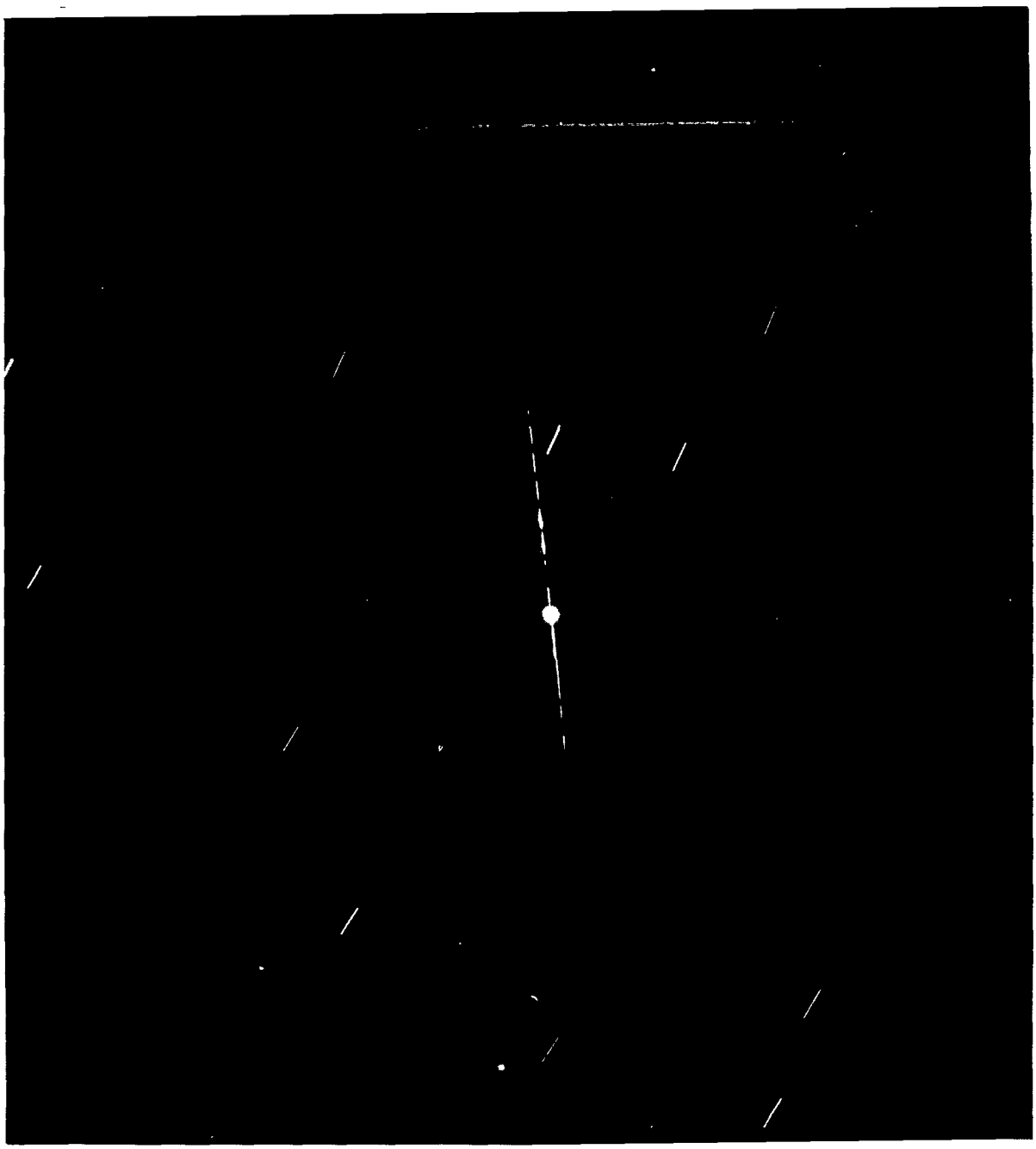

(e) Trailblazer Ic; camera location: Coquina Beach, N.C.; trace chopped at 5 chops per second. L-63-9260

Figure 29.- Continued.

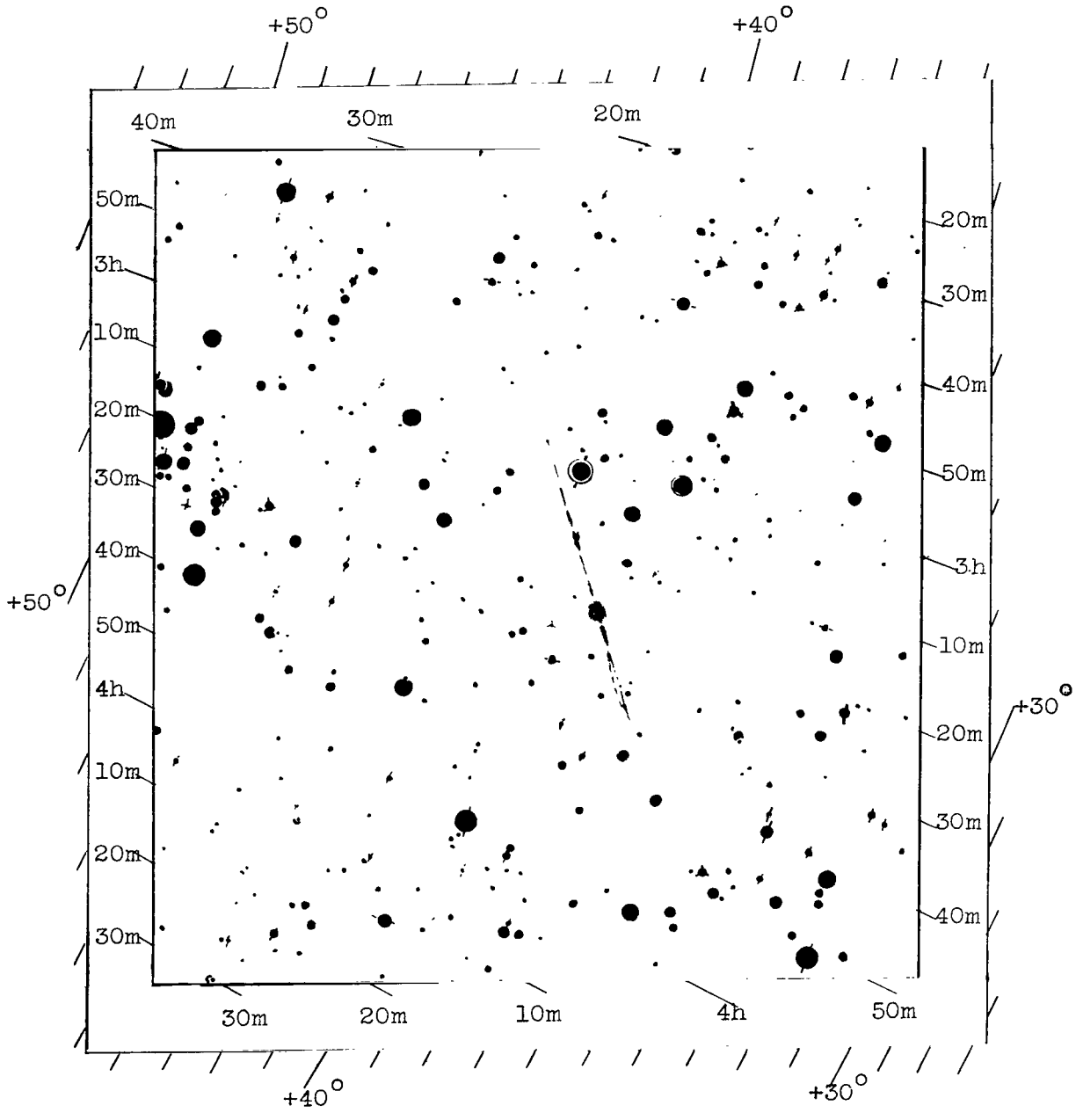


Note: Inner scale - right ascension, hr, min

Outer scale - declination, deg

(f) Sketch of star background for Trailblazer Ic; camera location: Coquina Beach, N.C.; trace chopped at 5 chops per second.

Figure 29.- Concluded.

(a) Trailblazer Id; camera location: Wallops Island, Va.; trace unchopped.

Figure 30.- Photographs of sixth-stage reentry for Trailblazer Id. L-63-9261

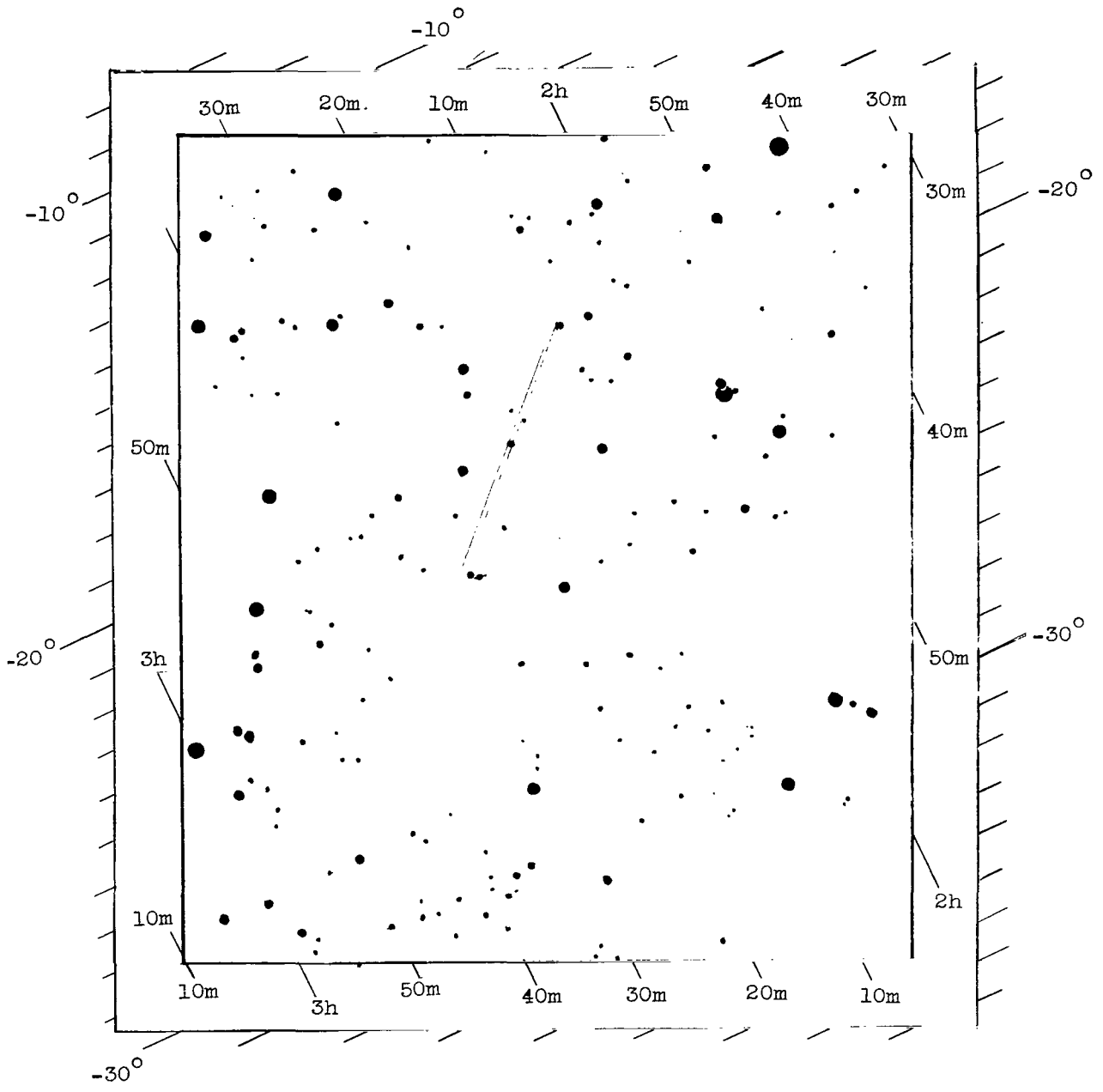


Note: Inner scale - right ascension, hr, min

Outer scale - declination, deg

(b) Sketch of star background for Trailblazer Id; camera location: Wallops Island, Va.; trace unchopped.

Figure 30.- Concluded.

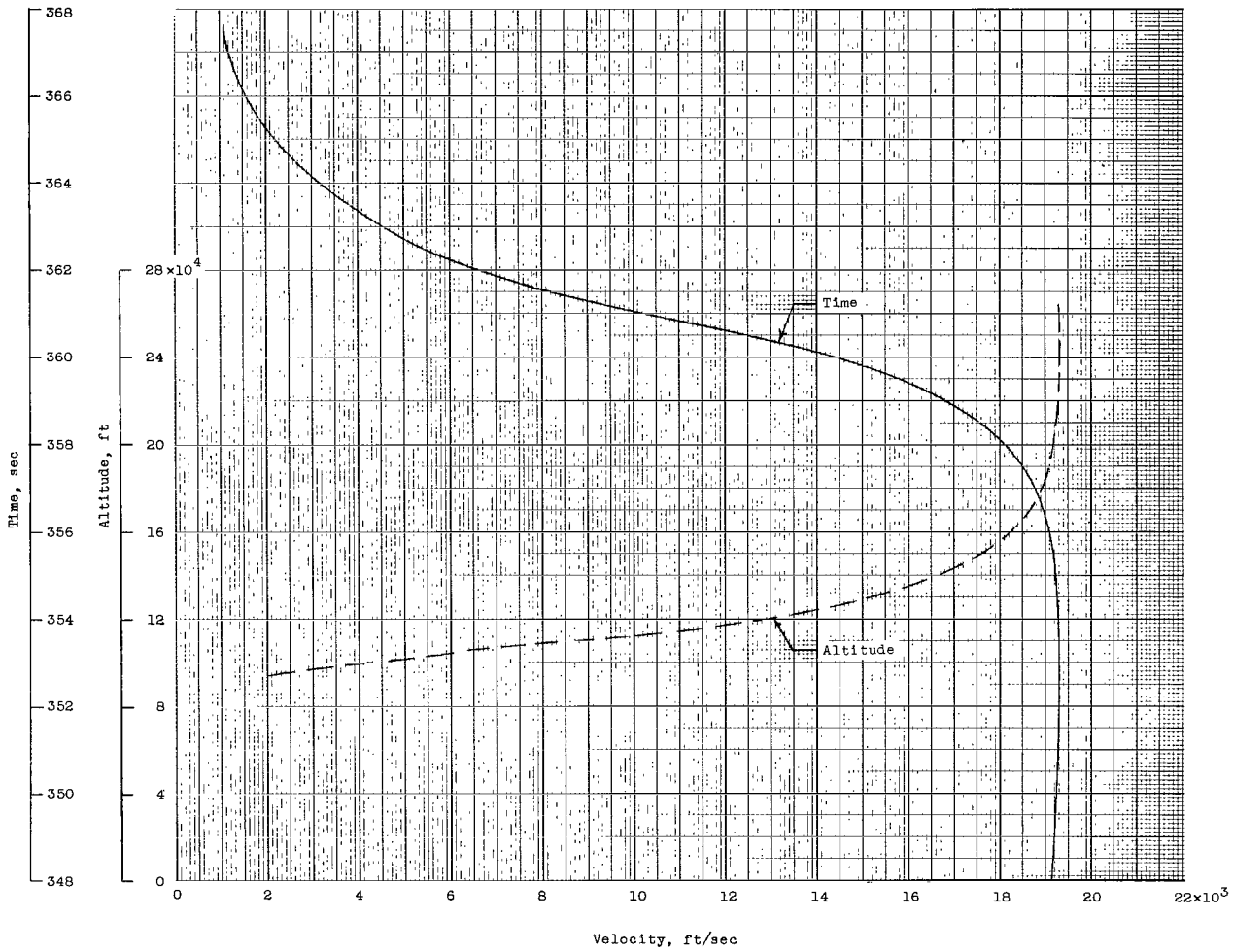


Figure 31.- Variation of reentry velocity with altitude and time for Trailblazer Ie.

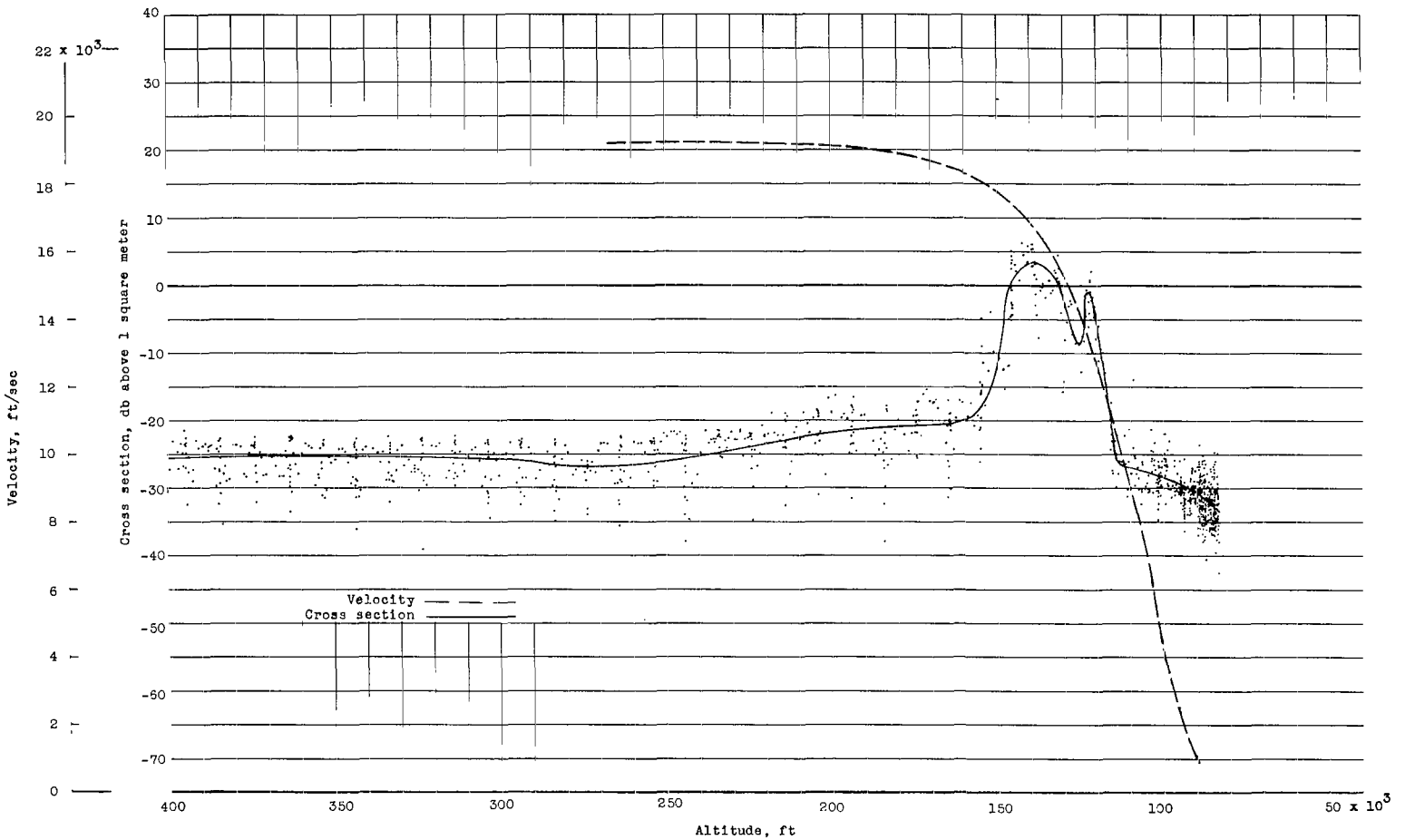


Figure 32.- Variation of cross section and velocity with altitude for Trailblazer Ie 5-inch sphere. MIT S-band radar.

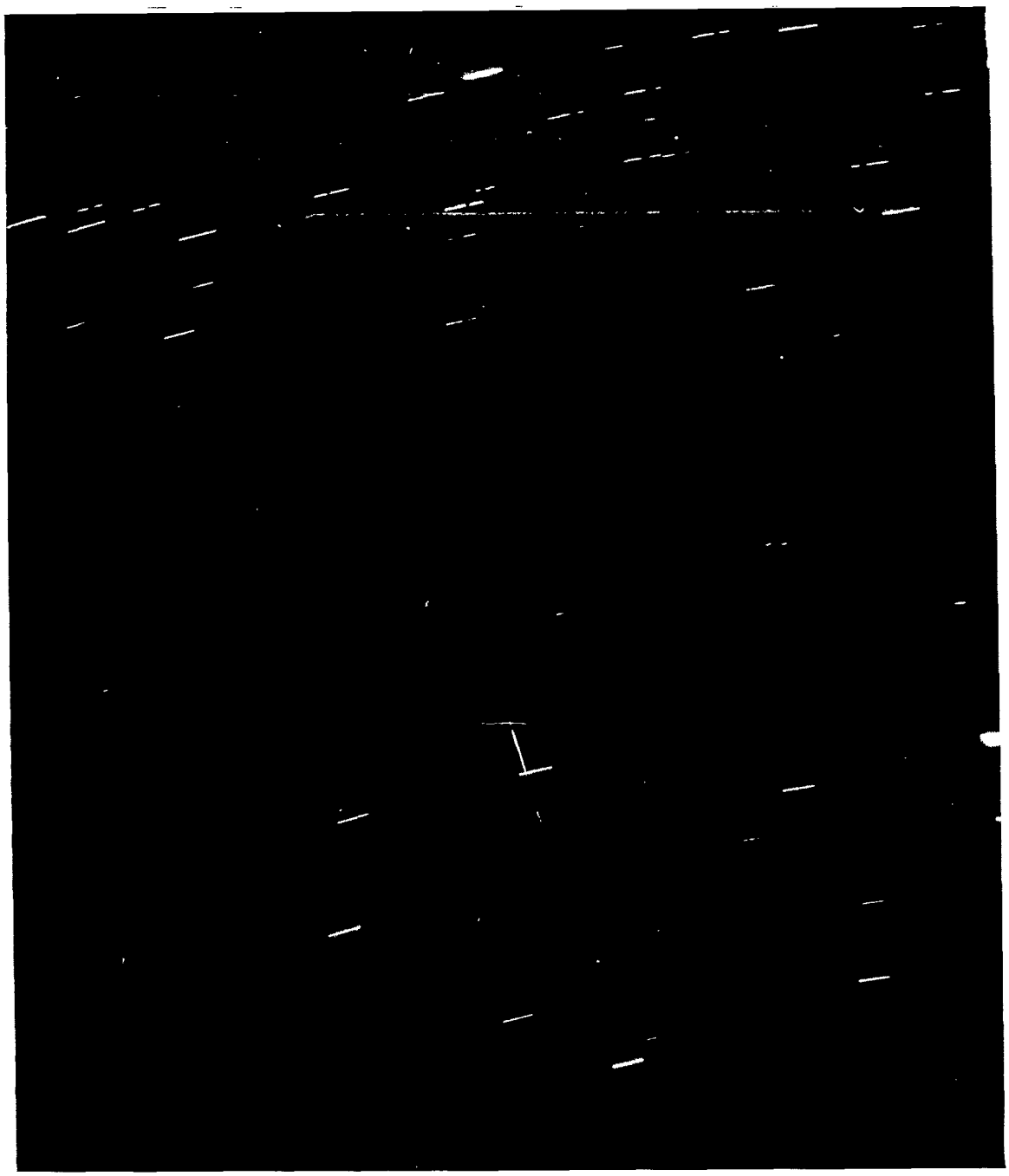

(a) Trailblazer Ie; camera location: Wallops Island, Va.; trace unchopped.

Figure 33.- Photographs of sixth-stage reentry for Trailblazer Ie. L-63-9262

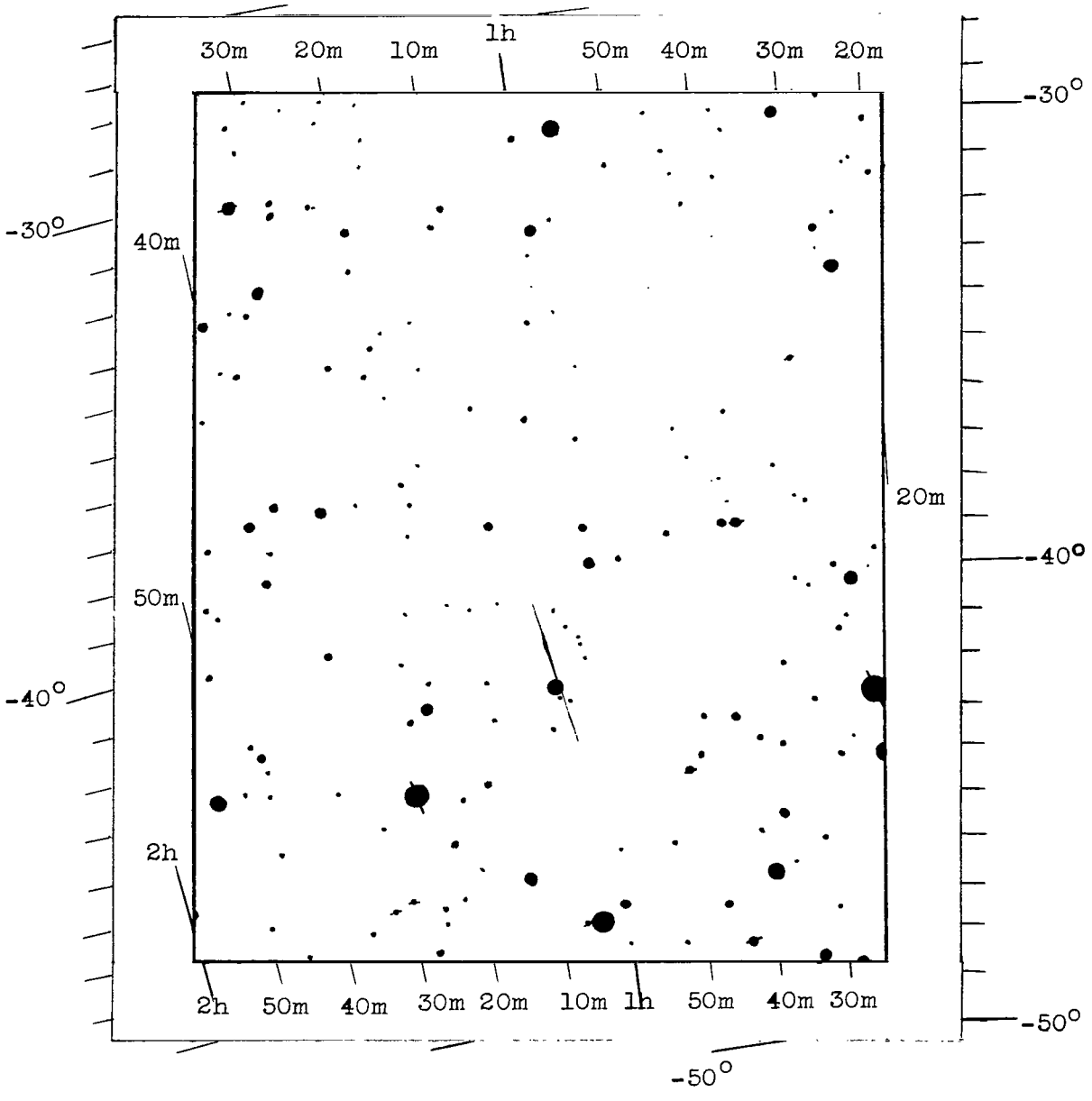


Note: Inner scale - right ascension, hr, min

Outer scale - declination, deg

(b) Sketch of star background for Trailblazer Ie; camera location: Wallops Island, Va.; trace unchopped.

Figure 33.- Continued.

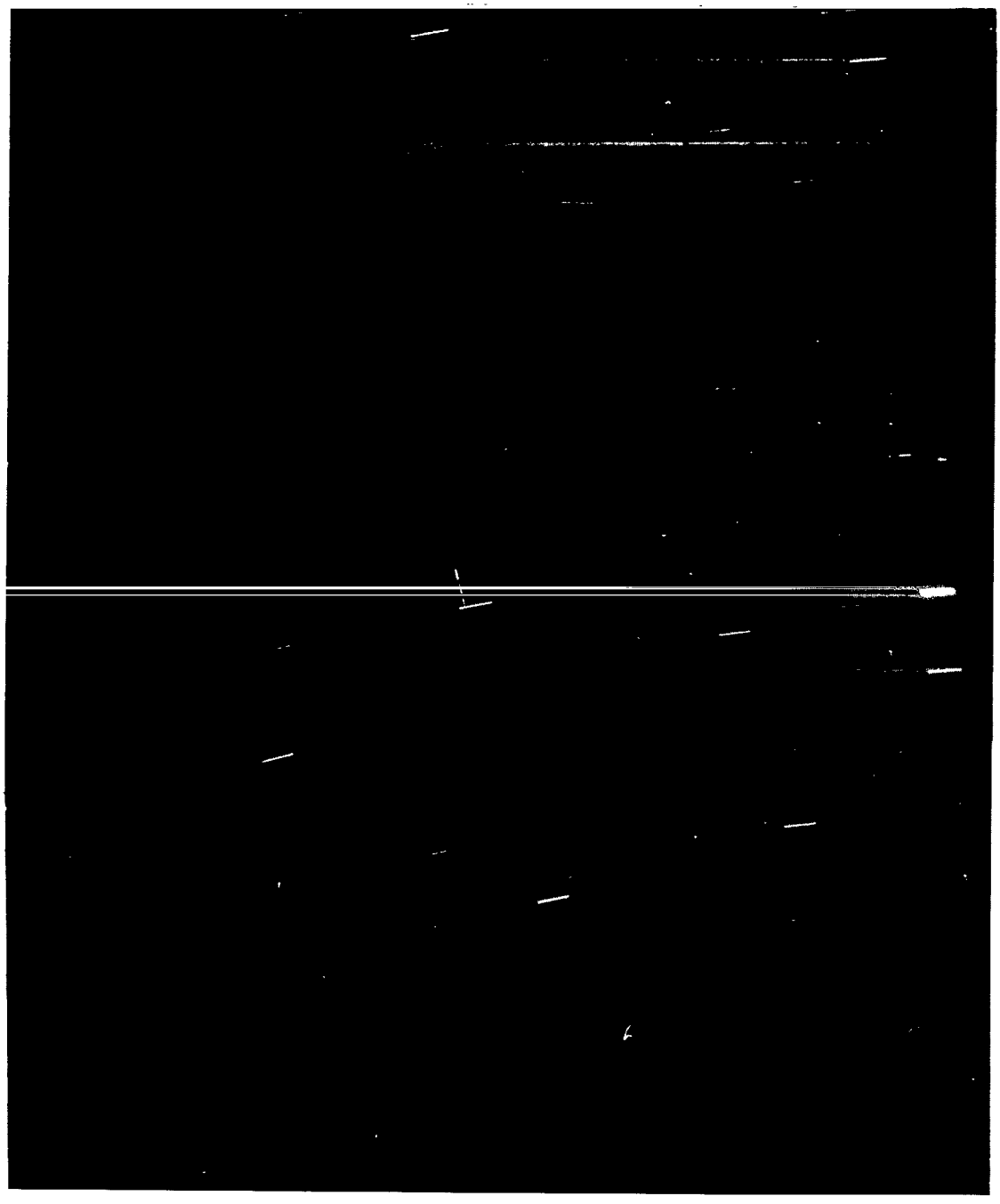

(c) Trailblazer Ie; camera location: Wallops Island, Va.;
trace chopped at 5 chops per second.

Figure 33.- Continued.

L-63-9263

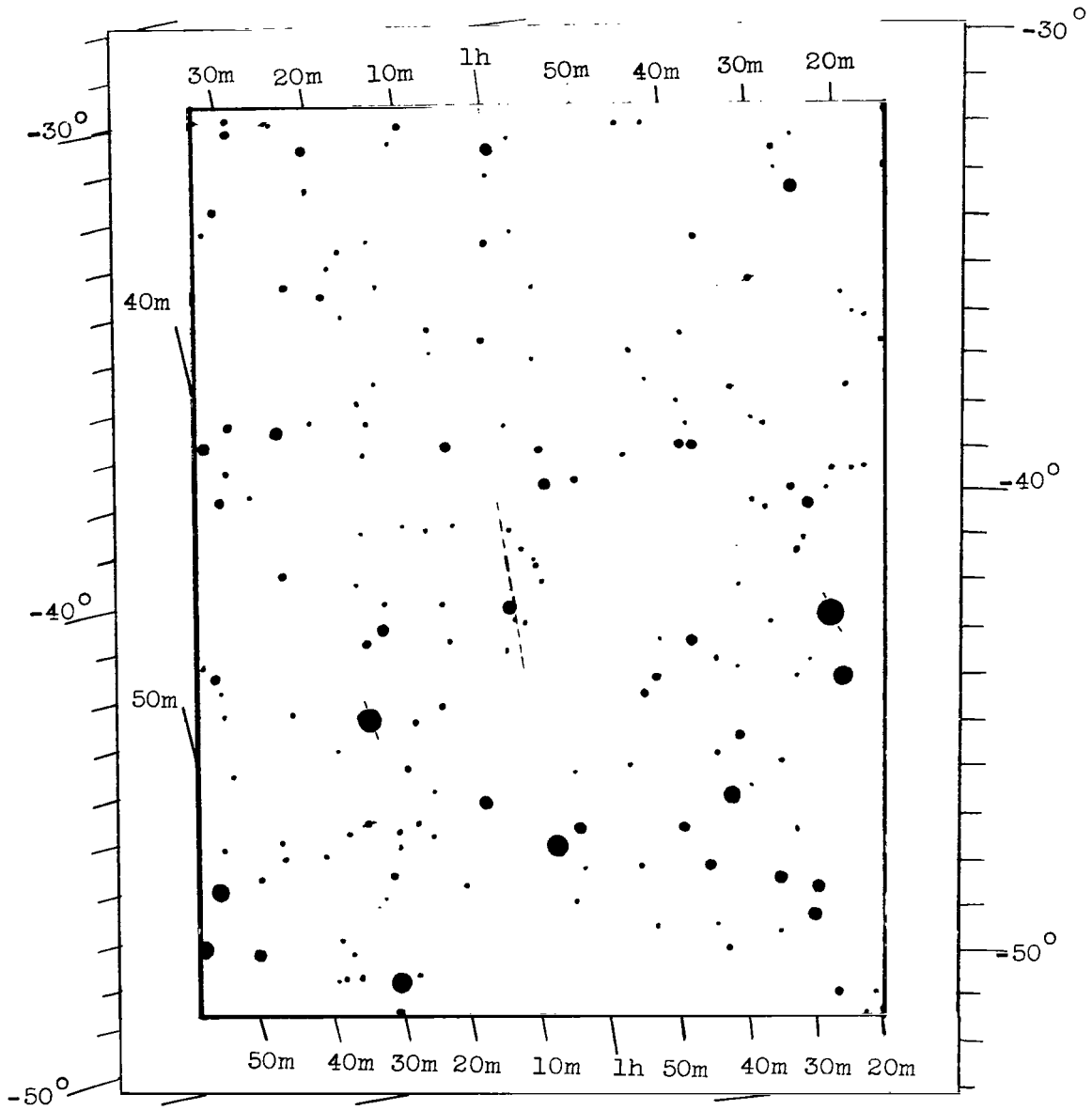


Note: Inner scale - right ascension, hr, min

Outer scale - declination, deg

(d) Sketch of star background for Trailblazer Ie; camera location: Wallops Island, Va.; trace chopped at 5 chops per second.

Figure 33.- Continued.

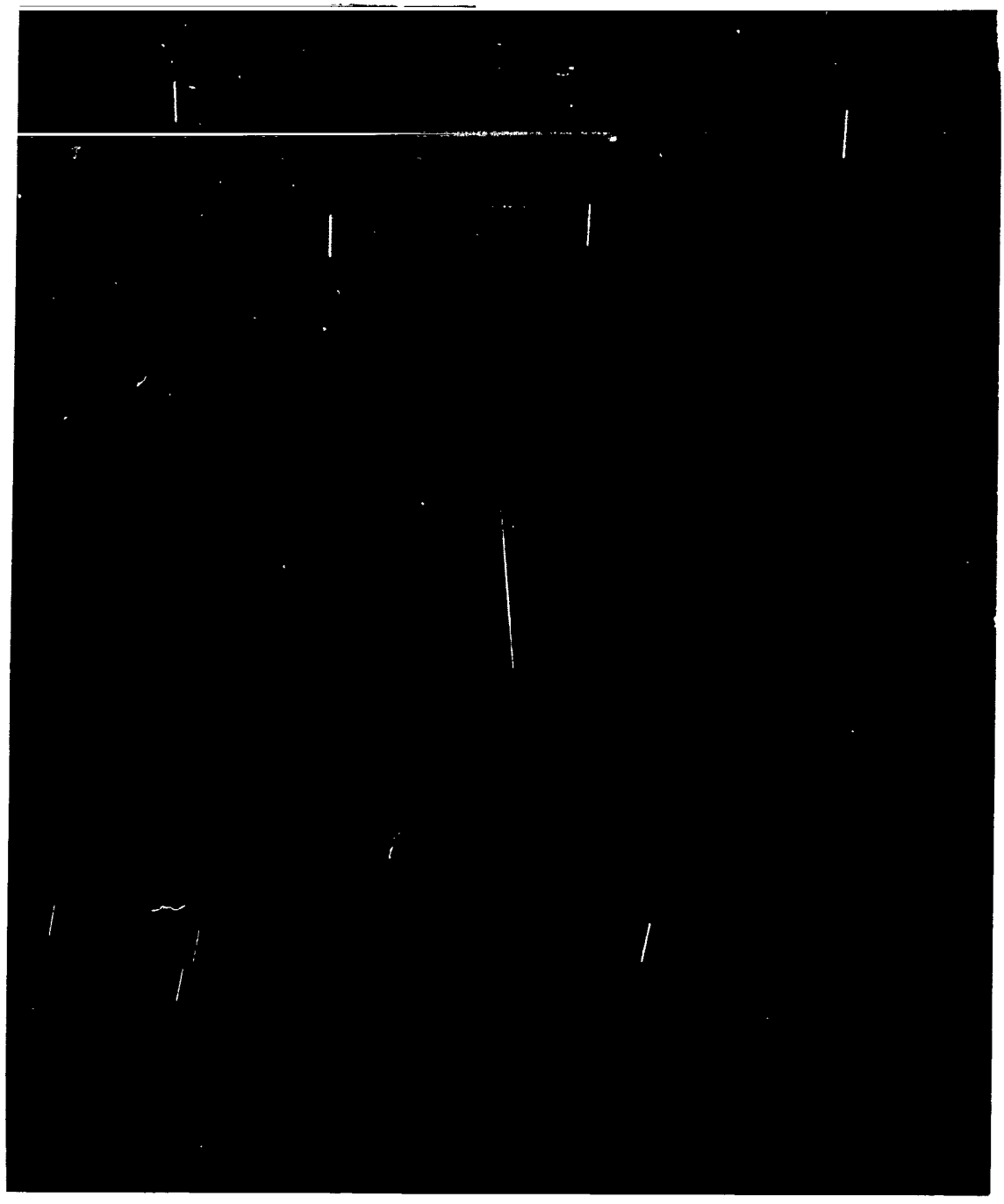

(e) Trailblazer Ie; camera location: Coquina Beach, N.C.; trace unchopped. L-63-9264

Figure 33.- Continued.

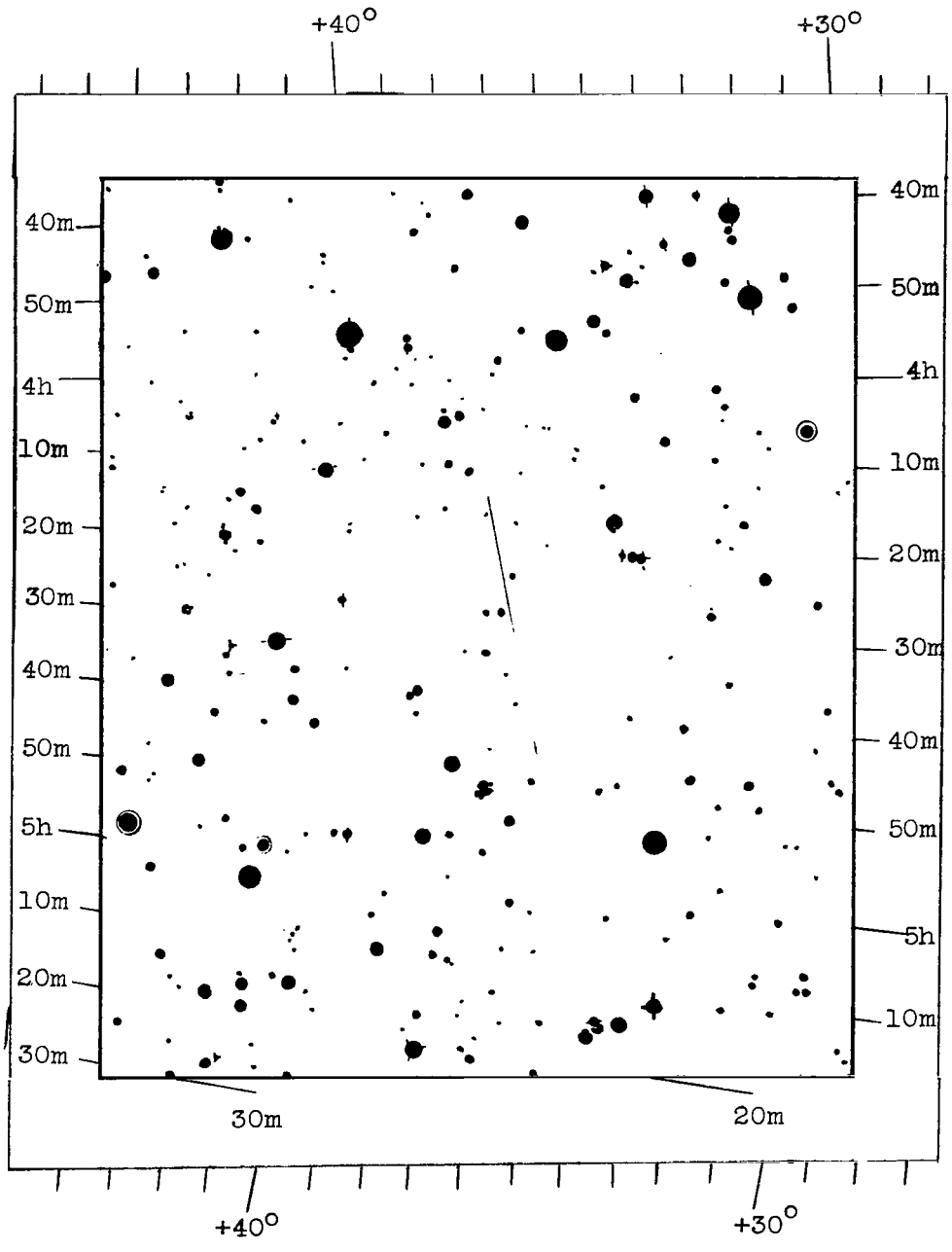


Note: Inner scale - right ascension, hr, min

Outer scale - declination, deg

(f) Sketch of star background for Trailblazer Ie; camera location: Coquina Beach, N.C.; trace unchopped.

Figure 33.- Concluded.

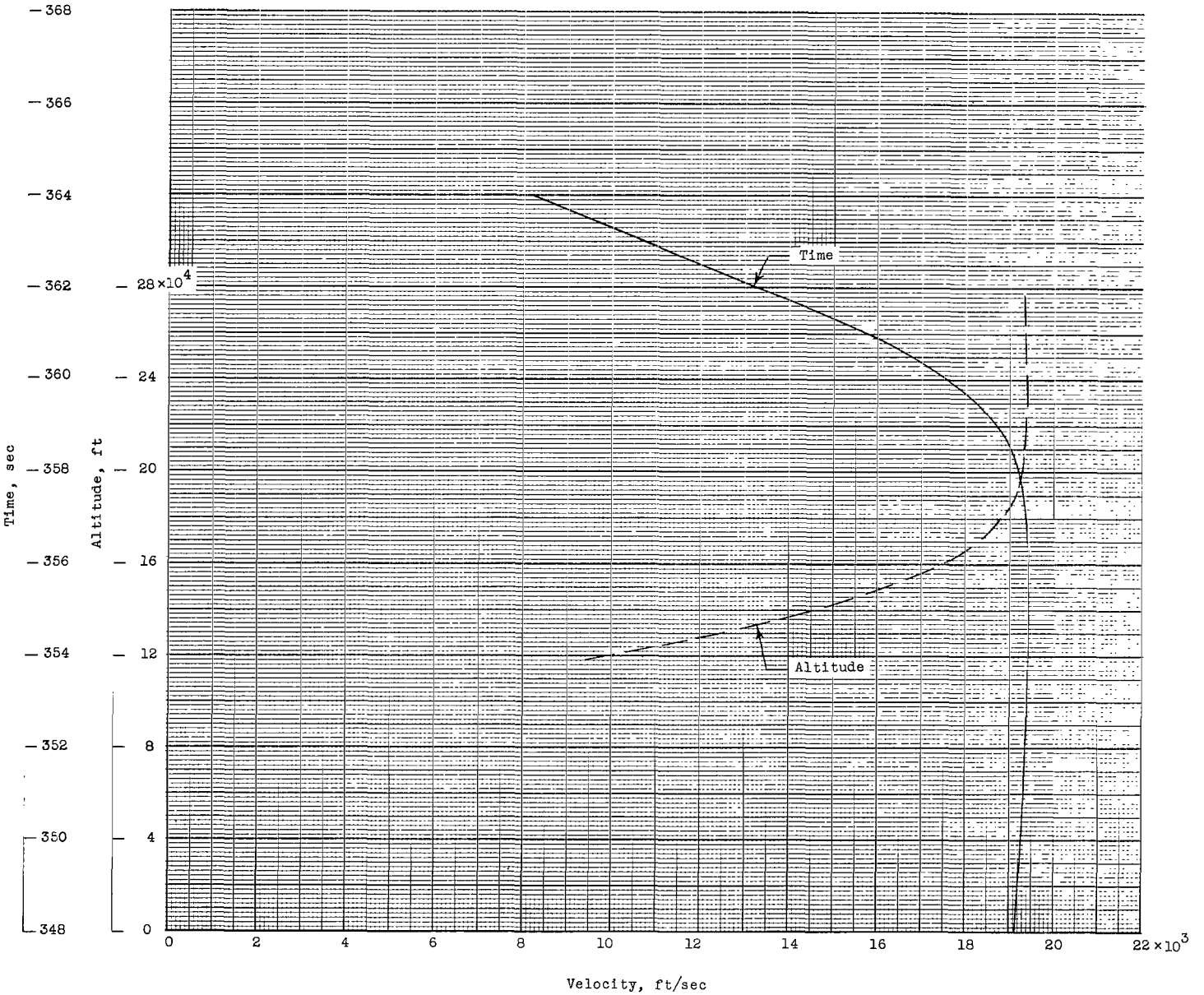


Figure 34.- Variation of reentry velocity with altitude and time for Trailblazer If.

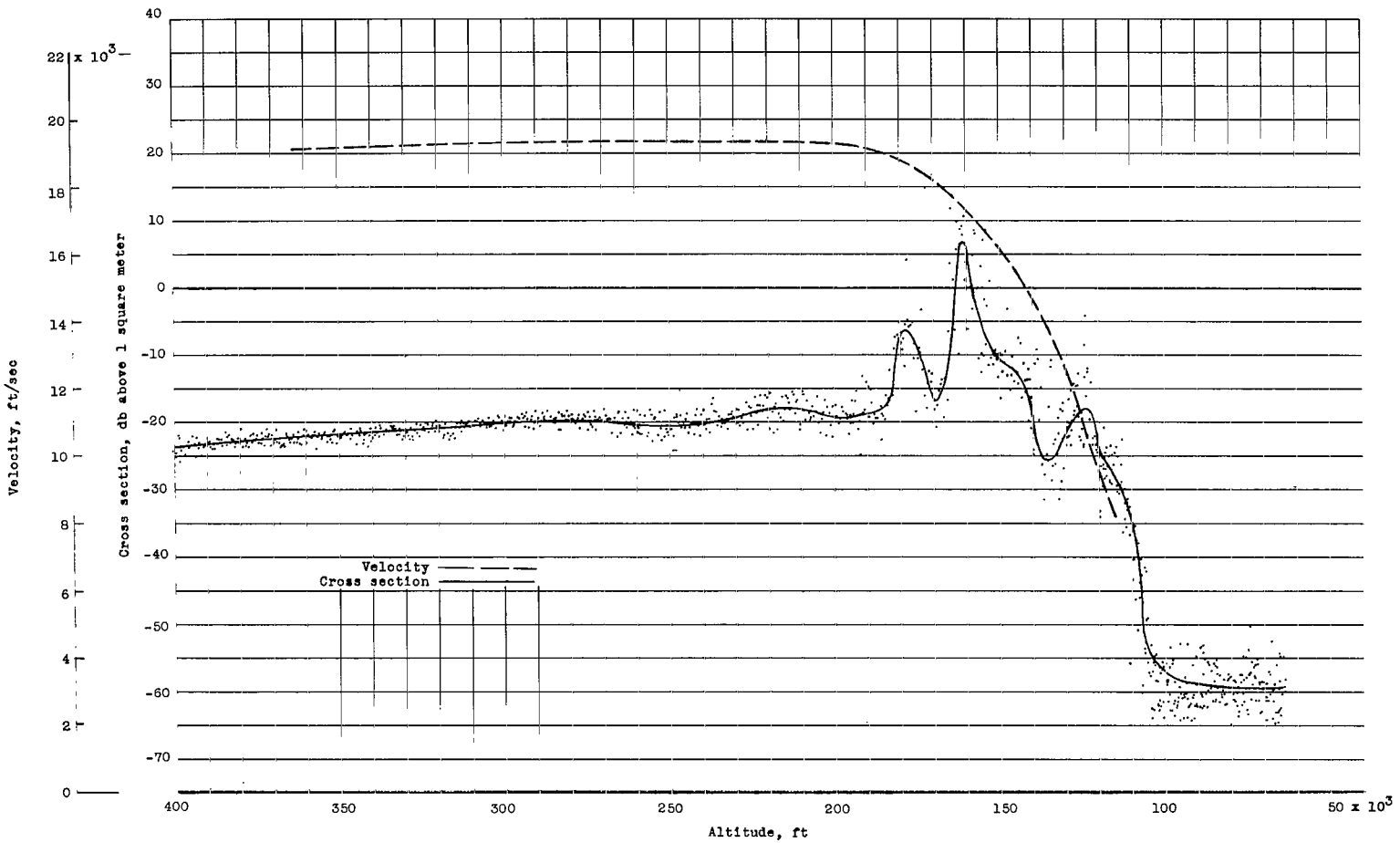


Figure 35.- Variation of cross section and velocity with altitude for Trailblazer If 5-inch sphere. MIT S-band radar.

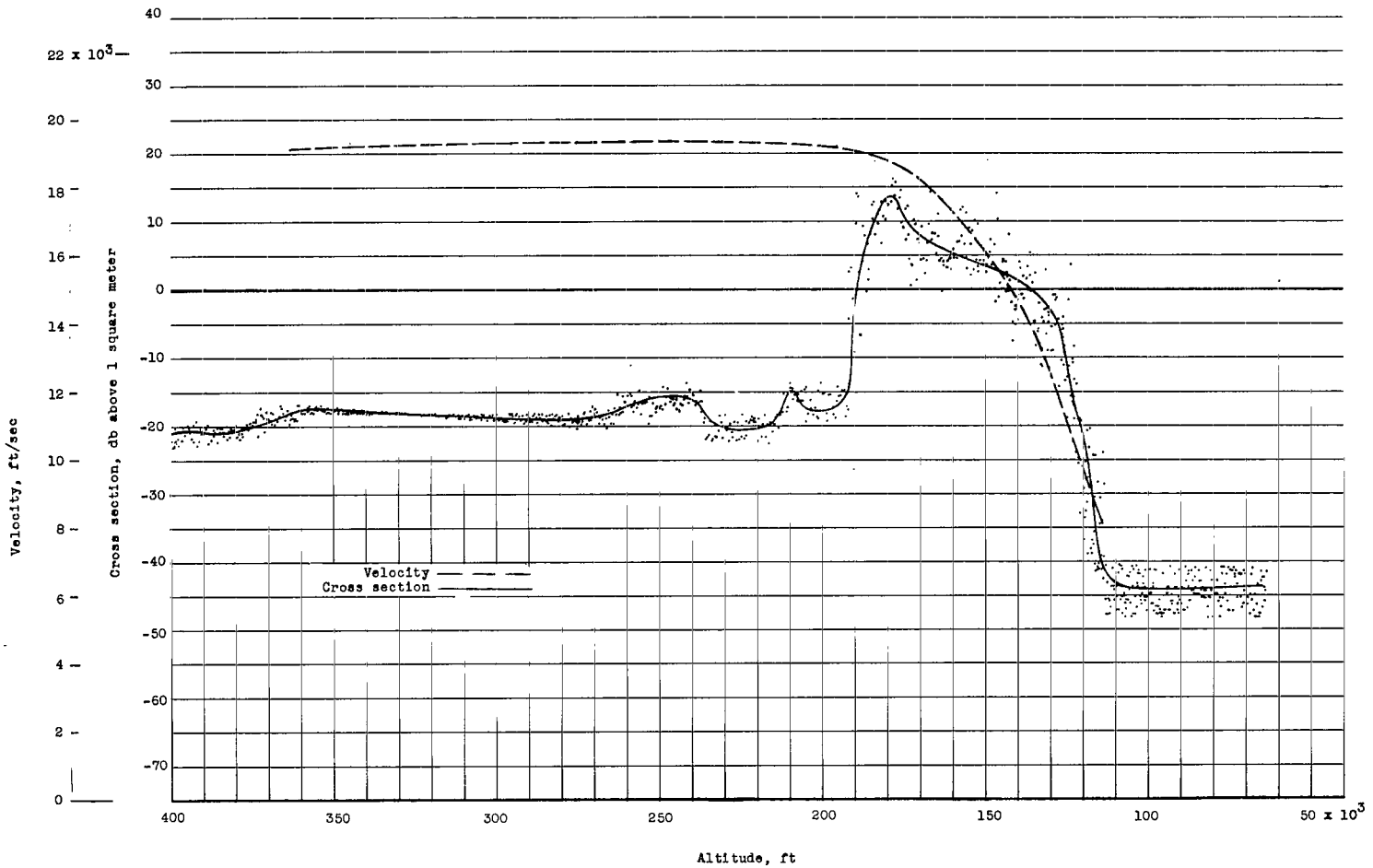


Figure 36.- Variation of cross section and velocity with altitude on Trailblazer If 5-inch sphere. MIT UHF-band radar.

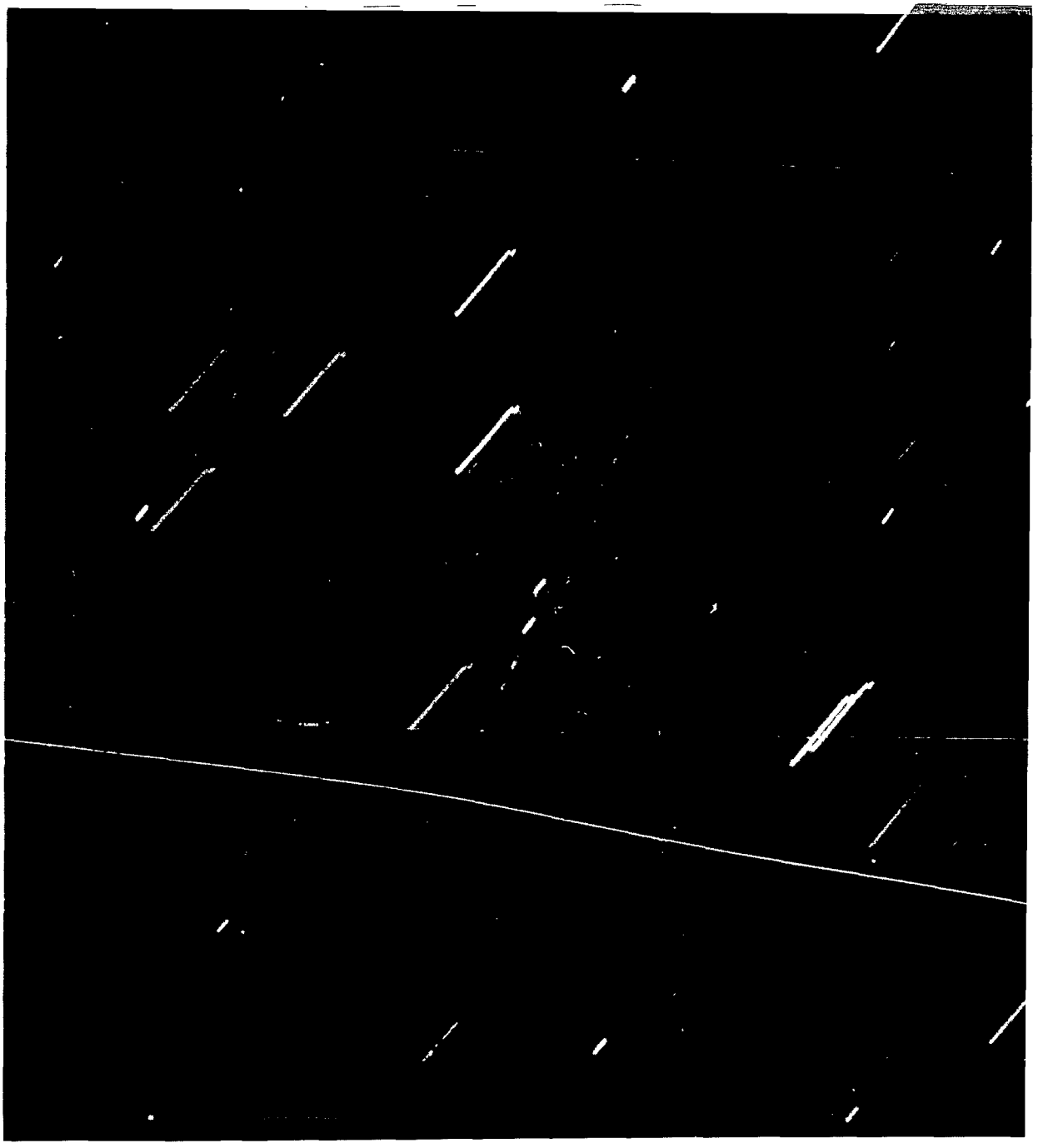

(a) Trailblazer If; camera location: Fentress, Va.;
trace chopped at 5 chops per second.

Figure 37.- Photograph of sixth-stage reentry for Trailblazer If. L-63-9265

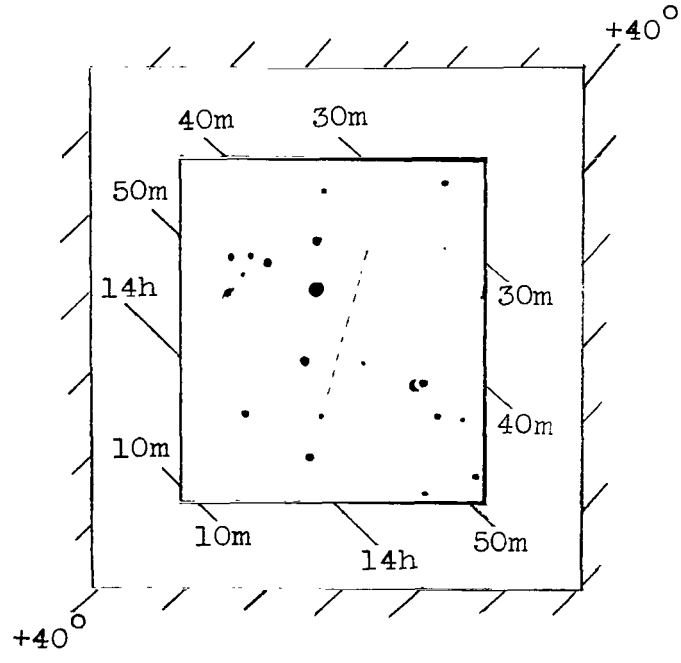


Note: Inner scale - right ascension, hr, min

Outer scale - declination, deg

(b) Sketch of star background for Trailblazer If; camera location: Fentress, Va.; trace chopped at 5 chops per second.

Figure 37.- Concluded.

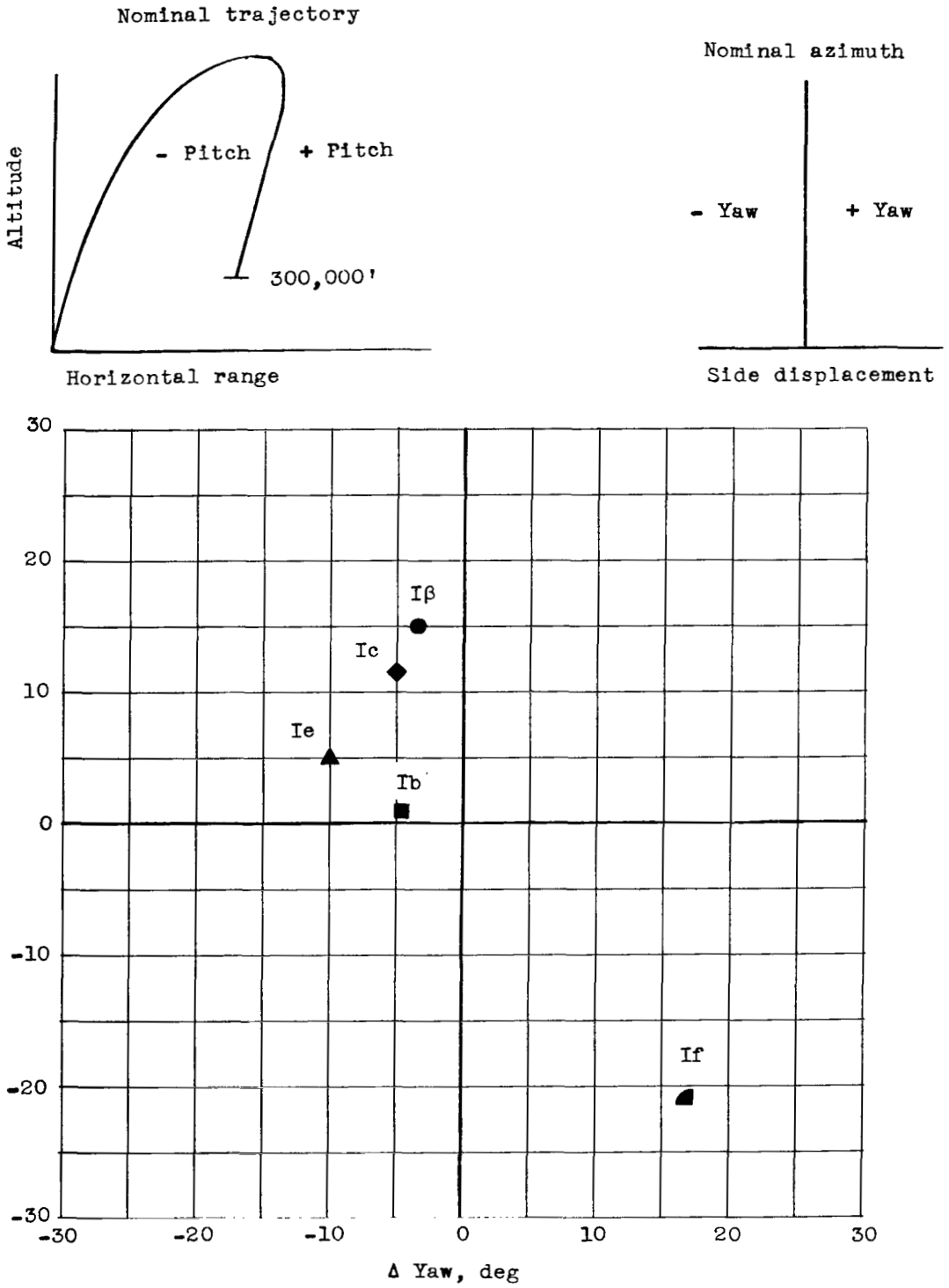


Figure 38.- Deviation of flight-path angle from nominal reentry trajectory for Trailblazer I vehicles.

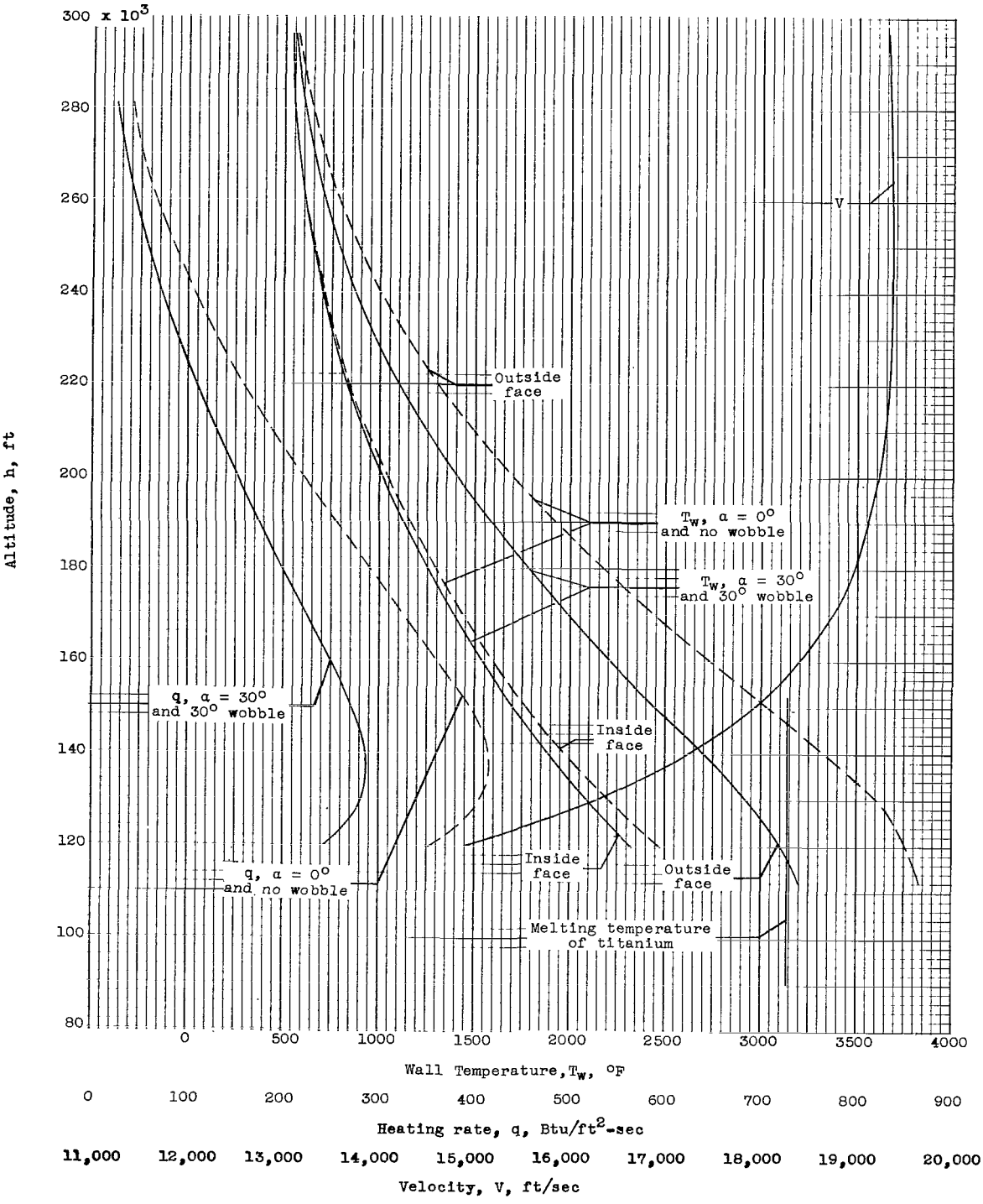


Figure 39.- Variation of wall temperature, heating rate, and velocity with altitude during reentry of Trailblazer Ic. Titanium case.

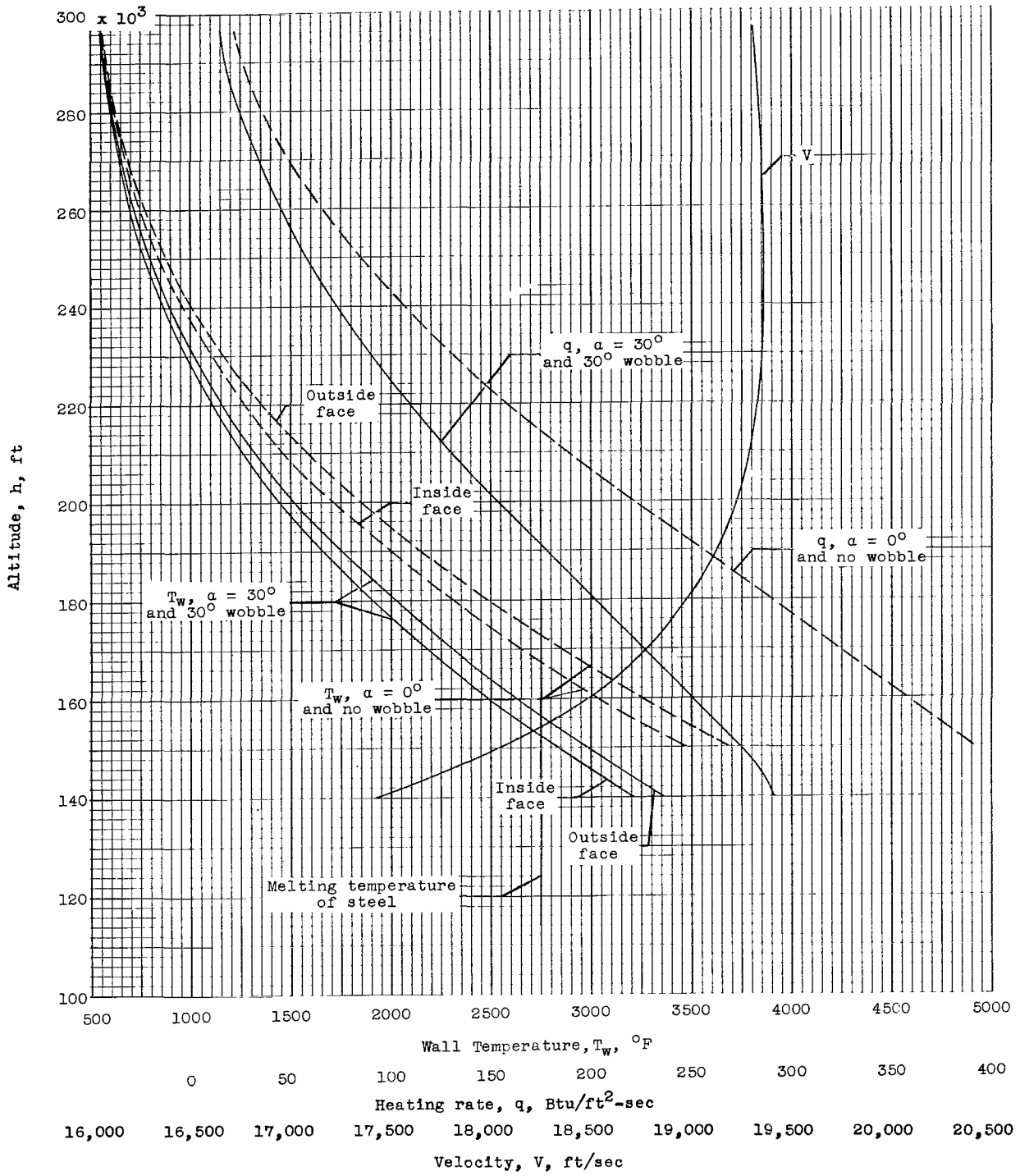


Figure 40.- Variation of wall temperature, heating rate, and velocity with altitude during reentry of Trailblazer Ie. Steel case.

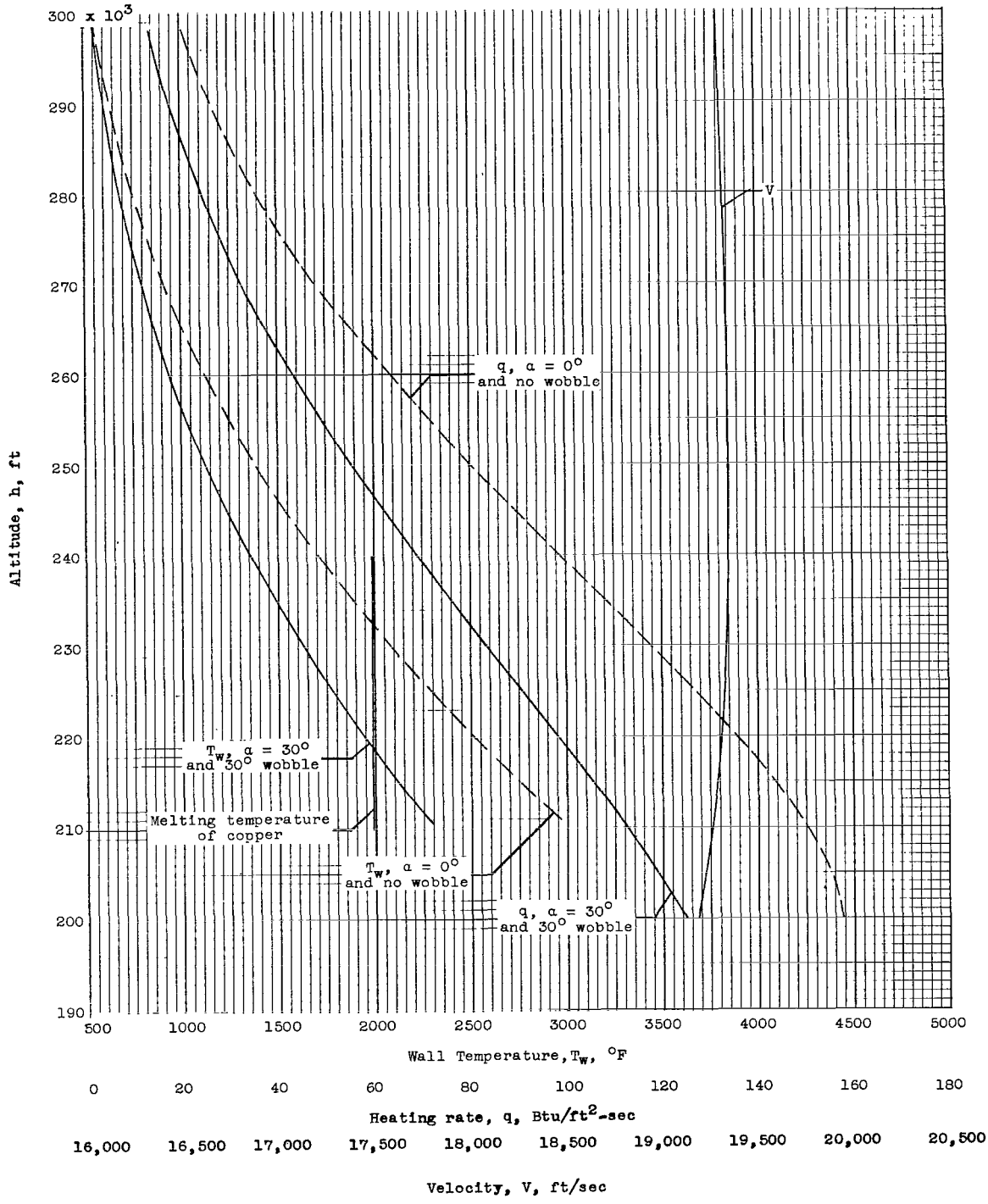


Figure 41.- Variation of wall temperature, heating rate, and velocity with altitude during reentry of Trailblazer If. Copper heat-shield cover.

2/7/6 3

*"The National Aeronautics and Space Administration . . . shall . . . provide for the widest practical appropriate dissemination of information concerning its activities and the results thereof . . . objectives being the expansion of human knowledge of phenomena in the atmosphere and space."*

—National Aeronautics and Space Act of 1958

# NASA SCIENTIFIC AND TECHNICAL PUBLICATIONS

TECHNICAL REPORTS: Scientific and technical information considered important, complete, and a lasting contribution to existing knowledge.

TECHNICAL NOTES: Information less broad in scope but nevertheless of importance as a contribution to existing knowledge.

TECHNICAL MEMORANDUMS: Information receiving limited distribution because of preliminary data, security classification, or other reasons.

CONTRACTOR REPORTS: Technical information generated in connection with a NASA contract or grant and released under NASA auspices.

TECHNICAL TRANSLATIONS: Information published in a foreign language considered to merit NASA distribution in English.

TECHNICAL REPRINTS: Information derived from NASA activities and initially published in the form of journal articles or meeting papers.

SPECIAL PUBLICATIONS: Information derived from or of value to NASA activities but not necessarily reporting the results of individual NASA-programmed scientific efforts. Publications include conference proceedings, monographs, data compilations, handbooks, sourcebooks, and special bibliographies.

*Details on the availability of these publications may be obtained from:*

SCIENTIFIC AND TECHNICAL INFORMATION DIVISION

NATIONAL AERONAUTICS AND SPACE ADMINISTRATION

Washington, D.C. 20546